LBNL-38845
CONF-9509356--
UC-426

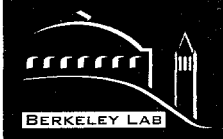

ERNEST ORLANDO LAWRENCE
BERKELEY NATIONAL LABORATORY

Proceedings of the Workshop on Vacuum Arc Ion Sources

Ernest Orlando Lawrence Berkeley National Laboratory September 18–20, 1995

Ian Brown, Editor
Accelerator and Fusion Research Division

August 1996

LBNL-38845
CONF-9509356
UC-426

Proceedings of the Workshop on Vacuum Arc Ion Sources

September 18–20, 1995

Ian Brown, Editor

Accelerator and Fusion Research Division
Ernest Orlando Lawrence Berkeley National Laboratory
University of California
Berkeley, California 94720

August 1996

This work was supported by the Division of Advanced Energy Projects of the U.S. Department of Energy under Contract No. DE-AC03-76SF00098.

FOREWORD

The custom has developed of holding a workshop on vacuum arc ion sources just before or just after the International Conference on Ion Sources. The ICIS'95 was held at Whistler, Vancouver, Canada, in September '95, and this workshop was held in Berkeley following this ion source conference, on September 18-20, 1995

The meeting was small and informal. The record of the proceedings collected here summarizes the presentations given at the workshop.

Ian Brown
LBL

CONTENTS

Mevva Development for the new GSI High-Current Injector

B.H.Wolf, H.Emig and P.Spädtke,
Gesellschaft für Schwerionenforschung, GSI,
Planckstr.1, 64291 Darmstadt, Germany

Abstract

To increase the intensity of the heavy ion synchrotron SIS for heavy elements by a factor of ~50, a new prestripper accelerator is planned for Unilac and the heavy ion synchrotron SIS. It is designed to accept ions with mass/charge $\leq$ 65 and an injection energy of 2.2 keV/u.
A vacuum arc ion source with a strong axial magnetic field will deliver 15 mA of U^{4+} as heaviest element at a repetition rate of 1 Hz and a pulse length of 300 μs. The investigation of the Mevva ion source with pulsed magnetic field of several kGauss have shown that ion currents of 8 mA U^{4+} can be measured at our test bench after 5m of transport and charge analysis (transmission at the test bench 25% only).
The noise on the extracted ion beam was already $\leq$25%, a value similar to the Pig ion source in the sputter mode, but efficient high current beam transport probably requests further improvements.

1 New prestripper linac RFQ and IH

The proposed prestripper [1] (fig. 1) consists of a RFQ accelerator with an acceptance of $\epsilon_n = 0.3$ πmm mrad and an injection energy of 2.2 keV/u instead of 11.7 keV/u at the present Wideroe. The final energy of this structure will be 120 keV/u and the rf frequency 36 MHz. The mass over charge ratio is $A/q \leq 65$. The heaviest single charged ion accepted is copper and for uranium charge state 4^+ is required instead of U^{10+} in the present prestripper.
The RFQ will be followed by two 36 MHz IH structure accelerator tanks with an end energy of 1.4 MeV/u. At this energy the ions will be stripped to the charge state required by the Unilac poststripper accelerator (e.g. U^{28+}). The overall length of the new prestripper is 32 m and will fit into the space of the Wideroe it will replace.

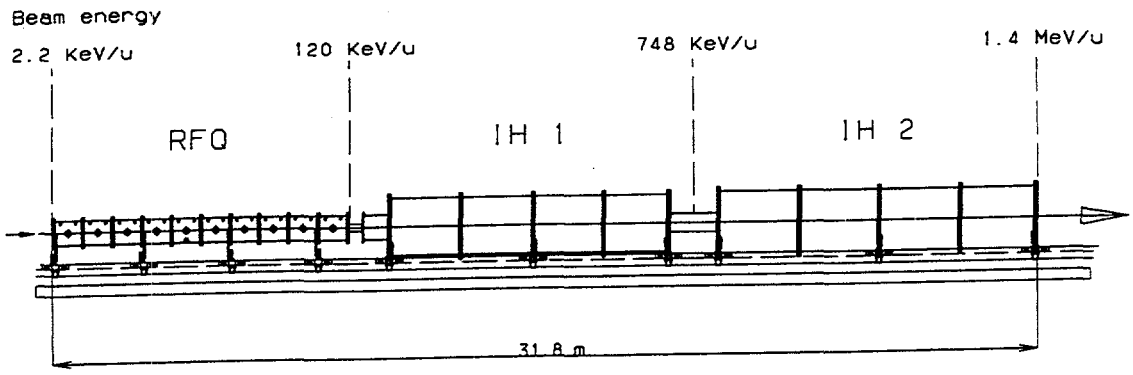

Figure 1 High current injector linac

2 Position of charge analysis

There are two possibilities to do the charge analysis in the new injector:

- Analysis on the high voltage platform after extraction with 30 to 50 kV. This has the advantage of a lower current load on the 120 kV high voltage power supply of the post-acceleration (at present 300kV), but the space charge related problems of high current ion beam transport at relatively low velocities.
- Acceleration of the total current directly after extraction to 2.2 keV/u and following charge and isotope analysis at ground potential.

An acceleration gap with a variable width of 5 to 27 cm allows to optimize the acceleration optic to the space charge forces of different ion species and ion currents. Further investigations of the two possibilities are necessary before a final decision will be made.

3 Mevva with magnetic field for U^{4+}

Metal evaporation by vacuum arc is a relatively new possibility for multiple charged metal ion production which is especially effective in the presence of an axial magnetic field.

- With increasing magnetic field (up to 1 Tesla) in the arc region the charge state distribution can be shifted towards higher charges.
- The limited acceptance of the linac of $\epsilon_n = 0.3\ \pi$ mm mrad requires a matched emittence of the ion source (at 30 kV $\epsilon \sim 300\ \pi$ mm mrad). Within this emittance the total ion current is about 100 mA.

4 Experimental Setup

The experiments described here were carried out using the GSI version of the vacuum arc ion source with grids and magnetic field [2] at the high current test bench, which has been described in detail in [3]. In these experiments we made some modifications of the ion source (Fig.2). Instead of the large coil on the outside of the expansion area, we used a small one with an internal diameter of 3 cm and 4 cm length which was mounted inside the anode region near the cathode to produce a solenoidal magnetic field. This coil has about 250 turns of copper wire of 1.05 mm diameter with the total resistance of about 1 Ohm. It was possible to obtain 40 G per ampere of coil current.

To avoid cooling problems, the experiments were made with a pulsed (5 ms) magnetic field only. We fed the coil and the arc by one power supply and two pulsing units. With separate resistors we had some control over different ratios of arc and coil

current. Sometimes we used two separate power supplies.

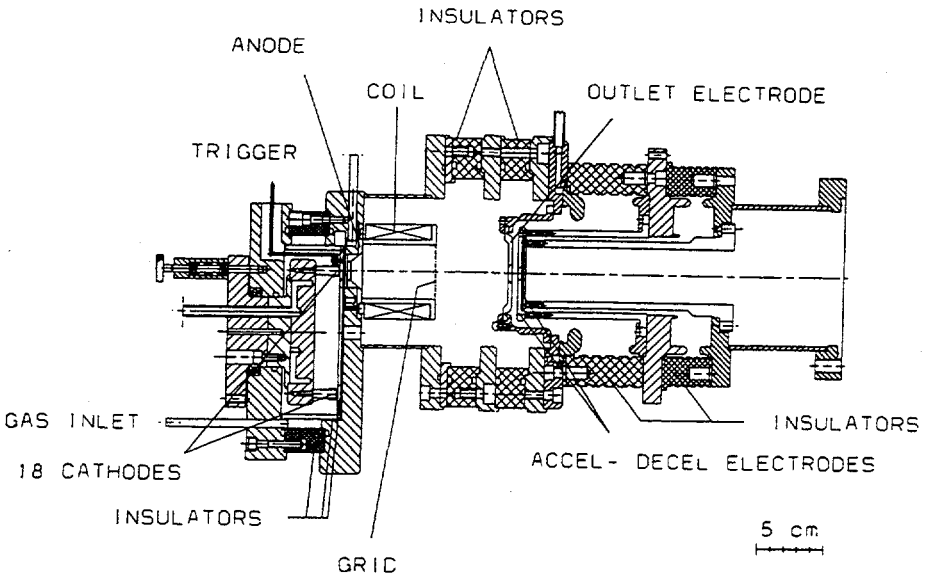

Figure 2 GSI vacuum arc ion source with magnetic field

A circuit scheme is shown in fig. 3.

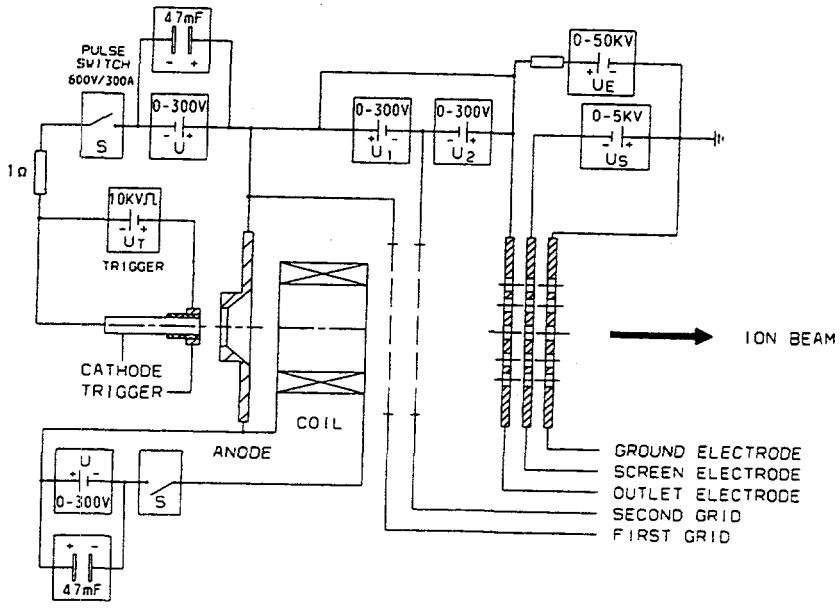

Figure 3 Circuitry of Mevva with pulsed coil

With the pulsed power supply the solenoid can produce a magnetic field of up to 6 kG at the centre of coil. The distribution of the magnetic field for 100 A current

along the axis of the coil is shown in fig. 4. The different profiles of the two different coils are obvious. We obtained a rather narrow profile with the small coil and the field at the extraction system was already 100 time lower than the maximum of the magnetic field. For iron or nickel cathodes the profile was nearly the same but the magnetic field at the cathode surface was twice as high compared to non-magnetic cathodes.

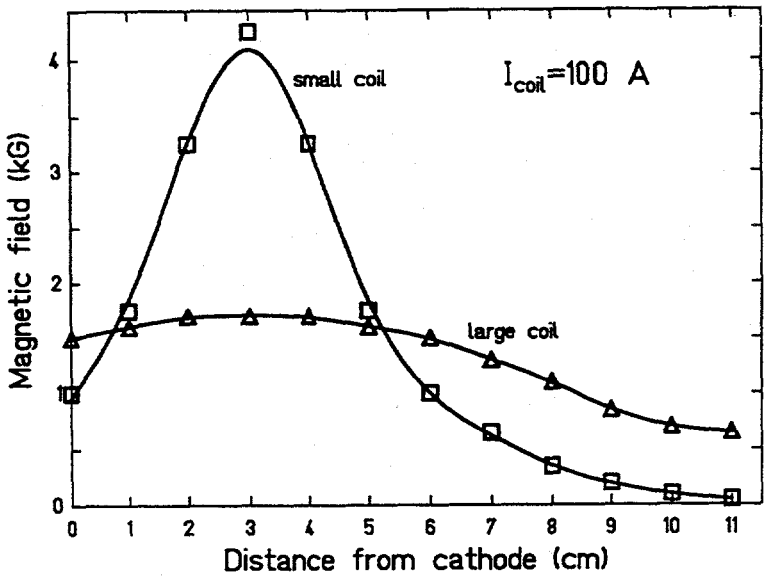

Figure 4 Magnetic field distribution on axis

The discharge current was typically in the order of 120-250 A, 0.4 ms, 1 Hz. As shown in Fig. 2 the coil was at anode potential. Both sides of the anode were terminated by metallic grids. We used double grids made from Ta (0.75 mm x 0.75 mm and 0.2 mm thickness). In order to improve pumping from the cathode region six holes of 10 mm diameter were drilled in the anode flange.

5 Experimental Results

The magnetic field has an essential influence on the vacuum arc, particulary on the discharge voltage which increased from about 20 V to more than 30 V at 0.2 Tesla.

The influence of the magnetic field with Ni-cathode and the grid at anode potential is presented in Fig. 5. By increasing the magnetic field not only the total current was increasing, but we obtained a change of the charge state distribution as well. One can see from Fig. 5 that the low charge states decrease and at the same time

the higher charge states increase.

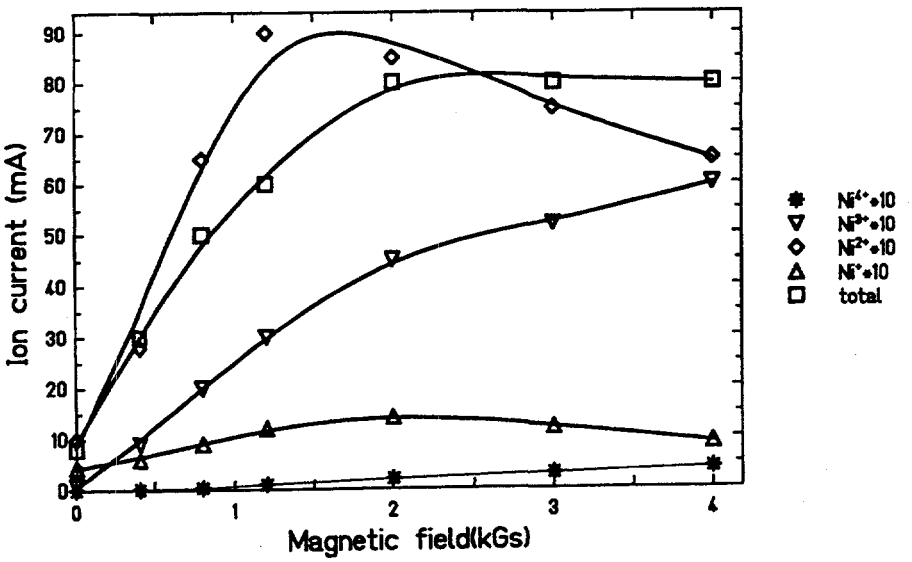

Figure 5 Ion current versus magnetic field for Ni-charge states

With an U-cathode (Fig.6), the experimental results were very close to the data which had been obtained by I. Brown [4] in an earlier experiment. The maximum value of the U^{4+} current was up to 8 mA on the end of the beam line (25% transmission) and the average charge increased from 2.7 to 3.5 at 0.4 Tesla (fig. 7).

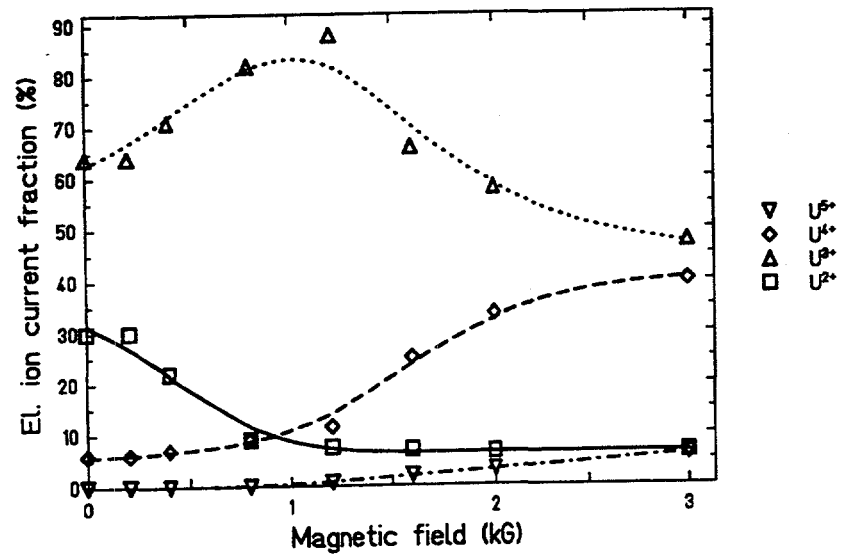

Figure 6 U-charge state distribution versus magnetic field

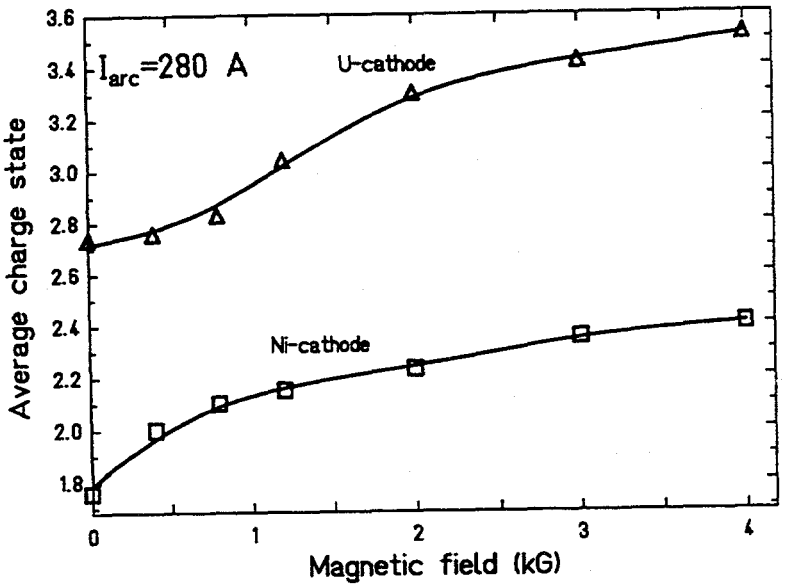

Figure 7 Average charge state versus magnetic field for Ni and U

The increase of the total current is followed by the beam noise reduction. It means that under the strong magnetic field the plasma density became rather high. Because of reflection of electrons by the accelerating potential in the region between the grid and the outlet electrode there is only a reduced ion beam space charge neutralization in that region. Thus in this gap a space charge limited ion flow is formed. As has been shown in [2] the space charge limited mode of the mevva source operation leads to a noise reduction.

Tab. 1 summarizes the yield of multiple charged ions for a variety of elements for a Mevva with strong magnetic field. These measurements have been carried out by E. Oks at LBL with a similar ion source as ours.

Table 1 Multiple charged particle yields (% of total particle current) of Mevva with and without magnetic field [5]

Ion	No magnetic field					With magnetic field						Arc	Magnet
	1	2	3	4	5	1	2	3	4	5	6	A	Tesla
C	96	4				29	58	13				3200	0.32
Mg	51	49				5	95					220	0.375
Al	38	51	11			5	11	85				1200	0.12
Sc	23	66	11			16	23	59	2			220	0.375
Ti	11	76	12	1		1	6	15	58	20		1300	1.0
V	11	72	15	2		13	31	48	8			220	0.375
Cr	14	70	15	1		4	9	20	53	12	2	800	0.62
Mn	48	52				26	47	25	2			220	0.375
Fe	28	68	6			6	20	34	38	2		2200	0.22
Co	34	59	7			5	46	47	2			400	0.6
Ni	43	50	7			1	9	19	32	27	12	3400	0.34
Cu	28	53	18	1		10	22	32	32	4		600	0.46
Y	7	63	29	1		6	9	77	8			220	0.375
Nb	3	40	39	16	2	0	6	11	29	51	3	1200	0.12
Mo	7	30	40	20	3	0	10	19	32	27	12	700	0.54
Ag	13	61	25	1		7	23	37	30	3		700	0.54
Ba	3	97				2	41	53	3	1		220	0.375
La	4	65	31			3	16	61	20			220	0.375
Gd	8	81	11			1	43	41	15			220	0.375
Er	8	62	30			2	12	70	16			220	0.375
Hf	7	26	48	18	1	1	5	11	39	41	3	600	0.46
Ta	1	17	39	39	4	1	5	13	40	41	2	220	0.375
W	1	17	35	35	12	1	5	16	39	32	7	220	0.375
Pt	12	70	18			1	16	34	46	3		1200	1.0
Pb	40	60				1	75	24				220	0.375
Bi	89	11				7	27	57	9			600	0.46
U	20	40	32	8		1	20	32	28	16	3	600	0.46

6 Conclusions

The Mevva with axial magnetic field has proven to deliver high currents of multiple charged ions with the beam quality requested by linear accelerators. We already accelerated Ti^{2+} and Ni^{3+} (the limit for the present linac) from the Mevva ion source for experiments with SIS energies and more than 10^9 particles per spill. The ion source worked reliable and the lifetime of one cathode was more than one day.

References

[1] U. Ratzinger et al. Rep. GSI-95-01, p 232 and 233 GSI Darmstadt 1995; and 'Beam Intensity Upgrate of the GSI Accelerator Facility', (A Technical Status Report), Rep. GSI-95-05, GSI Darmstadt 1995.

[2] E. Oks, P. Spädtke, H. Emig and B.H. Wolf. Rev. Sci. Instrum., 65, 3109 (1994).

[3] B.H. Wolf, H. Emig, D. Rück and P. Spädtke. Rev. Sci. Instrum., 65, 3091 (1994).

[4] I.G. Brown. Rev. Sci. Instrum., 65, 3061, (1994).

[5] E. Oks Proc. ICIS95 and this Workshop.

Vacuum Arc Ion Source Development at GSI

P. Spädtke, H. Emig and B.H. Wolf
GSI Darmstadt,
Postfach 11 05 52, 64220 Darmstadt

Some Remarks About the Development of the Mevva at GSI

Ion beams produced by the Mevva ion source are well suited for the injection into a synchrotron accelerator due to the low repetition rate (0.2 ... 5 Hz, the higher repetition rate is for the optimization of the linear accelerator only) and the short pulse length (up to 0.5 ms).

From the beginning of our experience with the Mevva ion source at GSI we tried to improve the reliability of pulse-to-pulse reproducibility and to minimize the noise on the extracted ion beam. For accelerator application this is highly necessary, otherwise the accelerator tuning and optimization becomes very difficult or even impossible. Already the beam transport becomes difficult for a noisy beam, because space charge compensation can be destroyed (at least partially). Furthermore a noisy dc-beam results in some rf-buckets which might be even empty.

The trigger problem, which we have had in the beginning could be solved by increasing the trigger voltage and the energy of the trigger power supply. We replaced the PFN (pulse forming network) with a normal power supply, feeding a large capacitor (47 mF), the discharge is switched by a GSI-made transistor pulsing unit. The advantage of this is a more flexible setting of the pulse length.

Fig. 1 shows already the second version of the Mevva ion source at GSI. The original extraction system has been exchanged to the extraction system used regularly for the Chordis ion source. The reason for that was simply to adopt the Mevva to the GSI vacuum system, but also to compare the emittance of the beam extracted from the Mevva ion source with the beam extracted from the Chordis ion source. All emittance measurements which have been made up to now, show similar results compared to Chordis emittance measurements. We conclude that the emittance is mainly given by the extraction system, the ion temperature within the plasma is negligible.

In the next version (fig. 2) the drift section behind the anode has been replaced with the Chordis anode chamber, equipped with a magnetic multi-pole structure. This structure is build by permanent magnets. We had hoped to quieten the plasma with the magnetic field, however, it has found (by removing the magnets) that the influence of the multi-pole field is negligible[2].

The next figure (fig. 3) shows already a multi cathode version of the Mevva ion source (some intermediate versions might be missing here). The holder for the permanent magnets is empty, the anode chamber simply acts as drift section.

One further idea to reduce the noise was to increase the arc current. Some improvement of the extracted beam has been observed, however, it remained unclear whether the effect was due to a quieter plasma or simply a better matching of the plasma to the extraction condition[1].

In a similar experiment, we have found some influence of introducing gas into the anode chamber on the extracted current and on the charge state distribution. It turned out later, that this method could be used to create ion beams with mixed element fractions. Whereas this is a promising application for material application, this method is not (beside some exceptions) applicable for accelerator beams. The noise reduction caused by the additional gas seem to be a similar effect as with increasing the arc current.

Fig. 4 shows a version with a coil to produce a magnetic solenoidal field and two grids. The distance of the grids is about one mm and by applying a small voltage between both grids, they are used to create a space charge limited flow of ions between the anode and the extraction system. This method has been already described by Humphries[3]. The extractable current density is decreased with that method and is not sufficient any more. This can be balanced by introducing the magnetic field which keeps the plasma electrons (and therefore the plasma ions as well). The total current density is increased by this means if front of the grids, which allows to cut off the large amplitude intensity fluctuations at that location. The action of both, the grids and the magnetic field is shown in fig. 8 and 10.

The last of this series of figures (fig. 5) shows the version of the source with a smaller coil close to the cathode and only one grid installed within the drift section. With the higher magnetic field, it was possible to influence the charge state distribution (see fig. 9). Depending on the specific required charge state, it might be necessary to have both coils simultaneously, one to influence the charge state distribution, the other to control the current density in front of the extraction.

The comparisment of the magnetic field produced by both coils is described in [4].

High Current Test Bench

The test bench where most of the experiments have been carried out is shown in fig. 6. The length of the test bench is about 5 m. Charge analysis is made with a 90 degree magnetic sector magnet. Further beam optics is provided by magnetic triplet lens which is installed directly behind the source. The distance between this triplet and the bending magnet is unnecessarily long which has only historic reasons (there was an emittance measurement device installed in previous times). Nevertheless 100% beam transmission should be possible with a beam emittance measured directly behind the source. This is shown in a simulation in fig. 7. Already 0.1 mA current results in 3% losses and 0.5 mA causes 45% losses of the beam. This effect could explain easily the measured transparency of the test bench of about 30%.

Measurements

In fig. 8 the effect of the installed grids together with a low magnetic field is shown. For this comparisment a Fe beam has been used. The left column shows the result without grids and magnetic fields, the right column is with grids and magnetic field. In the first row the total extracted beam is shown (measured in the first Faraday cup in the beam line). The next rows show the Fe^{+}, Fe^{2+} and Fe^{3+}, respectively.

The influence of the higher magnetic field close to the cathode is shown in fig. 9. In these oscillograms a Ni beam is extracted from the source, and the signal from two different Faraday cups are displayed. The first trace shows the Faraday cup directly behind the source (i.e. the total extracted ion beam is shown), the second trace is the signal from the Faraday cup behind the bending magnet which is than the analyzed current. The first column shows the Ni beam for low magnetic field, whereas in the right column the magnetic field close to the cathode is in the order of 0.35 T.

In fig. 10 the optimized U beam signal is shown. The upper trace is the total extracted beam, the second trace is the analyzed U^{4+} at the end of the beam line.

Requirements for the UNILAC

Up to now we inject the dc-ion beam into the Wideröe accelerator (the accelerator facility is shown in fig. 11). The specific input energy of this accelerator is 11.7 keV/u. For the dc acceleration up to 320 kV plus the extraction voltage of up to 50 kV is available. This requires a certain charge state for a given mass, without changing the existing hardware. Up to mass 25 we can accept singly

charged ions, up to mass 50 charge state 2 is required and so on. After upgrading the UNILAC with a high current injector (which will consists of a RFQ and an IH-structure, replacing the Wideröe accelerator) the specific input energy will be 2.5 keV/u. The design ion is U^{4+} (compared to U^{10+} now produced by the PIG-ion source) which requires about 150 kV total voltage for dc acceleration.

We will have to decide, whether the charge state separation will be made on the high potential terminal. In this case we can use the existing HV-power supply, which is restricted to 20 mA, but we would need a low energy beam line with additional lenses on the terminal, which requires a new power transformer to provide the necessary power on the terminal. If we would make the charge separation with the existing magnets on ground potential, we would need a new high voltage power supply (150 kV, 150 mA). In the moment we have checked, that the second possibility is working quite reasonable, and this would be a reliable solution.

The actual beam line between ion source and Wideröe accelerator is shown in fig. 12. To be able to focus the beam within the acceleration column a high focusing power is necessary. A single gap acceleration column is able to provide this focusing force. To provide some experimental data we have measured the emittance of the ion beam behind such a single gap system. For these measurements different gap width have been provided. This is shown in fig. 13, furthermore different ion sources have been used to compare different beams. The results are listed in tab. 1.

Simultaneously, a single gap structure with an adjustable gap length has been designed. The technical layout is shown in fig. 14.

The strong focusing properties of such a single gap structure as well as the strong influence of the space charge is shown with computer simulations (fig. 15 - fig. 20.). In all these simulations an Ar^{2+} with extraction voltage of 10 kV has been used. In Fig. 15 the space charge force is switched off, showing that an acceleration voltage of 60 kV is sufficient to focus the beam. If the space charge of the 10 mA beam is switched on, the beam explodes. Even if the acceleration voltage is set to 150 kV (which produces a strong over focusing for the zero space charge case: fig. 17), the space charge action is stronger than the focusing force of the gap (fig. 18). Introducing a negative screening electrode behind the acceleration column, keeps the secondary electrons in the beam. This is shown in fig. 19, the emittance at the location of the emittance measurement device is shown in fig. 20. This simulated emittance agrees perfectly with the measured emittance.

References

[1] P. Spädtke, unpublished.

[2] B.H. Wolf et al., Development of Heavy Ion Sources at GSI, Proceedings of the 3. ICIS, Review of Scientific Intstruments, Berkeley, 1989.

[3] S. Humphries et al., Ion Sources for Pulsed High Brightness Beams, The Physics and Technology of Ion Sources, edited by Ian G. Brown.

[4] B.H. Wolf, H. Emig and P. Spädtke, this workshop

Figure Captions

Fig. 1: Mevva II type with regular GSI accel-decel extraction system. U_t is the trigger electric, U_d the discharge power supply with a transistor pulsing equipment. The cathode C is in front of the anode A. The outlet electrode is connected to the anode via a $500\,\Omega$ resistor. The extraction power supply is U_e and the decel electrode is biased with the power supply U_s.

Fig. 2: The same abbreviations as in fig. 1 are used. The drift section of the Mevva source is here equipped with a multi-pol structure which is used for the Chordis ion source discharge chamber.

Fig. 3: The permanent magnets from the drift section has been removed. The empty Chordis discharge chamber simply acts as a drift section. A multi-cathode holder has replaced the previous single-cathode holder.

Fig. 4: The drift section has now been replaced by two grids, which can be connected to different potentials. To influence the plasma density close to the grids with a magnetic field, a coil has been added. The gas inlet can be seen at the top of the anode flange. We called that version GGB (grids, gas, magnetic field).

Fig. 5: An additional coil has been installed inside the vacuum, to create higher magnetic fields close to the cathode. Both coils can be operated in a pulsed mode, which allows the coil operation without cooling, even for high currents.

Fig. 6: The test bench at which most of the experiments have been carried out

Fig. 7: Simulation of an ion beam, transported through the test bench, assuming different degrees of space charge compensation. The beam for this simulation is Ar^+ with 20 keV energy.

Fig. 8: Faraday cup signals for Ni. The first column shows the result for the source without grids, but with the outer coil to match the plasma density to the extraction field strength via the magnetic field. In each oscilloscope figure the total extracted current is shown (upper trace) together with a specific analyzed charge state (lower trace) is shown. The singly charged ion beam is in the first row, the Ni^{4+} is in the fourth row. For the total current without mesh the scaling is 8 mA/div and 0.4 mA/div (Ni^+), 1 mA (Ni^{2+}), 0.4 mA (Ni^{3+}) and 0.02 mA/div (Ni^{4+}) for the specific charge state. For the beam with meshes and high magnetic field (0.35 T) to increase the charge states, the scaling is 40 mA/div for the total current, 1 mA/div (Ni^+), 4 mA (Ni^{2+}), 2 mA (Ni^{3+}) and 0.2 mA/div (Ni^{4+}) for the specific charge states.

Fig. 9: Comparison of the Mevva-IV (left column) with the version with grids and magnetic field (right column). First row shows the total current (20 mA/div). The second shows the singly charged Fe (left0.4mA/div, right 2 mA/div). The third shows the doubly charged Fe (left 2 mA/div, right 4 mA/div). The last row shows the Fe^{3+} (left 1 mA/div, right 2 mA/div).

Fig. 10: The design ion U^{4+}. The upper trace is the total extracted current (40 mA/div), the lower trace shows the analyzed U^{4+} (4 mA/div).

Fig. 11: The GSI-facility: IS is the injector building, HLI the new high charge state injector, UNILAC the linear accelerator, SIS the heavy ion synchrotron, FRS the fragment separator, ESR the experimental storage ring, TA the high energy experimental hall.

Fig. 12: The actual beam line from the high current source terminal to the Wideröe accelerator

Fig. 13: The experimental setup for emittance measurements. The accelerator gap is fixed for each measurement, can be readjusted by the insertion of distance rings. The emittance measurement device is installed in the diagnostic chamber.

Fig. 14: The technical layout of the new variable gap accelerator column.

Fig. 15 ... 20: Computer simulation of the beam used in the emittance measurements. The simulation was made with an Ar^{2+}-beam with 20 keV start energy.

Fig. 15: 60 kV acceleration voltage, no space charge forces.

Fig. 16: 60 kV acceleration voltage, with space charge.

Fig. 17: 150 kV acceleration voltage, no space charge forces.

Fig. 18: 150 kV acceleration voltage, with space charge.

Fig. 19: As fig. 18 but with negative screening potential, to keep the space charge compensating electrons within the ion beam.

Fig. 20: Emittance figure at the location of the emittance measurement device. The beam has been produced with the geometry described in fig. 19.

Tab. 1: Measured emittance.

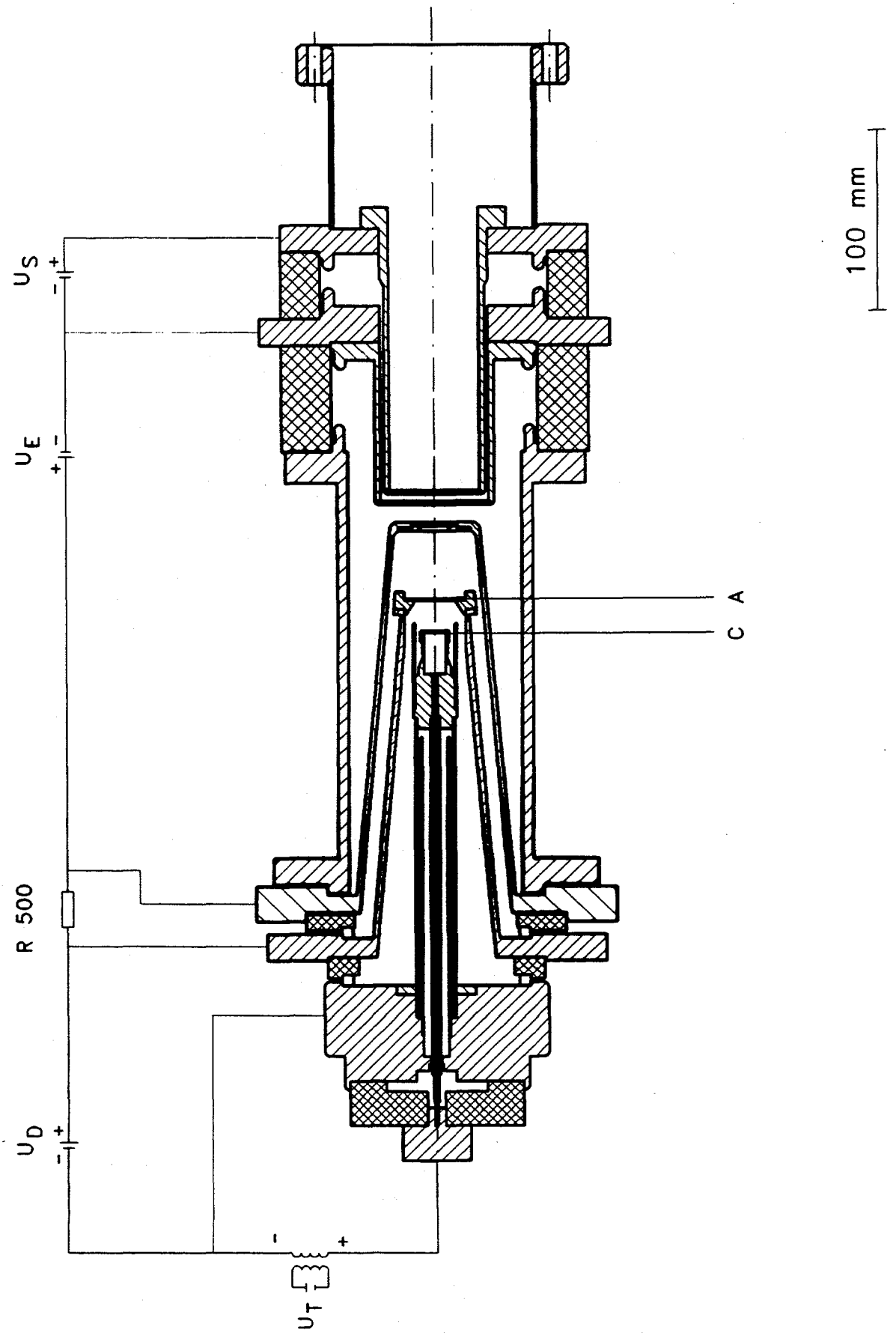
100 mm
U_S
U_E
U_D
R 500
C A
U_T

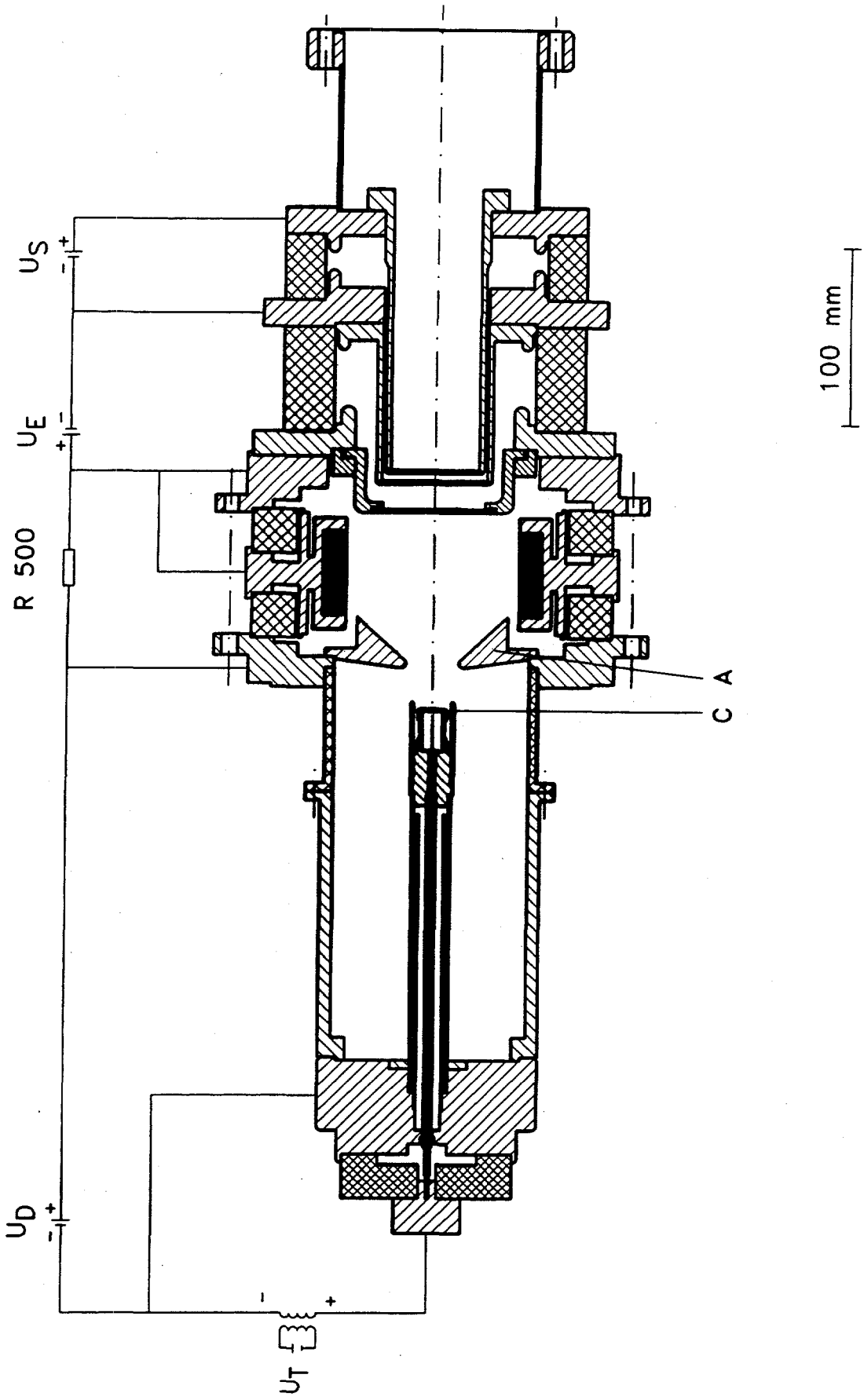
U_S
U_E
R 500
U_D
U_T
C A
100 mm

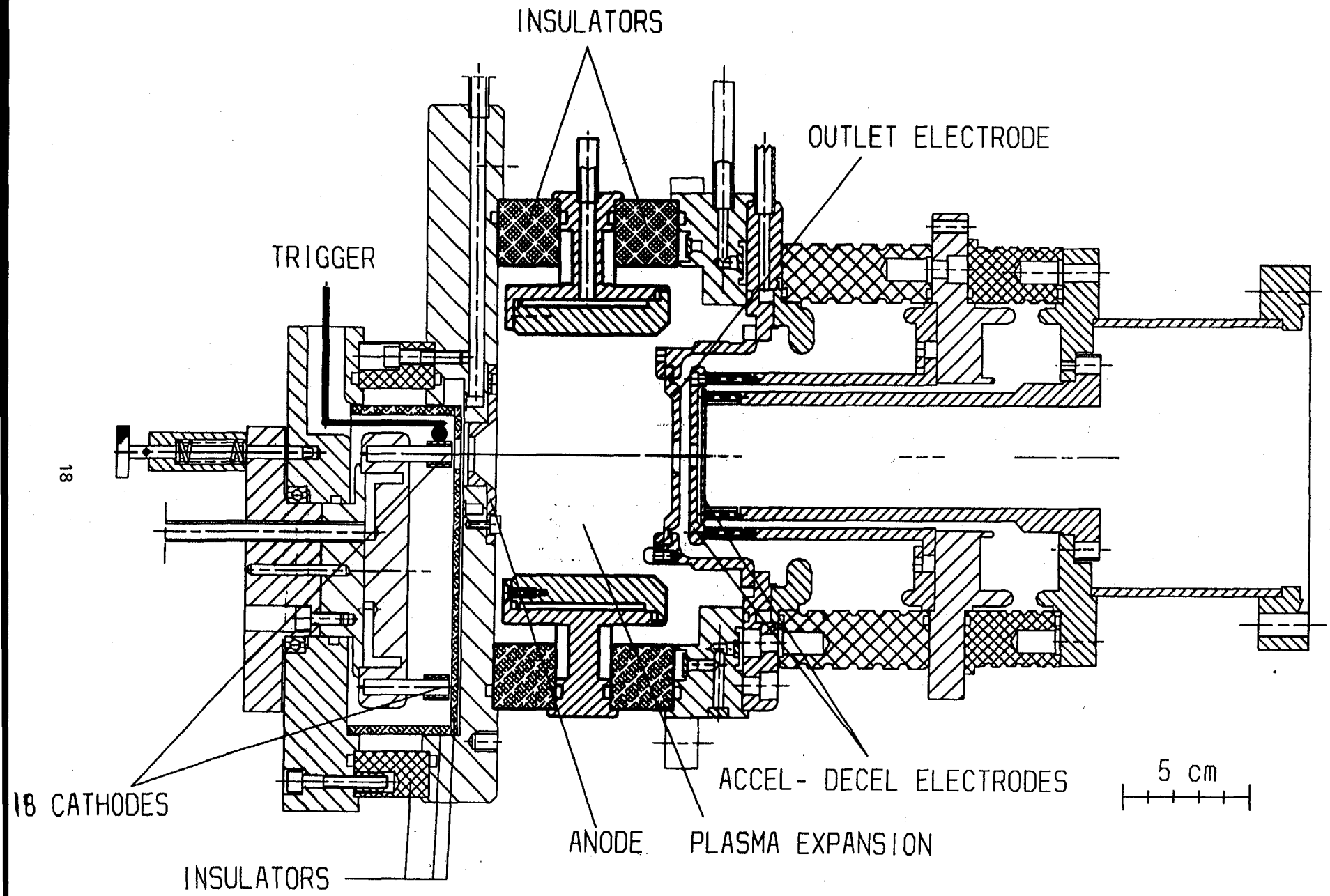

MEVVA IV GSI-VERSION

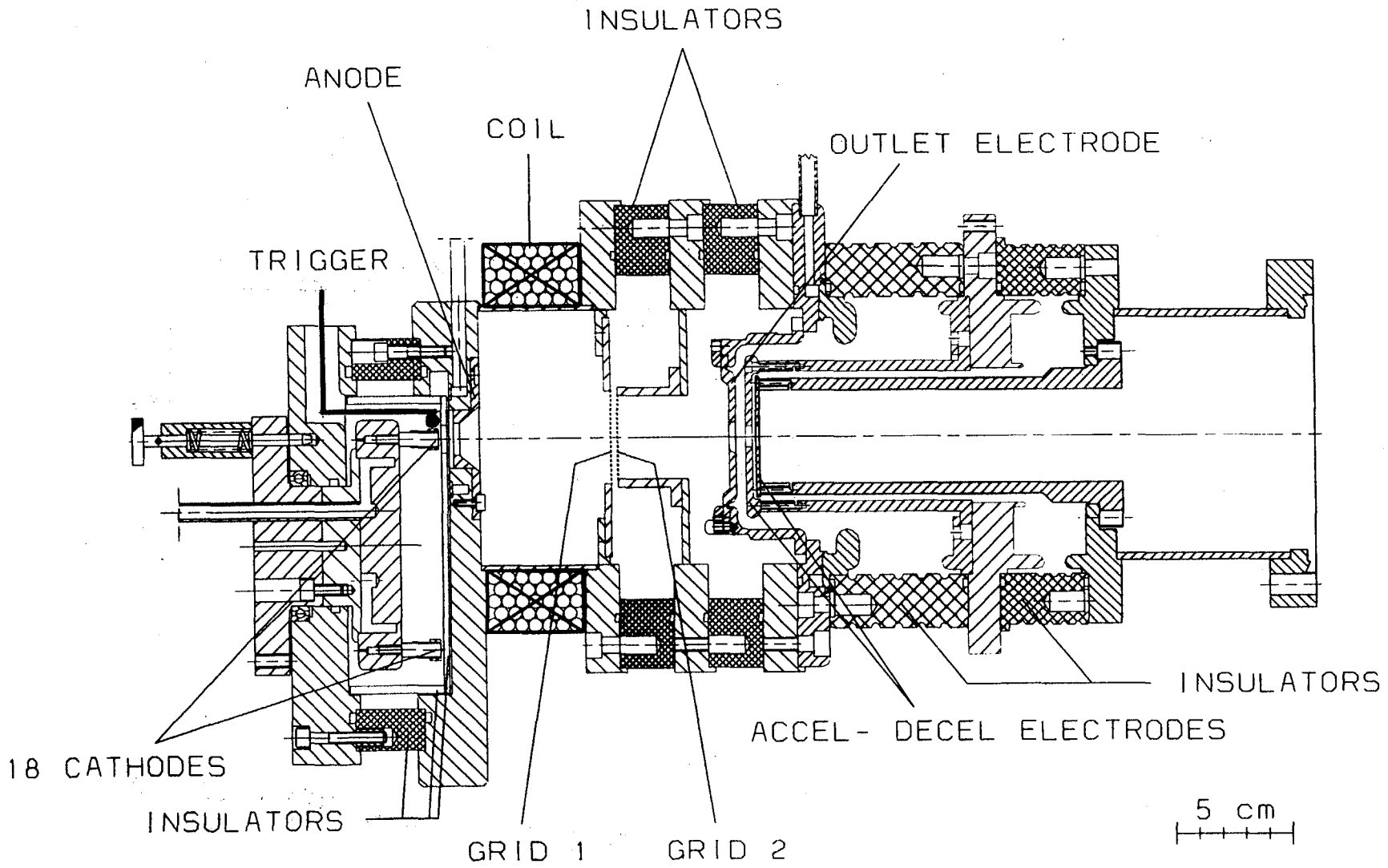

MEVVA IV-GGB GSI-VERSION

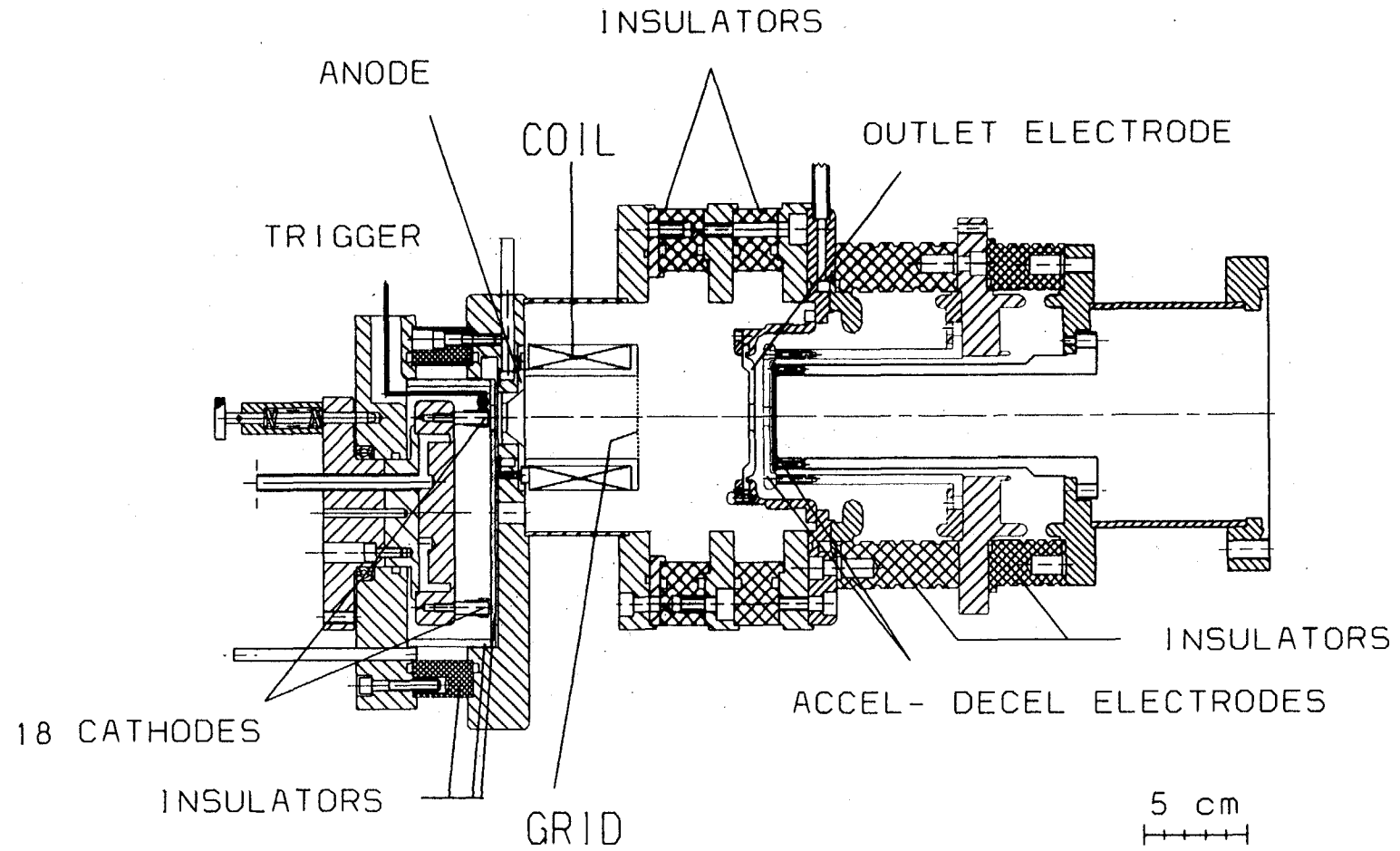

MEVVA IV WITH GRID
AND MAGNETIC FIELD

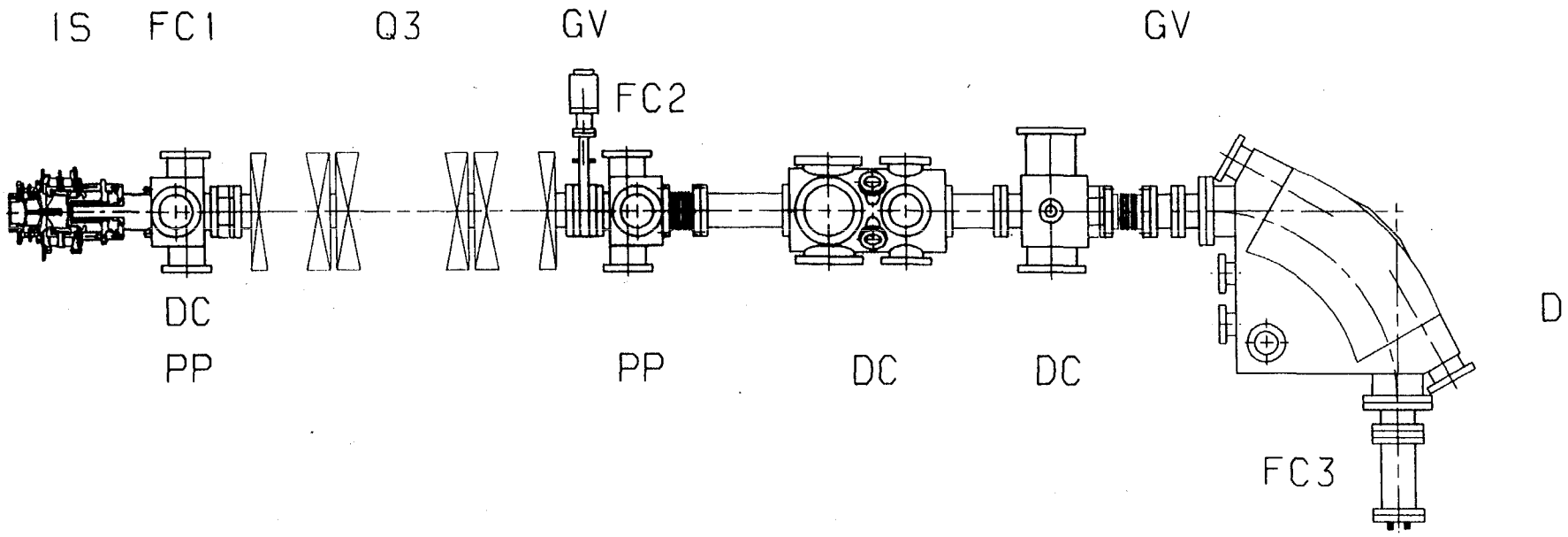

IS: chordis ion source

PP: pepperpot

DC: diagnostic chamber

Q3: triplet

D : dipole

GV: gate valves

FC1, FC2, FC3: faraday cups

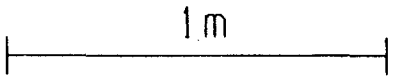

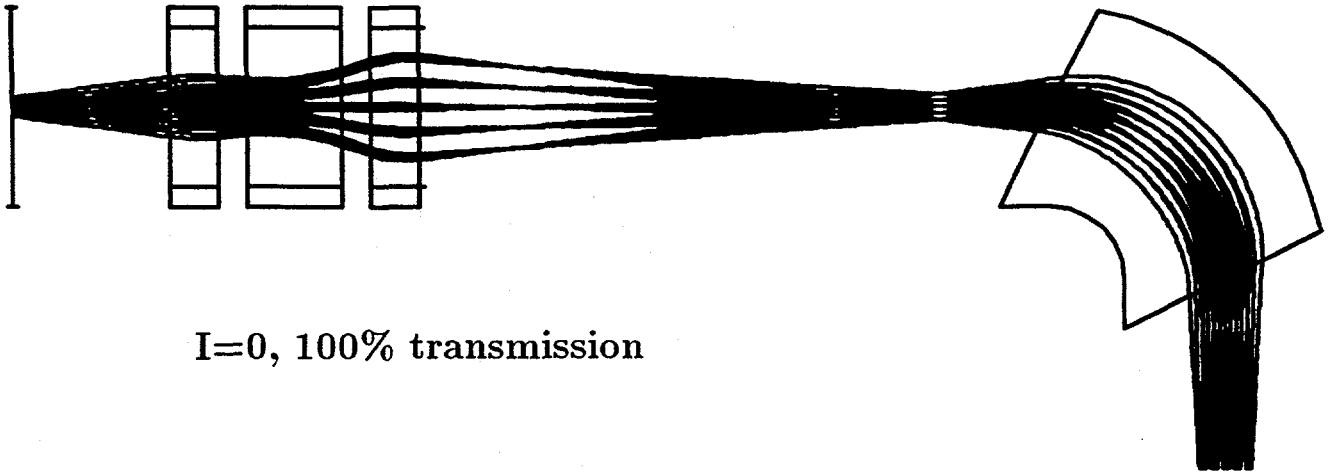

I=0, 100% transmission

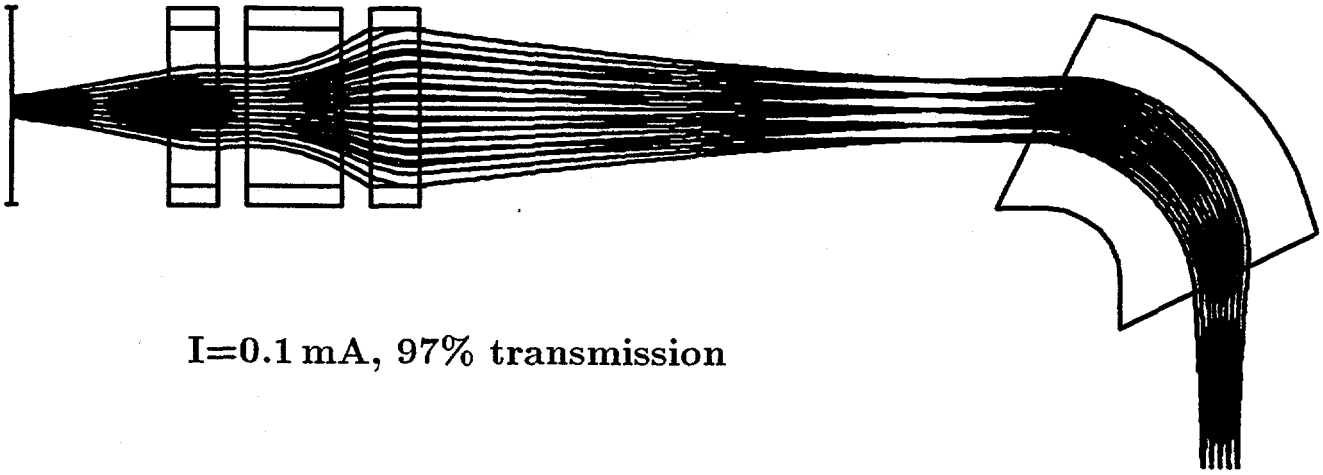

I=0.1 mA, 97% transmission

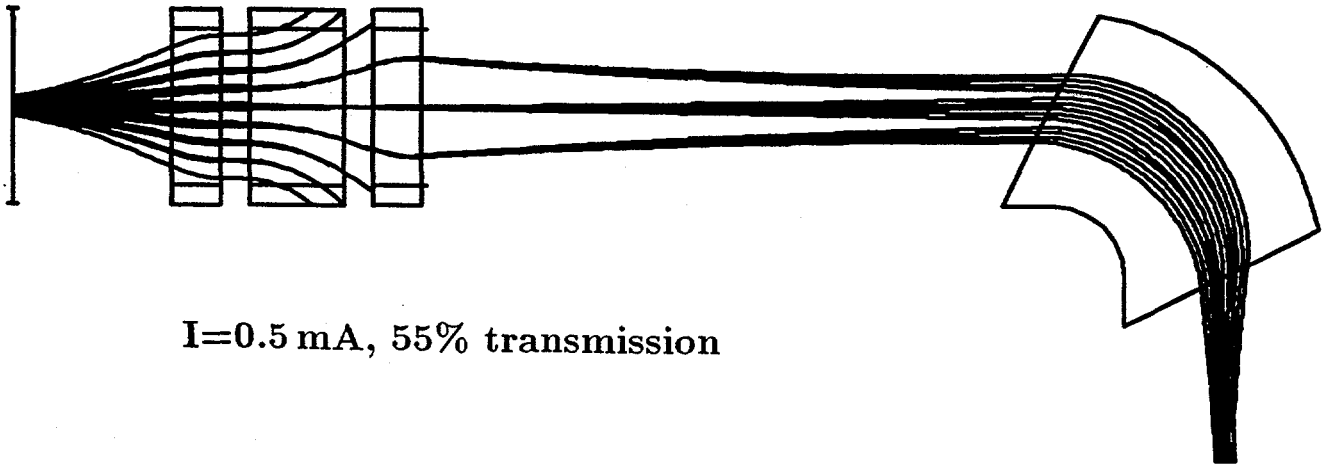

I=0.5 mA, 55% transmission

20 keV Ar^+ beam at the high current test bench
(total beam path 5 m)

Ni

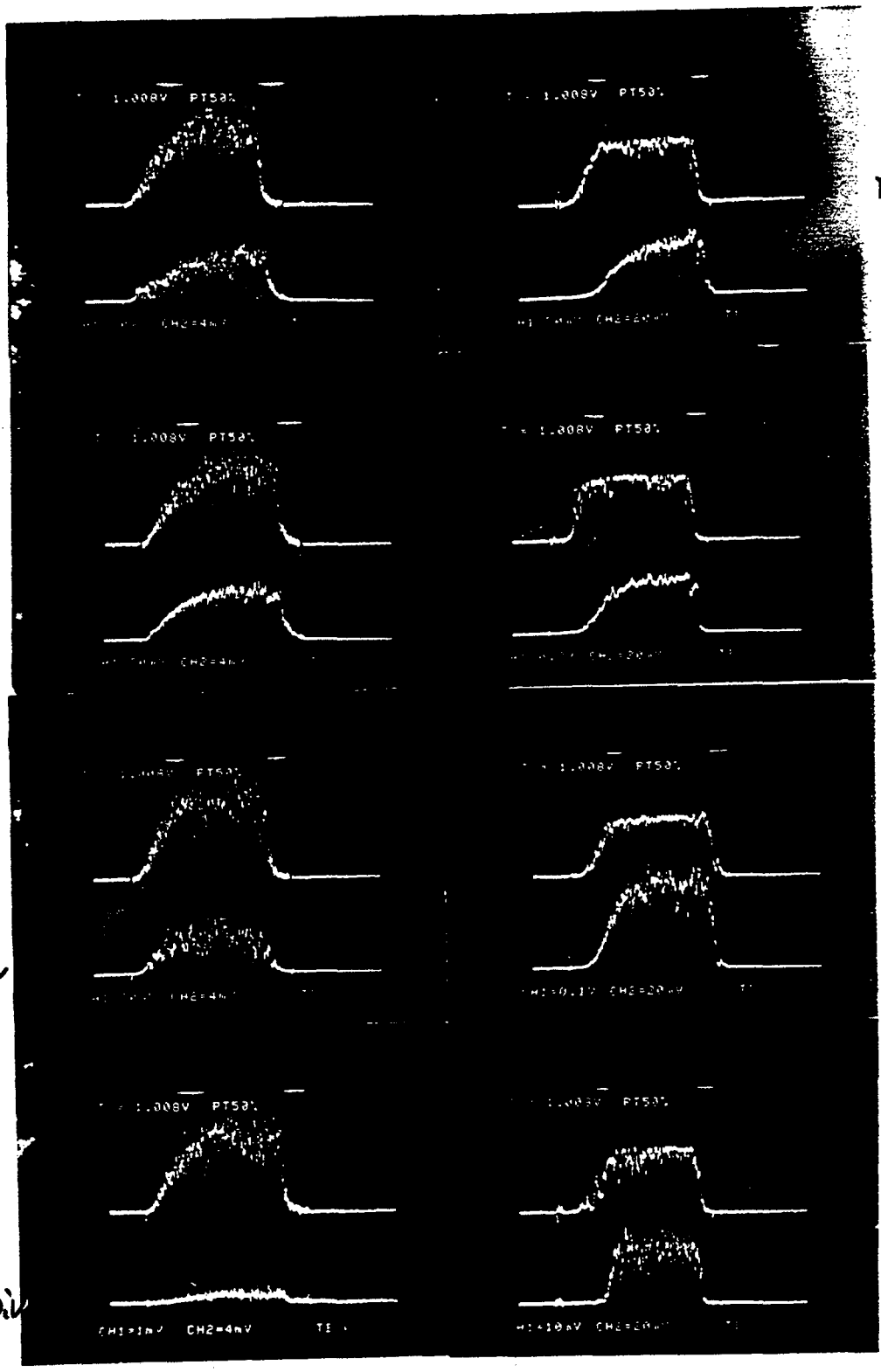
8mA/DIV
0.4mA/D
1mA/DIV
0.4mA/DIV
0.02mA/DIV
Ni 40mA/DIV
Ni+ 1mA/DIV
Ni
Ni2+ 4mA/DIV
Ni
Ni3+ 2mA/DIV
Ni
Ni4+ 0.2mA/DIV
0.02T
0.35T

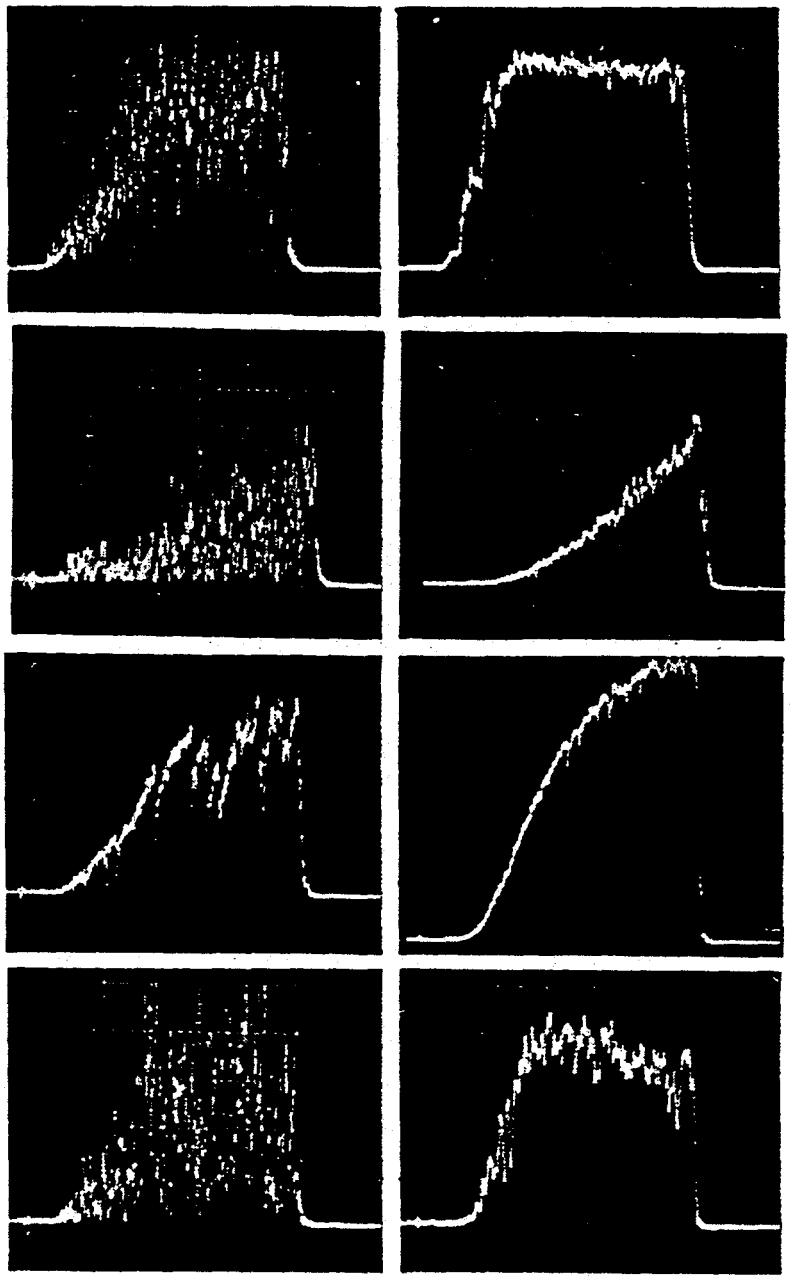

Comparison of the MEVVA-IV (left column) with the version with grids and magnetic field (right column). First row shows the total current (20 mA/div). The second shows the singly charged Fe (left 0.4 mA/div, right 2 mA/div). The third shows the double charged Fe (left 2.0 mA/div, right 4 mA/div). The last row shows the Fe^{3+} (left 1.0 mA/div, right 2 mA/div).

U

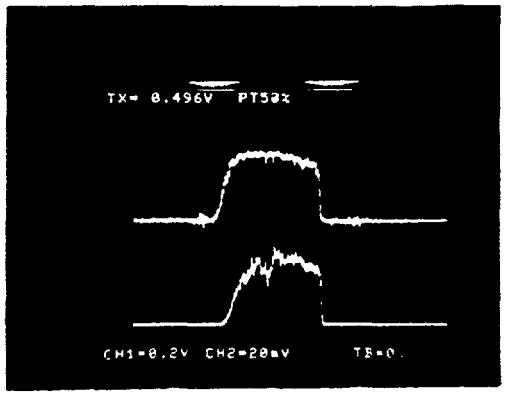

40mA IDiv U

4mA IDiv U++

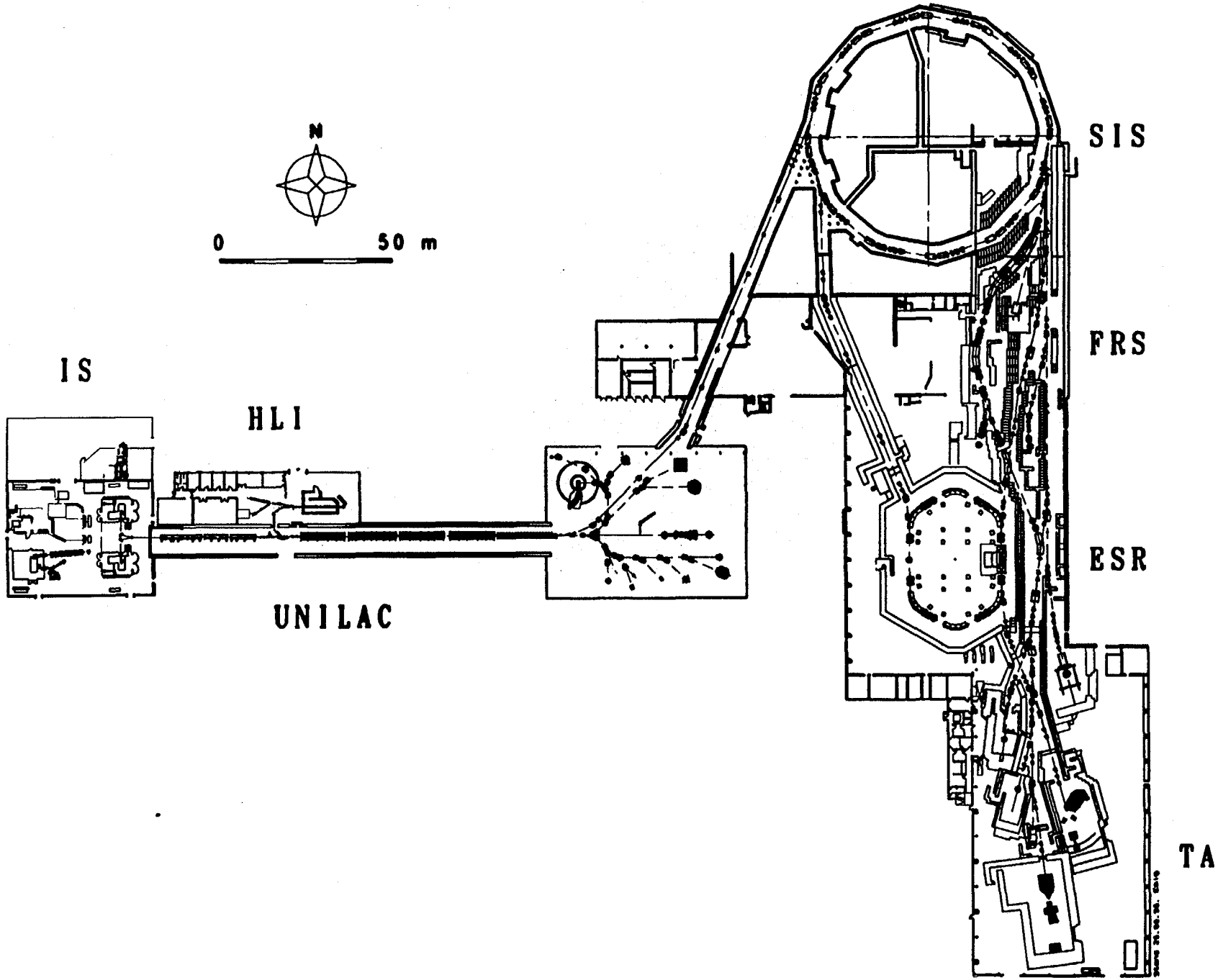
N
0
50 m
IS
HLI
UNILAC
SIS
FRS
ESR
TA

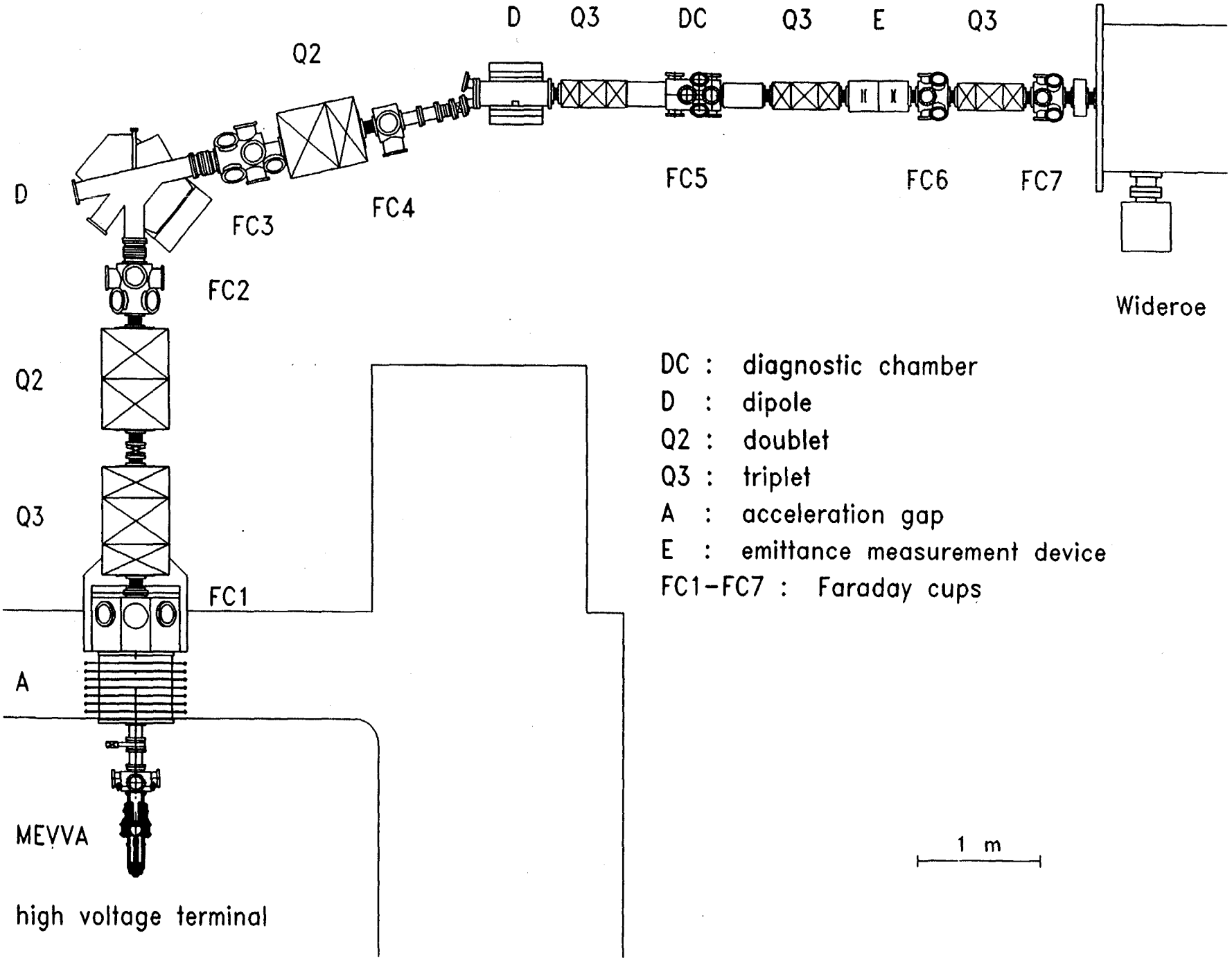
D
Q3
DC
Q3
E
Q3
Q2
D
FC3
FC4
FC5
FC6
FC7
FC2
Wideroe
Q2
Q3
FC1
A
MEVVA
high voltage terminal
DC : diagnostic chamber
D : dipole
Q2 : doublet
Q3 : triplet
A : acceleration gap
E : emittance measurement device
FC1-FC7 : Faraday cups
1 m

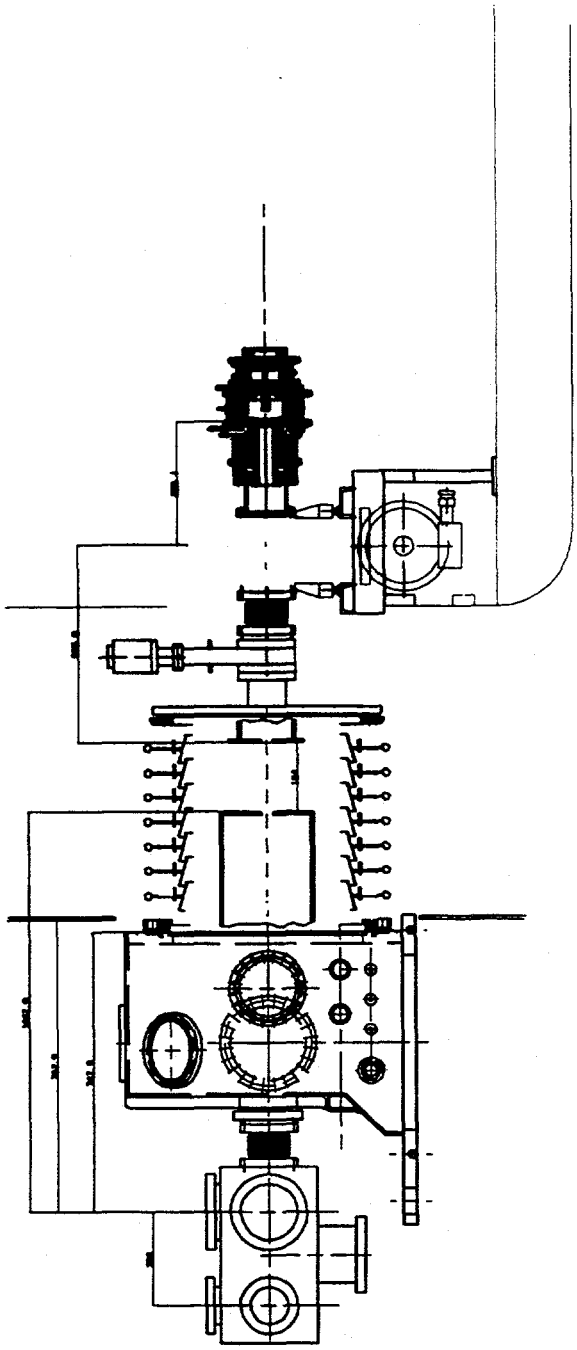

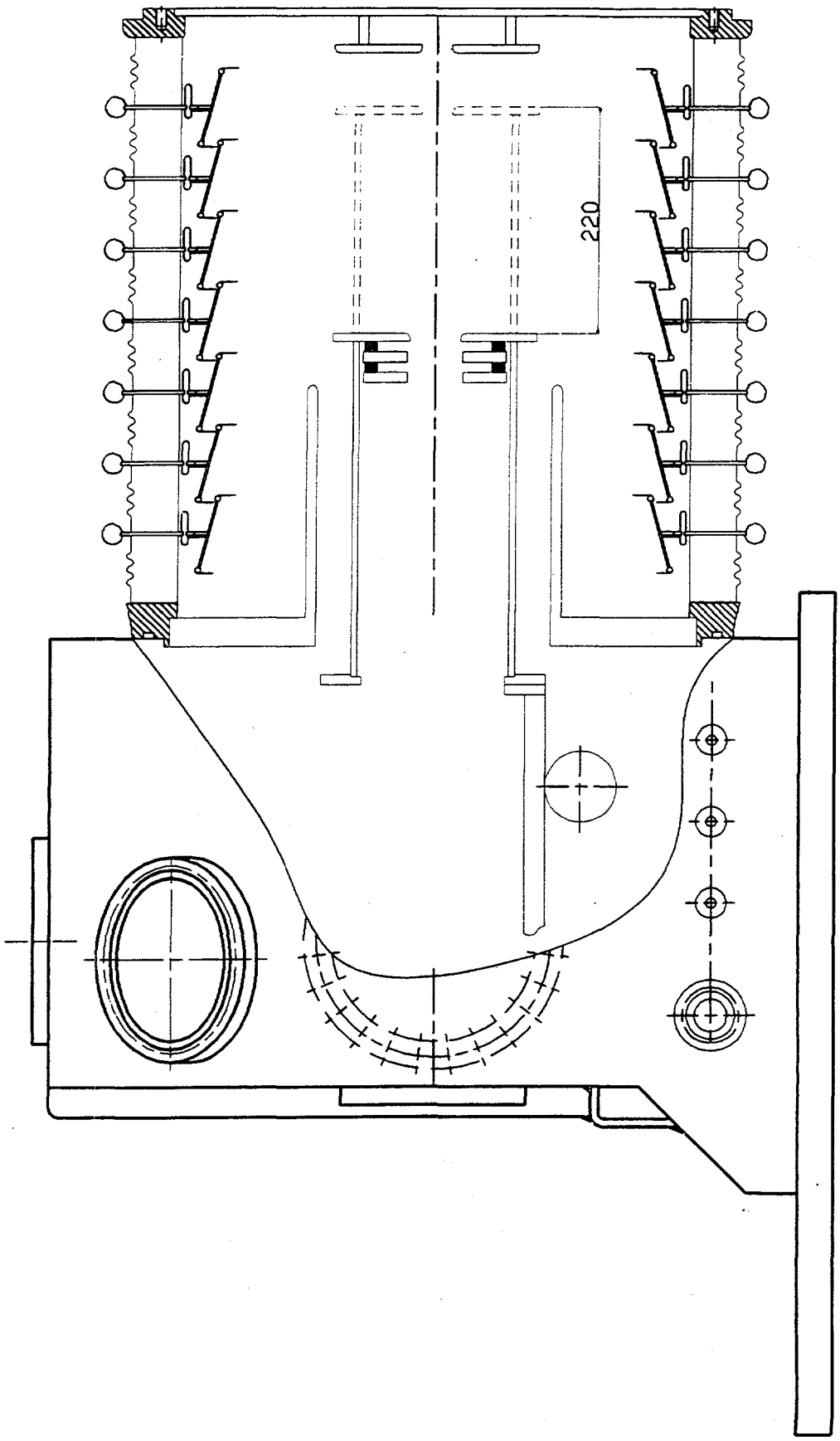
220

AXCEL-INP VERSION 3.42 potential and trajectory plot ITERATION 1

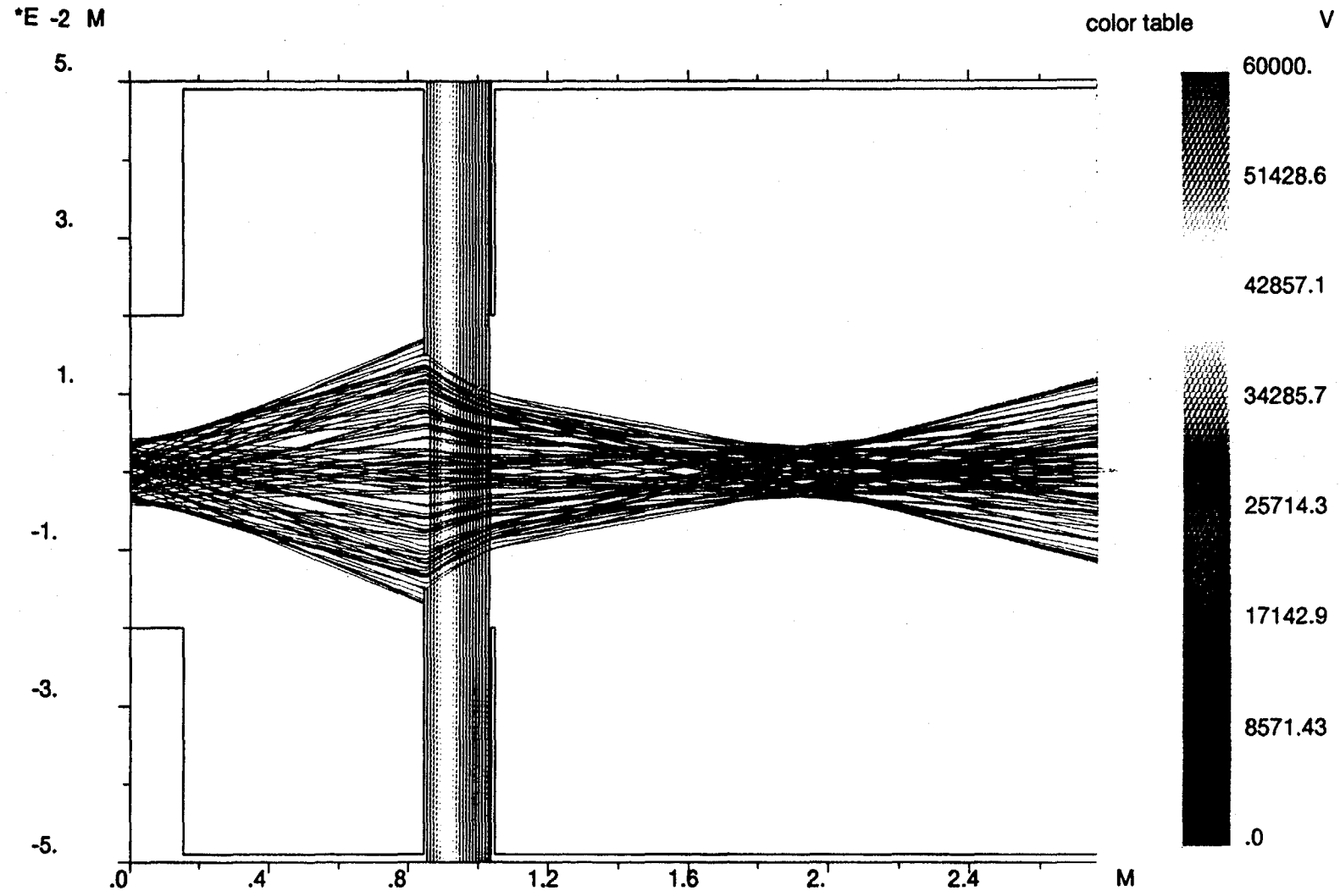

USER: INP Wiesbaden

COMMENT: Column 20+60kv Ar2+ DATE: 01/04/95 TIME: 21:06:02

AXCEL-INP VERSION 3.42 potential and trajectory plot ITERATION 7

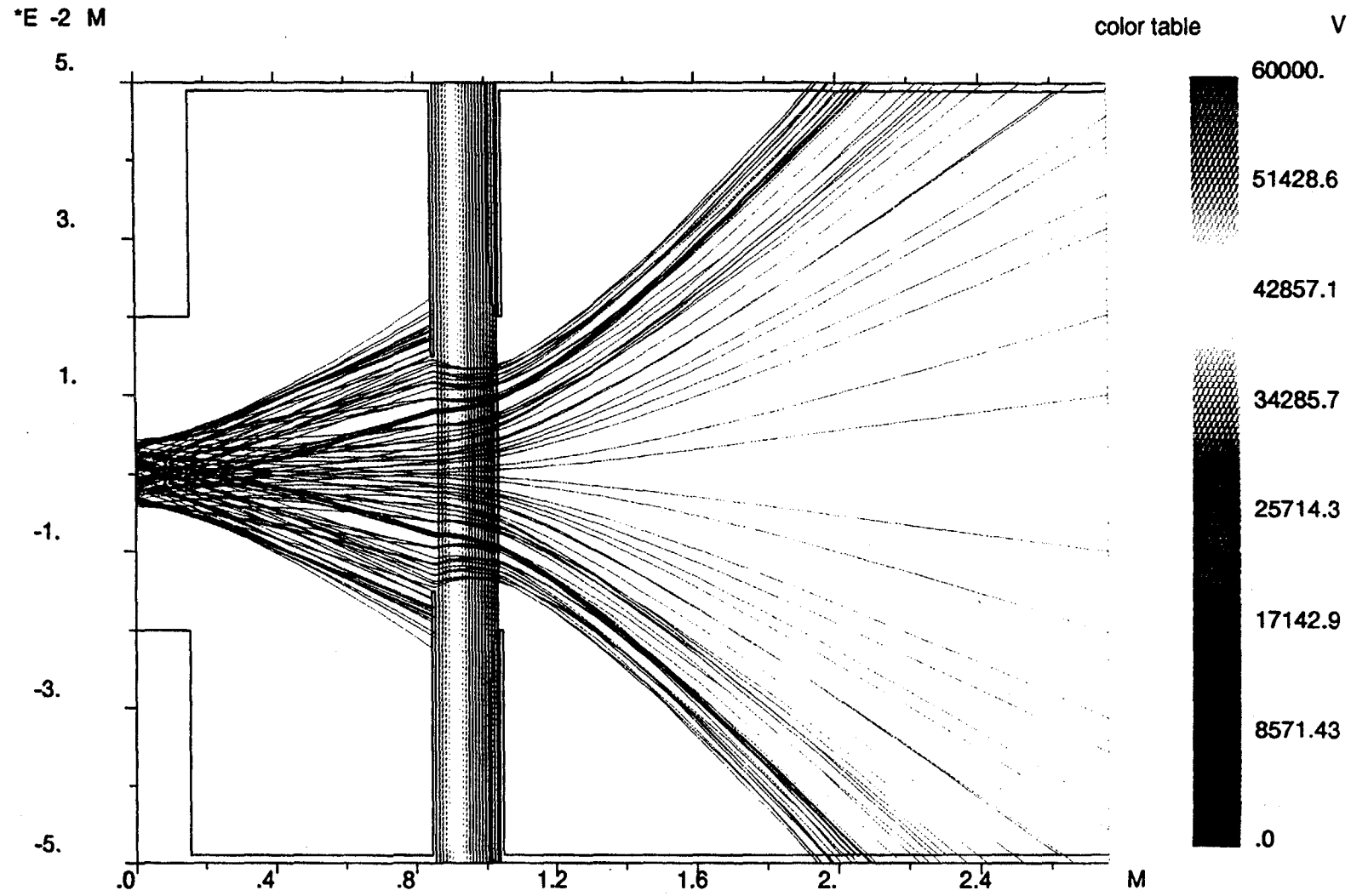

USER: INP Wiesbaden

COMMENT: Column +60kv Ar2+ DATE: 01/04/95 TIME: 21:34:28

AXCEL-INP VERSION 3.42 potential and trajectory plot ITERATION 1

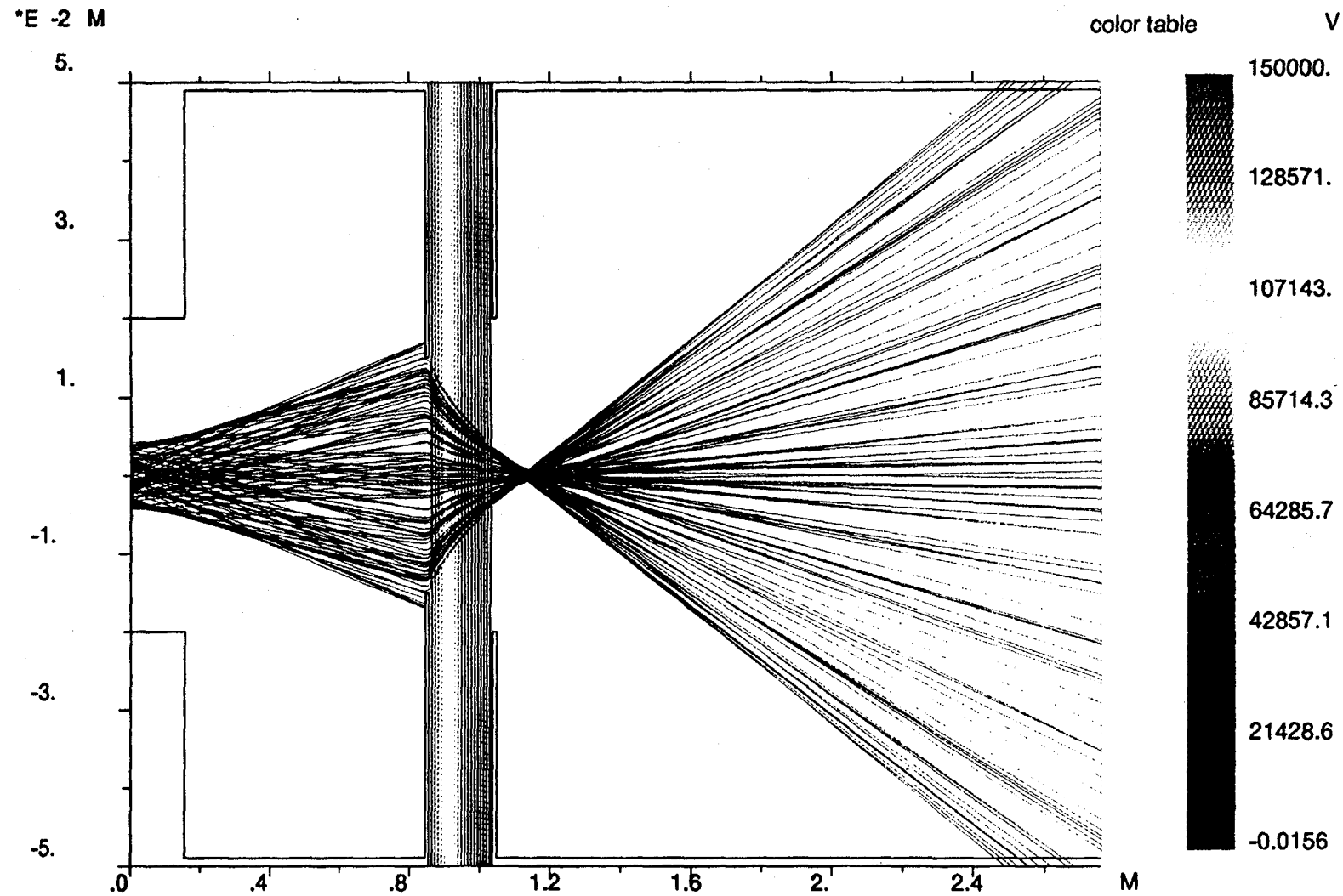

USER:

COMMENT: Column 20+150kv Ar2+ DATE: 01/04/95 TIME: 22:03:15

AXCEL-INP VERSION 3.42 potential and trajectory plot ITERATION 6

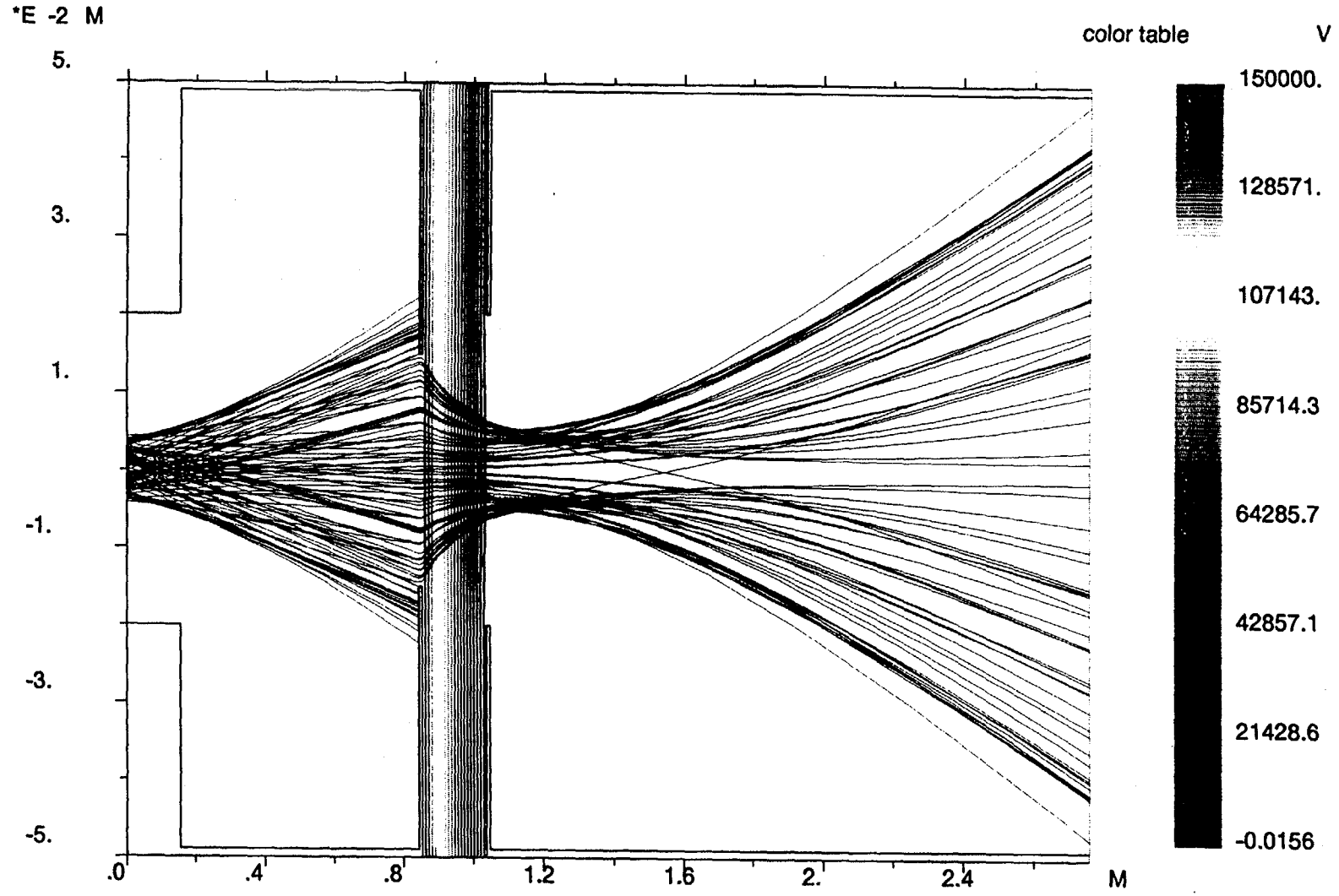

USER: INP Wiesbaden

COMMENT: Column 20+150kv Ar2+ DATE: 01/04/95 TIME: 22:21:53

AXCEL-INP VERSION 3.43 potential and trajectory plot ITERATION 6

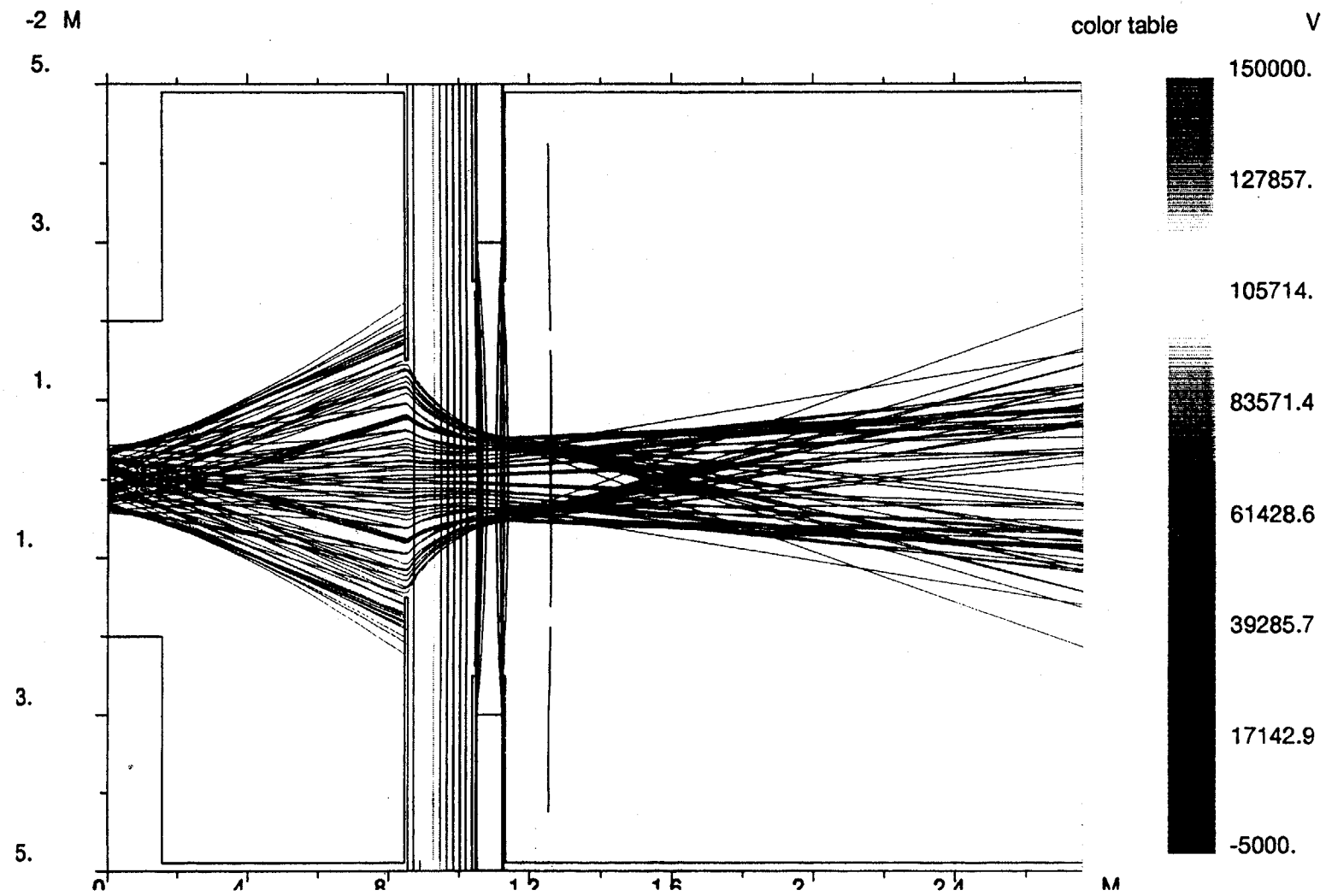

INP Wiesbaden (GERMANY)

COMMENT: Column 20+150kv Ar2+ DATE: 03/08/95 TIME: 22:48:58

AXCEL-INP VERSION 3.43 radial emittance ITERATION 6

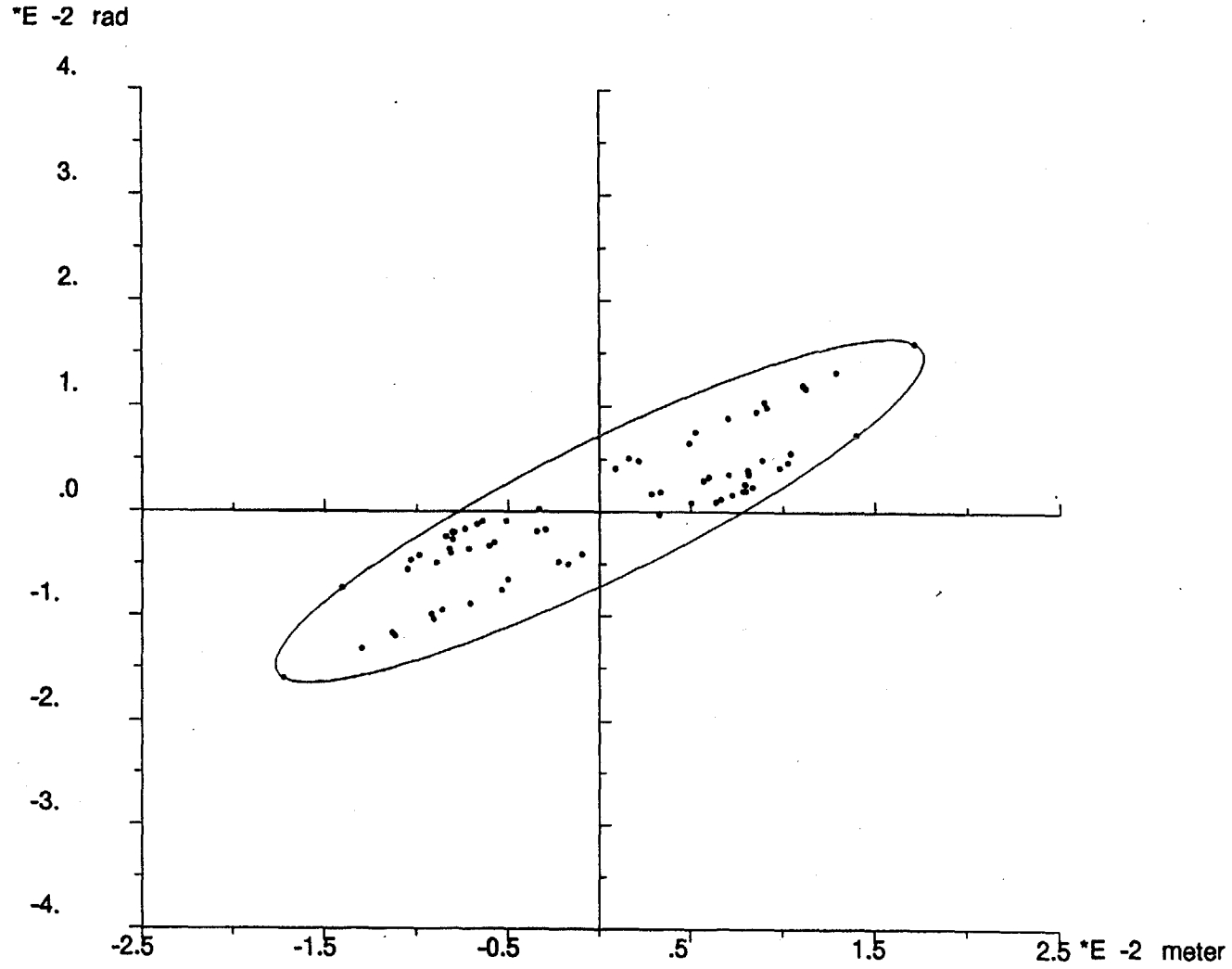

INP Wiesbaden (GERMANY)

COMMENT: Column 20+150kv Ar2+ DATE: 03/08/95 TIME: 22:51:30

U [KV]	gap [mm]	β	ε [mm mrad]	ε_n mm mrad	I [mA]
		Ar^+ Chordis Source			
30		$1.2 \cdot 10^{-3}$	100	0.12	
30+60	30	$2.2 \cdot 10^{-3}$	80	0.18	12
		Ne^+ Chordis Source			
30		$1.8 \cdot 10^{-3}$	100	0.18	
30+112	50	$3.9 \cdot 10^{-3}$	90	0.35	16
30+150	100	$4.4 \cdot 10^{-3}$	65	0.28	10
30+230	180	$5.3 \cdot 10^{-3}$	55	0.29	10
30+130	180	$4.1 \cdot 10^{-3}$	50	0.21	2
		Ni^{2+} Mevva Source			
30		$1.5 \cdot 10^{-3}$	100	0.15	
30+96	50	$3.0 \cdot 10^{-3}$	90	0.27	12
30+197	100	$4.1 \cdot 10^{-3}$	70	0.29	14
30+276	180	$4.7 \cdot 10^{-3}$	65	0.30	20
		Ar^{2+} PIG Source			
18+48	180	$2.7 \cdot 10^{-3}$	38/138	0.1/0.37	0.2

Report on ITEP Mevva Development

V.A.Batalin, Yr.N.Volkov, T.V.Kulevoy, S.V.Petrenko
and A.A.Kolomiets
Institute for Theoretical and Experimental Physics, Moscow, Russia

presented by B.H. Wolf, GSI

1. INTRODUCTION

The MEVVA ion source (version ITEP-90) designed and constructed at ITEP is used at the injector of the heavy ion RFQ linac (TIPr-1) which has been built as a driver prototype for heavy ion fusion program. The source operates in a pulse mode. Pulse length was from 5 to 140 μs, repetition rate is up to 1/2 Hz. The injection voltage is 50-70 kV. The modified version of the source with drift channel and electron gun has been named e-MEVVA. The first measurements of charge state distributions for e-MEVVA beam carried out by time-of-flight (TOF) method showed promising results. Copper ions with charge to mass ratio up to 1/3-1/5 has been detected.

The more detailed investigation of beams generated by MEVVA and e-MEVVA have been carried out in the framework of the agreement with GSI. It has been planned to measure the beam parameters at operation regimes those are close to GSI injectors ones. The main requirements of GSI specifications are:

- Charge to mass ratio.....1/8, 1/24, 1/60
- Pulse length .....> 400 μs
- Repetition rate.....>5 Hz

In the framework of this agreement the following works have been done:

- the new power supply units for MEVVA and e-MEVVA have been designed and manufactured;
- analyzing magnet have been installed between the injector and RFQ;
- the measurements of CSD for MEVVA and e-MEVVA ion source have been carried out by both time-of-flight method (TOF) and magnet mass-analyzer;

2. DIAGNOSTIC SYSTEM AND MEASUREMENT METHODS.

2.1. The layout of diagnostic system.

The heavy ion RFQ linac (TIPr-1) has been used as a test bench for experiments with the ion sources. Its diagnostic system allows to measure charge states distribution (CSD) using two methods:

- time of flight method (TOF) for short pulses with drift distance 14 meter;
- magnetic analyzer (MA) with electrostatic deflector (energy analyzer); later the new MA has been installed at the injector output directly.

The initial configuration of linac is shown in Fig. 1.(a).

The total current from the injector is measured by a Beam Transformer (BT) (4) and a Faraday Cup (FC) at the injector output. That FC is provided by permanent magnets which suppress secondary electrons. A FC (3) at the linac output is used for TOF and accelerated ion current measurements. These two FC can be removed from beam axes for beam passing. Ion current after MA is measured by FC (8) placed into Measurement Chamber.

There are electrostatic deflecting plates (bending angle is 45°, bending radius is 0.58 m and the gap width between them is 2 cm) into a chamber at the injector output. They transport the ion beam to MA (8). They can be removed from beam axes if whether TOF measurements or accelerating into the RFQ structure are carried out. Electrostatic lenses (5) are used for matching ion beam with RFQ structure. This deflector has been disassembled and the new magnet mass-analyzer has been installed at the injector output directly (Fig. 1.(b)). Magnet parameters will be described later.

2.2. Time-of-flight method and equipment.

The total length of linac (14 m) is used as a drift duct for TOF measurements. To form a short beam pulse (up to 5 μs) the special beam optic system has been used. The optic system is shown in Fig. 2.

The grid 3 placed between two extracting grids has a potential of +6 kV relatively to the anode of the ion source. It locks the ions extracted from the plasma boundary. And ions can pass through this grid while the short (duration of 5 μs) unlocking high voltage pulse of -7 kV is applied to it only.

A start position of the short pulse can be chosen at any time along the MEVVA arc current pulse duration. Changing this position with scanning step of 5 μs, the charge state distribution (CSD) for total beam pulse has been measured.

The obvious advantage of TOF method is that it allows to measure CSD corresponding to ion source output. Charge exchange processes can only change the ratio between amplitudes of measured separated pulses corresponding to different ion charge states. In addition, all charge states can be measured simultaneously for each pulse. Nevertheless the small acceptance of drift channel allows to measure CSD only for central part of beam. A very sensitive detector is needed because the total current measured at the linac output doesn't exceed 40 μA while TOF method is using.

2.3. Analyzing magnet equipment

2.3.1. Installation of new MA

In order to check results obtained by TOF method the CSD for uranium ion beam has been measured by the MA. The MA earlier installed at the experimental bench had bending radius 0.56 m and angle 45°, magnetic field is up to 0.8 T. It had a very small area with uniform field and as result very bad resolution and very small acceptance. Also the electrostatic deflector decreased the acceptance of this system. As a result only small part of the total ion beam could pass through the bending plates and the AM chamber and reached ion collector at the MA output.

A new magnetic mass-analyzer has been installed at TIPr-1 injector in order to improve measurements of the CSD for uranium ion beam generated by the ITEP MEVVA and the e-MEVVA. This magnet was a part of measuring line of ITEP proton linac ISTRA-36. Parameters of this magnet are given in Table 1

Table 1

bending angle	60°
bending radius	0.5 m
width of area with homogeneous field	48 mm
entrance aperture	20 x 48 mm
value of magnetic field range	0.006 - 0.8 T
current range	16 - 235 A
weight	1500 kg

Unfortunately, the original support for the magnet can't be installed at the TIPr-1 injector output. It is lower than it is necessary for new position of MA and moreover there is not enough place between injector and RFQ to set up that support. A new support for the magnet has been constructed.

The chamber with bending plates, the manifold with one of electrostatic lenses, the measuring chamber, old magnet and one of the flap valves have been dismounted. The support for this equipment has been taken away also. At the free place the new support has been mounted and the new magnet has been installed on it. Prior to the magnet mounting an alignment telescope has been adjusted to the linac axis. It has been used for the alignment of the magnet. The connection of magnet's flanges with both the injector output and the RFQ structure input has been made by an adapter of special design (without bellow). These adapters provide the vacuum connection of stationary flanges. A vacuum seal has been mounted between magnet and RFQ structure.

The measuring chamber has been mounted at the magnet output. Two motion seals have been installed at this chamber. The first one, nearest to magnet output, has a plate with a vertical slit with width of 5 mm and is placed at the magnet focal point. The second one has the same plate and current collector behind the slit. It is possible to measure beam current fallen at each plates and collector separately. The distance between plates is 285 mm. The plate with the slit with width of 5 mm has been installed at the magnet input to increase the mass-spectrometer resolution.

The magnet replacing results the increasing of cables length from magnet to its power supply. The resistance of these cables is comparable with the resistance of MA winding. So it has been necessary to upgrade the power supply to provide the needed magnetizing current. This upgrading has been done in framework of this work. Unfortunately the power supply provides the stable magnetizing current into two limited range (from 16 A to 170 A and from 20 A to 250 A). It is not possible to measure ion beam CSD from H^+ to U^+ without a range switching. But the ranges have a wide common part. It takes 20 minutes to change one range to another while power supply is switched off. The scanning step for magnetizing current at down range (0.2 A) is smaller than at upper range (0.5 A). It is very suitable for CSD measurements. To provide magnet cooling, the magnet has been connected to the linac cooling system.

2.3.2. *Method of measurements*

The total current from both plates and collector has been measured during CSD measurements for ITEP MEVVA. Moreover the slit at the MA input has been removed during this measurements. It is possible because magnet resolution is high enough to separate uranium ions with charge states generated by the conventional MEVVA. So it is possible to measure the absolute current for each charge state. It should be mentioned nevertheless that not more than 10% of beam current could pass through magnet due to its relatively small acceptance. As it was said above it has been necessary to switch the ranges of magnetizing current during measurements. To decrease the possible errors, the measurements for several points from common part of two ranges have been done. It has been found that the results obtained for these points after the switching coincide with ones obtained before this switching.

The current fallen at the collector has been measured during e-MEVVA CSD measurements. To increase the accuracy for CSD measurements by magnet analyzer, the following method has been used. For each given magnet analyzer current, I_{ma}, the total ion current at the analyzer input has been measured by current transformer. It allows to normalize value of measured collector current to total beam current and decrease the influence of beam instability. Every point of spectra is the mean value of 3-4 measurements. The measurements have been carried out for every point both for e-beam operation regime and for without e-beam operation regime. One spectrum includes about 500 points. It has to be mentioned that these measurements require a lot of time. One full cycle of measurement took usually 6 - 8 hours and more.

2.4. Acceleration in 6 MHz RFQ.

Acceleration of U^{4+} ion beam into the TIPr--1 linac is a most direct method to check quality and quantity of ion beam generated. It is known that RFQ structure is a focusing channel for some of unaccelerated particles. So if beam pulse length is long enough the FC at the linac output will measure the sum current of accelerated and non accelerated ions. Two methods for real accelerated ion beam current measurements have been used. First of them is the short ion beam (as for TOF measurements) acceleration. In such way the U^{4+} ions' peak appears for 15μs earlier than without acceleration while other peaks stay at their old position

Also it is possible to measure the accelerated current when long ion beam is accelerated. The frequency of the RF field for TIPr-1 is 6.2 MHz. So accelerated current have a RF structure that can be seen on the oscilloscope. Non accelerated current have not such RF structure and on oscillograms they are as a non modulated pedestal.

3. ION SOURCES LAYOUT

3.1. MEVVA ion source

ITEP MEVVA has been described in details previously[1]. A scheme of MEVVA ion source is shown in Fig. 3. An arc current modulator with current up to 150 A, pulse length up to 140 μs and repetition rate up to 1/2 Hz had been used as power supply for main arc. This power supply has been upgraded and now provides the pulse length up to 500 μs and repetition rate up to 5 Hz. A trigger pulse has length of 15 μs and 15 kV amplitude. A MEVVA extraction opening has a 10 mm diameter. A repetition rate of 1/4 Hz and the arc current about 60 A has been used during the experiment. To increase the U^{4+} component of uranium beam from ITEP MEVVA, the additional independent pulse power supply has been connected to trigger electrode (Fig. 4).

The length of voltage pulse from the additional power supply is 50 μs and voltage magnitude is 2.5 kV. This power supply can be switched on at any chosen time. It has been found that while this power supply is working the U^{4+} component into uranium beam increases.

3.2. E-MEVVA ion source

The modified version of source [2] with drift channel and electron gun has been named e-MEVVA. In this modification the arc plasma passes through the drift channel (0.7 m), which has the axial magnetic field (0.02 T). The external electron beam with the energy of a few keV and pulse length about 50 μs from the independent electron gun is injected into the drift channel along the axis in the direction of plasma motion. As a result plasma ions are interacting with high energy electrons beam during the whole plasma drift time. A scheme of e-MEVVA ion source is shown in Fig. 5

The standard operation regime which has been used during measurements and parameters of the electron beam pulse are given in **Table 2**

It should be noted that the value of t_{eb} and I_{eb} are coupled, therefore instability of I_{eb} leads to instability of t_{eb}. The instability of e-beam current reaches 10 - 20 % for newly made cathode and rises to about 50% after a few hours of continuos operation. It is resulted by the e-gun cathode heating and deterioration of the vacuum condition during a long operation time.

Table 2

Electron gun			
Generator of e-gun	duration	Δt_{ge}	50μs
	voltage	U_{ge}	2 kV
E-gun high voltage	voltage	U_{eb}	2-10 kV
Electron beam	duration	Δt_{eb}	20-100 μs
	current	I_{eb}	10 - 100 A
MEVVA			
Trigger pulse generator	duration	Δt_{tr}	15 μ s
	voltage		15 kV
Arc discharge power supply	duration	Δt_{arc}	0,4 ms
	current	I_{arc}	up to 100 A
rate of pulses repetition		t_{rep}	0,25 Hz
Drift channel			
Potential	voltage	U_{ch}	250 V
Solenoid	current	I_s	1 A
	field	B_s	0.02-0.03 T

The voltage from the storage capacitor (U_{eb}) applies to the gap accelerating the electron beam (e-beam). U_{eb} can drop to zero, when the e-beam current is too high. The energy of the e-beam changes from maximum value to almost zero during the e-beam pulse.

4. THE INVESTIGATION OF ION BEAMS GENERATED BY MEVVA AND E-MEVVA ION SOURCES.

4.1. MEVVA ion source.

The main aim of the MEVVA ion source investigation was the increasing of the U^{4+} ions component of the generated ion beam. To achieve this aim the additional independent power supply has been connected to trigger electrode. The CSD of generated ion beam has been measured by using both the TOF method and MA. In Fig. 6. the typical CSD measured by TOF method is shown. One can see that without additional power supply (picture A) practically only uranium ions with charge +2 and +3 are present. U^{4+} ions component does not exceed a few percents. In picture B it can be seen that with additional power supply U^{4+} component increases up to ≈30%. It has been found in our measurements that this component can reach 40% of total beam current.

CSD has been measured by magnet mass-analyzer also. One broad plate without any slits has been used as the current collector. The resolution for uranium components of the ion beam generated by conventional MEVVA has been high enough. The accelerating voltage has been 35 kV that results the total beam current has been 5-8 mA. Results of those measurements are shown in Fig. 7. The current is given in absolute magnitudes. The spectra in Fig. 7 are in good agreement with TOF results. Only one difference is the presence of the charge exchange peak of (3+ to 2+).

Fig. 7.(A). corresponds to the time moment when the voltage pulse from the additional power supply pulse is applied to electrodes. As it was mentioned above the length of

additional voltage pulse was 50 μs. The power supply unit with longer pulse length is now under preparation.

Some difference in results obtained by two methods can be explained by the fact that the current pulse for any charge state indicated at the MA output has not rectangular form and the maximum value of that current pulse has been measured. So the CSD composed from maximum value for every charge state measured by TOF method should be compared with the MA CSD.

The changing of CSD during the ion beam pulse has been investigated by TOF method. The results are shown in Fig. 8.

The amplitude of currents is shown in arbitrary units, as percentage to total current. As it was expected the CSD isn't changed during almost all beam pulse. Only at the end of pulse U^+ and U^{2+} components increase while other decrease. It should be noted that a form of the current pulse measured by MA for each charge state is the same as one obtained from TOF measurements for total beam length

The U^{4+} ions have been accelerated into the TIPr-1. The accelerated current up to 4 mA has bean measured. When the new power supply has been used the accelerated ion current increased up to 15 mA.

4.2. E-MEVVA ion source

First of all the CSD for e-MEVVA operation without e-beam has been measured (Fig. 10). It is easy to identify the peaks of H^+, H^{2+}, U^{3+} and U^{2+}. The group of peaks from area with specific masses from 11 to 19 (below this area will be named as area "A") consist of residual gas ions (C^+, O^+, H_2O^+ ...). The group of peaks from area with specific masses from 23 to 32 (below this area will be named as area "B") consist of "dirt" ions which we can't identify. The peak of U^{4+} ions is present in CSD but has a very small amplitude. The measured peaks have some width. This width increases for higher specific mass. This effect can be observed in Fig. 10. The H^+ peak is the most narrow and the U^{2+} peak is the most wide. It is very important to note that almost all peaks have not a smooth shape. To identify real peaks placed near each other, it is necessary to take into account not only the position of peaks but also the width of peaks which depends on specific mass of ions. Certainly the U^+ ions are present in beam but they couldn't be detected during these measurements (the magnetic field is not high enough to bend U^+ ions when accelerated voltage at the injector is 50 kV).

It is interesting to compare CSD in Fig. 10 with CSD measured for ITEP MEVVA (see Fig. 7). The main component of CSD for ion beam generated by e-MEVVA without e-beam is U^{2+} ions. It is a result of the fact that the plasma drifts through the channel with axial magnetic field for a long time and there are not electrons with high energy into the plasma. So the recombination process predominate during the plasma drift time.

The shape of the measured ion current pulse at the injector output for e-MEVVA has a valley with duration about 50 μs when the operation regime with e-beam is used. This valley appears at the moment when e-beam is switched on. The measured ion current along this valley is close to zero. Then the ion current appears again and first ≈50 μs of the restored ion beam pulse are a most interesting place for our investigation.

The CSD has been measured for four different time moments during the ion beam pulse. First one corresponds to the beginning of beam pulse which consists of the ions generated by trigger pulse. Second one corresponds to the time between the trigger and e-beam pulse. Next one corresponds to the time of 50 μs after the e-beam switching-on (below we will name the data obtained at this point as a data for e-beam). And last one corresponds to the end of the ion beam pulse. Results are shown in Fig. 11 and Fig. 12.

Let us to compare these CSDs with the one measured for e-MEVVA ion beam without e-beam operation.

First of all we can note that beam CSDs measured before (Fig. 11b) and after e-beam (Fig. 12b) look like the CSD measured without e-beam operation (Fig. 10). The presence of peaks with specific masses 6, 40 and 100 in CSD corresponded to the "after e-beam" moment can be explained by measured method. It is more suitable to give this explanation after discussion of CSD for "e-beam".

The CSD measured during the trigger pulse (Fig. 11a) contains an appreciable parts of U^{3+} and U^{4+} ions. It is possible to assume that there are U^{5+} ions also in the beam during the trigger pulse. It can be explained by the known fact that the electron energy into trigger arc plasma is higher than into the main arc. It should be mentioned that C^{2+} peak appears in CSD.

The CSD measured for points of ion beam corresponded to the e-beam operation (Fig. 12a) differs from CSDs measured both for all other points and for without e-beam operation regime.

The main differences are:

- amplitudes of low charge state uranium peaks decreased,
- amplitudes of peaks from areas "A" and "B" increased,
- the groups of new peaks appear,

Peaks with specific masses of 6 and 8 correspond to C^{2+} and O^{2+} ions. The most interesting peaks appear in areas of specific masses from 38 to 43 (below this area will be named as area "C"), 48 to 57 (below this area will be named as area "D") and from 63 to 70 (below this area will be named as area "E"). The groups D and E can't be explained as wide U^{4+} ion peak. As it was discussed above the width of U^{4+} ion peak can't be so large. The same reason give possibility to conclude that these peaks are not iron and copper peaks. They can't be any pure uranium ions too, but they can be the peaks of charge exchanged uranium ions. The pressure into both the ion source and the MA channel has been about 1-3 x 10^{-6} Torr, so the recombination processes during the time of beam passing through the measuring channel are strong enough. If this assumption is correct the peaks of ions which did not loose charges by recombination have to be to the left from these groups. Areas "A" and "B" are the only place where these ions can exist. One can see that amplitudes of peaks from these areas increased in comparison with regime without e-beam. It can be resulted by increasing of the residual gas ionization. But if one assumes that there are the uranium ions (charge states from 7 to 21), their current is added to "dirt's" ions current and provides the same increasing of peaks from these areas. Moreover the lower specific mass the more increasing of peak amplitudes. The current of U^{21+}, U^{20+} and U^{19+} ions have to be added to current of C^+ ions while current of U^{13+} ions can only be added to current of H_2O^+ ions.

It is clear that the area "B" can include the charge exchanged uranium ions also. In this case there are uranium charge states from 13 to 21 into ion beam. The areas "D" and "E" can contain the peaks corresponding to the recombination of listed above uranium ions up to charge states 7-9. These peaks have highest amplitudes between all recombined uranium ions. The area "C" can consist of charge exchange ions too (for mentioned above high charged uranium ions, the final charge states are 9-11). The presented in Fig. 12 A spectrum is very typical for numerous measured results. The mentioned above groups of peaks always exist. We have to say that some charge exchanged peaks which should be present in spectra never were detected in our measurements. We can't explain this phenomena now. Peaks with specific masses 97 and 100 can also be recombination peaks of U^{20+} and U^{21+} to the 7+ charge state.

Now it is just in time to explain the appearance of peak with specific mass of 6, 40 and 100 into CSD for "after e-beam" moment. We noted above that the pulse length of e-beam is unstable and can reach 80 μs. Sometimes the e-beam length has been long enough and the ion charge states generated for this moment could be measured as the ones corresponded to the "after e-beam" moment.

The results discussed above have been obtained while the e-beam accelerating voltage has been 6 kV and total beam current at the injector output has been at least 10 mA. The same measurements have been done for e-beam accelerating voltage of 5.5 and 7 kV. Results are given in Fig. 13. The measurements have been done up to mass of 60.

The same measurements has been done when the additional slit has been installed at the MA input. Results for e-MEVVA operation without and with e-beam are shown in Fig. 14. The CSD for e-beam operation corresponds to moment of "e-beam". The e-beam accelerating voltage has been 7 kV. One can see that results are the same as it has been discussed above.

The TOF method for CSD measurements of ion beam generated by e-MEVVA ion source has been used also. Moreover this method was the first that we used for investigation of the high charged ion beam production. As it was said above this method permits to measure CSD of ion beam corresponding to the injector output and recombination processes don't influence on the result.. Typical CSDs measured by TOF method for e-MEVVA ion beams are shown in Fig. 15. One can see that the peaks corresponded to U^+, U^{2+} and U^{3+} are present in the CSD for ion beam when the "without e-beam" operation regime is used. H^+ ions are present in CSD also. The small peak near the H^+ correspond to the specific mass group which was named as "group A" during the MA measurements. The main distinguish of this TOF CSD from the MA one is the presence of the U^+ peak. As it was mentioned above it is explained by the fact that the U^+ ions couldn't be detected during MA measurements.

The CSD measured for e-MEVVA during the e-beam operation contains peaks of U^+, U^{2+} ions with very small magnitudes. But the new peaks appear in the CSD. We marked them as I, II and III. They can correspond to the high charged uranium ions. We made this conclusion after the testing of the main MEVVA discharge regime. We didn't see the any valley in the arc current pulse. We think that uranium ions have to present into ion beam. The only place in CSD where they can be present is the new peaks.

Specific masses and possible ion charge states corresponded to these new peaks are given in Table 3. To determine their specific masses, the peaks of U^+ and U^{2+} (those are present in both CSD) have been used for calibration. It is important to note that they don't change their time position, so one conclude that the accelerating voltage doesn't change when e-beam is switched on.

Table 3

Peak mark	Specific mass	Charge states
I	2 -3	H_2^+, H_3^+,C^{4+}
II	8-9	U^{28+} -U^{26+}, O^{2+}
III	13-15	U^{18+} -U^{16+}, N^+, CH^+,CH_2^+

The peak III corresponds to the specific masses from the "group A" (MA measurements). Unfortunately the resolution of TOF method is not high enough. Using results of TOF method, we can only estimate the generated uranium charge states. But it is impossible to distinguish uranium ions from "dirt's" ones. It is interesting to note that TOF CSD for e-beam operation doesn't contain peaks of ions with mass 48-57 and 63-70. This fact speaks for our assumption that corresponding peaks in MA CSD are peaks of the uranium ions which lost some charges by recombination.

5. CONCLUSION

The measurements of CSD for ion beams generated by ITEP MEVVA and e-MEVVA ion sources have been done in framework of agreement with GSI. The measurements have been done by TOF method and with magnetic MA. The new MA has been installed at the TIPr-1 linac injector to provide these measurements. The power supply for MEVVA ion source has been upgraded to approach its operation regime to GSI injectors operation regime.

It has been found that it is possible to increase the U^{4+} component into ion beam generated by MEVVA ion source. It can reach up to 40% of the ion beam.

Results obtained for e-MEVVA ion source allow to suppose that this ion source can generate high charged uranium ion beams with charge states from U^{13+} to U^{21+}. Phase density of U^{21+} current estimated at MA output is ≈3 mA/cm.mrad. The total current at MA input with e-beam operation was at least 10 mA.

Analysis of described work results showed that for further investigations of e-MEVVA it is nesessary to do the following:

- to improve the vacuum conditions both in ion source and in measuring channel;
- to provide cooling of e-gun cathod;
- to upgrade beam diagnostic system.

Up to present time the e-gun with cathode cooling has been designed and now is under preparation. The drawings of the new version of e-MEVVA were prepared. This new version provides the possibility to connect vacuum pump directly to the source.

The test cycle of the e-MEVVA operation at the MA magnet showed that it is necessary to continue both the investigations of e-MEVVA beam parameters and development ion source itself.

6. REFERENCES

[1] V.A.Batalin, Yr.N. Volkov, T.V.Kulevoy, S.V.Petrenko, Preprint ITEP, 1991-37;

[2]V.A.Batalin, Yr.N. Volkov, T.V.Kulevoy, S.V.Petrenko, Preprint ITEP 33 - 94 Moscow 1994; Proceeding of the 1994 International Linac Conference, Tsukuba,Japan. p. 390 - 392.

7. FIGURES

Fig. 1. Layout of heavy ion injector. a) Old configuration b) Upgraded configuration 1- Ion source, 2- Beam transformer, 3- Deflector, 4- Analyzer magnet, 5- Measuring chamber at the MA output, 6- Faraday cup at the linac input, 7- Electrostatic lens, 8- Cavity of TIPr-1, 9- Faraday cup at the linac output.

Fig. 2. TOF optic. 1- Ion source expander, 2- extractor grids, 3- lock grid, 4-"focusing" electrode, 5- accelerating electrode.

Fig. 3 . Scheme of ITEP MEVVA ion source. 1- cooling channel, 2- bellow, 3- cathode, 4- insulator, 5- trigger, 6- anode.

Fig. 4 Schemes of power supply for ITEP MEVVA a) Usual power supply, b) Power supply with additional independent modulator.

Fig. 5. Scheme of the e-MEVVA ion source. 1- e-gun, 2- diaphragm, 3-MEVVA cathode flange, 4- coil for e-beam, 5-, 6- MEVVA trigger , 7- MEVVA anode, 8- drift channel, 9- coil, 10- expander, 11- extractor grid.

Fig. 6. Photo of TOF oscillograms. a) without, b) with additional power supply. Scanning step 10 μs.

Fig. 7. Magnet CSD for MEVVA. a) with and b) without additional power supply.

Fig. 8. TOF CSD during the beam pulse for MEVVA operation without additional power supply for U^{+}, U^{2+} and U^{3+} components.

Fig. 9 TOF CSD during the beam pulse a) for MEVVA operation without additional power supply for U^{4+} and U^{5+} components, and b) for MEVVA operation with additional power supply for U^{4+} component.

Fig. 10. MA CSD for e-MEVVA operation without e-beam

Fig. 11 MA CSD for e-MEVVA operation with e-beam. At a) trigger, b) before e-beam.

Fig. 12 MA CSD for e-MEVVA operation with e-beam. At a) for e-beam, b) after e-beam time points.

Fig. 13. MA CSD for e-MEVVA operation with e-beam. E-beam accelerating voltage 5.5, 6 and 7 kV.

Fig. 14 MA CSD for e-MEVVA operation a)without and b) with e-beam. E-beam accelerating voltage 7 kV.

Fig. 15. TOF CSD for e-MEVVA operation regime without (upper one) and with e-beam (down one).

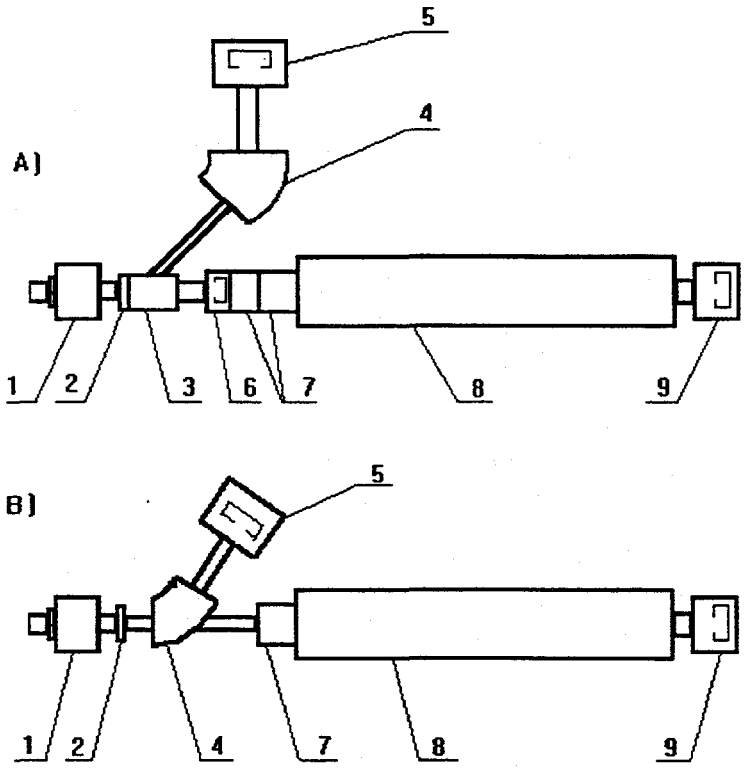

Fig. 1.Layout of heavy ion injector. A) Old configuration , B) Upgraded configuration: 1- Ion source, 2- Beam transformer, 3- Deflector, 4- Analyzer magnet, 5- Measuring chamber at the MA output, 6- Faraday cup at the linac input, 7- Electrostatic lens, 8- Cavity of TIPr-1, 9- Faraday cup at the linac output.

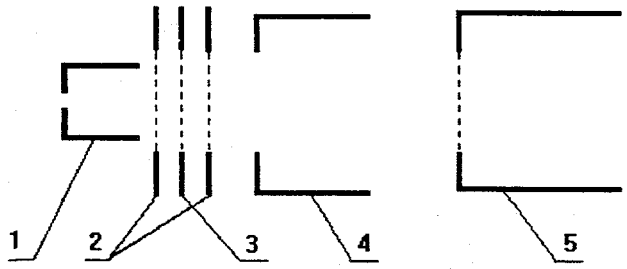

Fig.2. TOF optic. 1- Ion source expander, 2- extractor grids, 3- lock grid, 4-"focusing" electrode, 5- accelerating electrode.

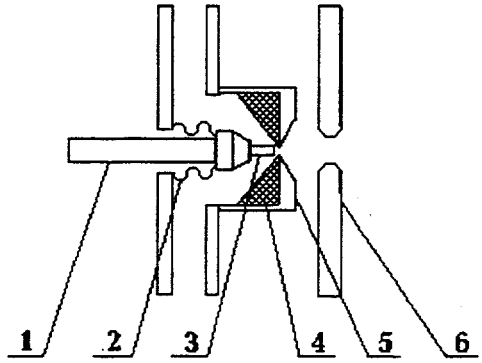

Fig 3. Scheme of ITEP MEVVA ion source: 1- cooling channel, 2- bellow, 3- cathode, 4- insulator, 5- trigger, 6- anode.

a)

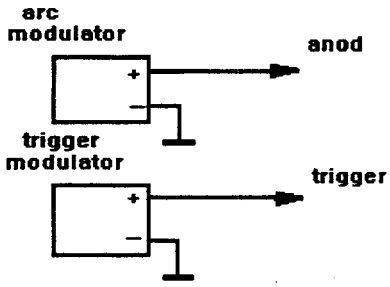

b)

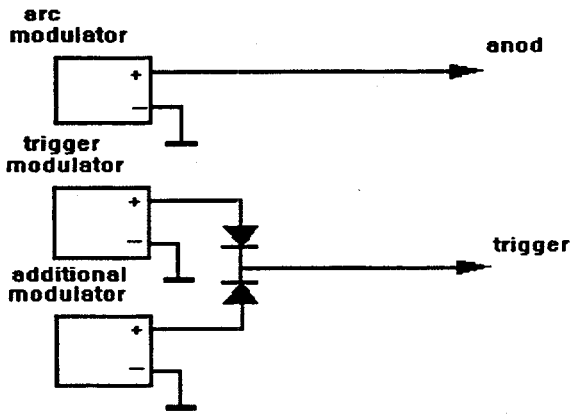

Fig.4. Schemes of power supply for ITEP MEVVA:
a) Usual power supply,
b) Power supply with additional independent modulator.

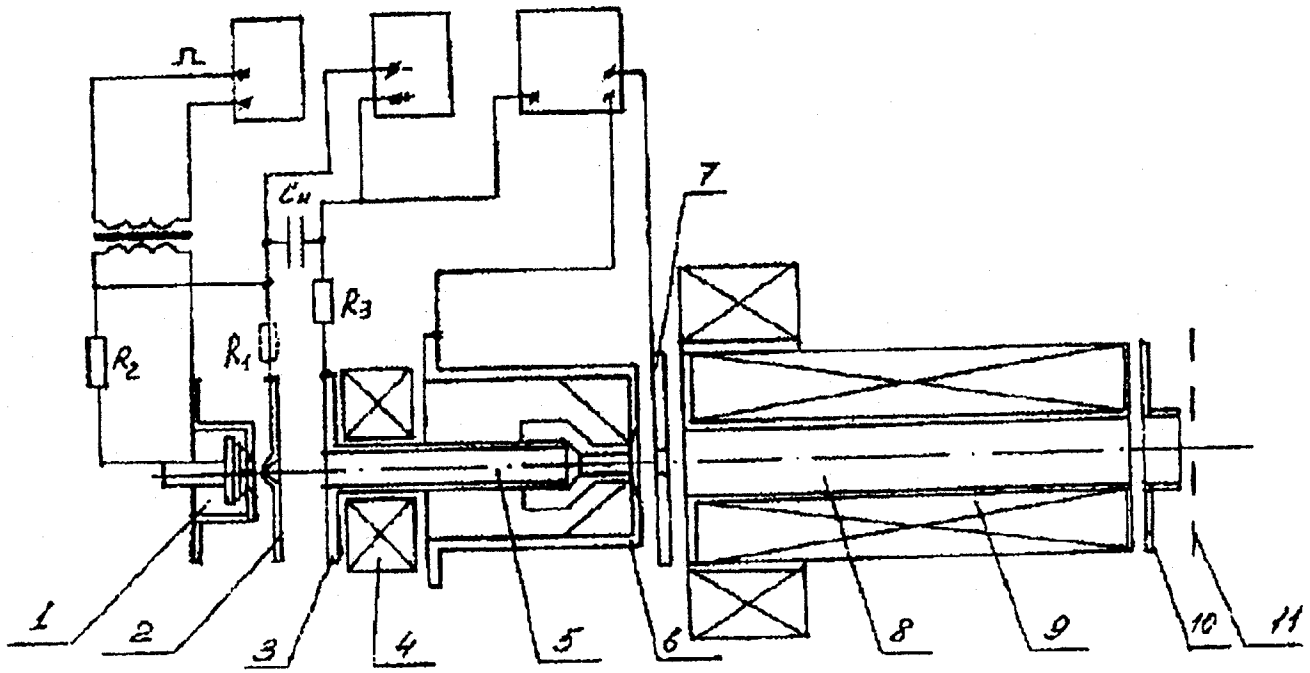

Fig 5. Scheme of the e−MEVVA ion source: 1− e−gun, 2− diaphragm, 3−MEVVA cathod flange, 4− coil for e−beam, 5−cathode support, 6− MEVVA trigger , 7− MEVVA anod, 8− drift channel, 9− coil, 10− expander, 11− extructer grid.

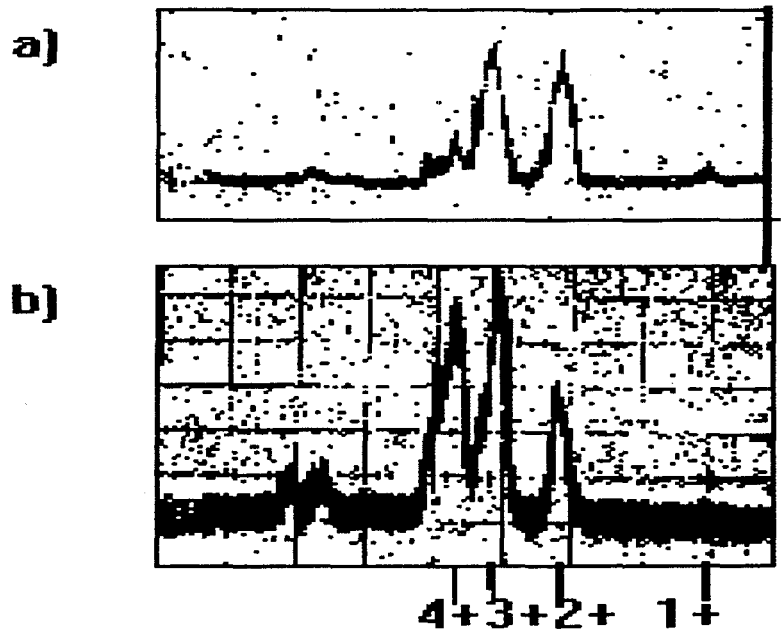

Fig.6. Photo of TOF oscillograms. a) without, b) with additional power supply. Scanning step 10 μs.

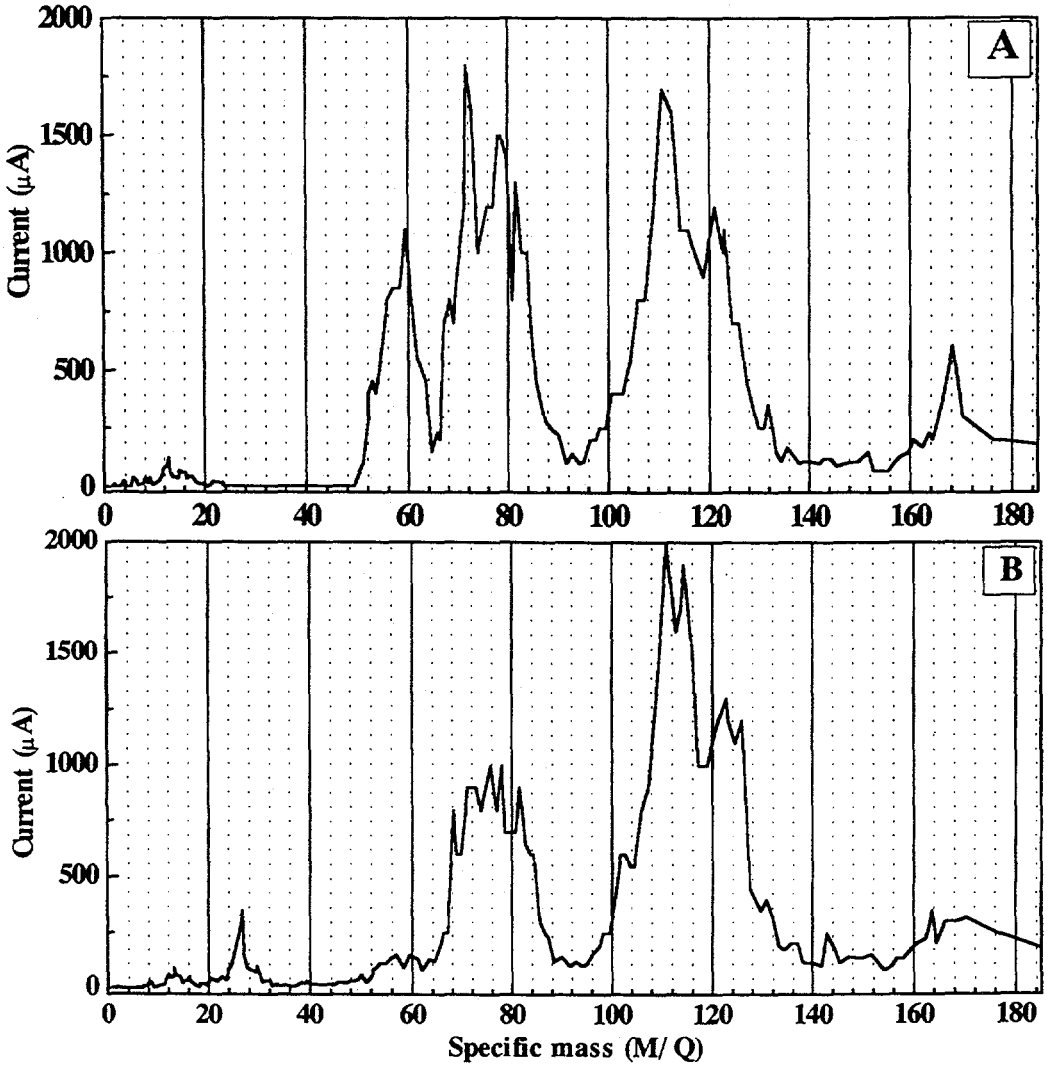

Fig.7. Magnet CSD for MEVVA: a) with and b) without additional power supply.

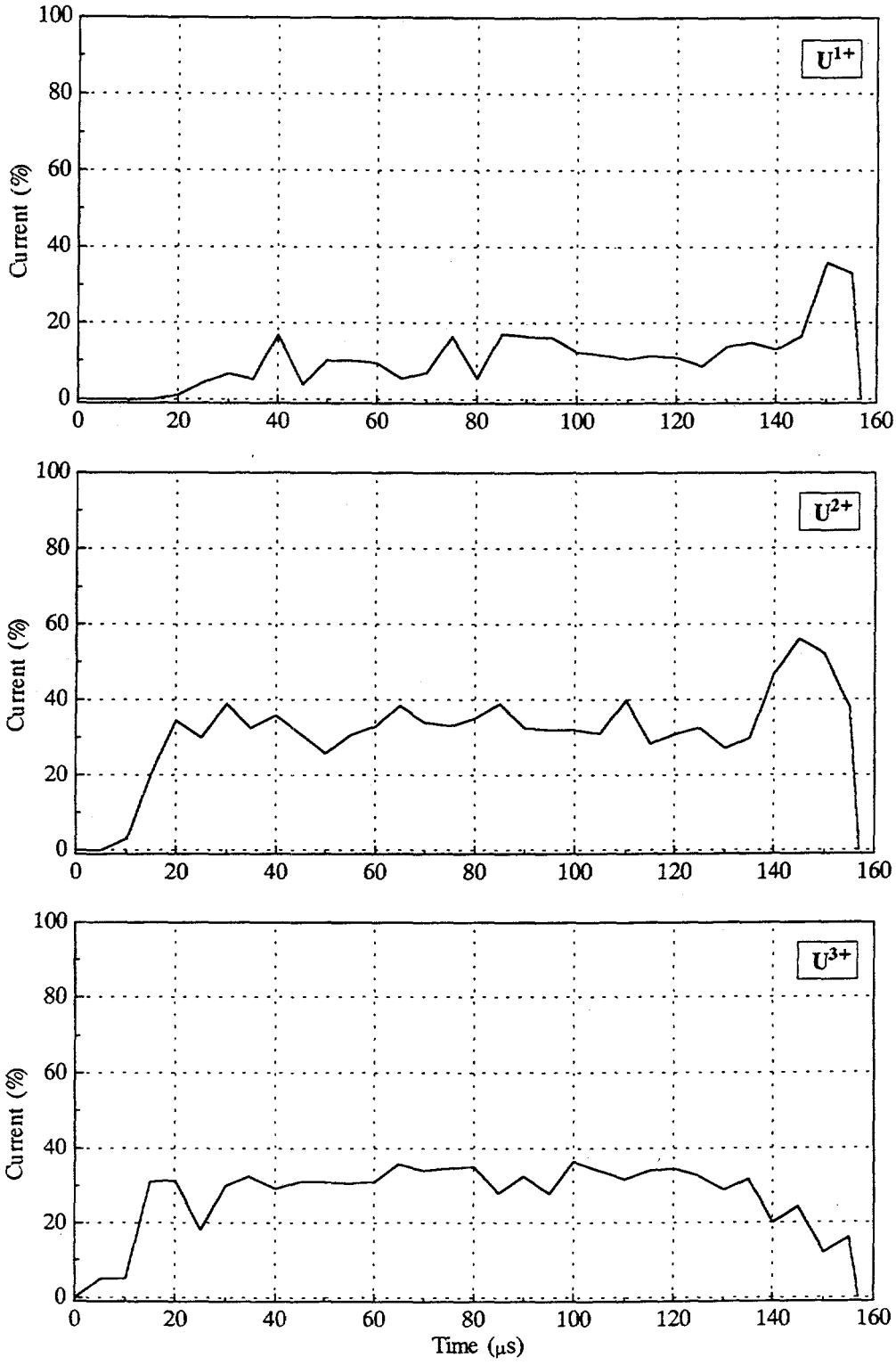

Fig.8. TOF CSD during the beam pulse for MEVVA operation without additional power supply for U^{+}, U^{2+} and U^{3+} components.

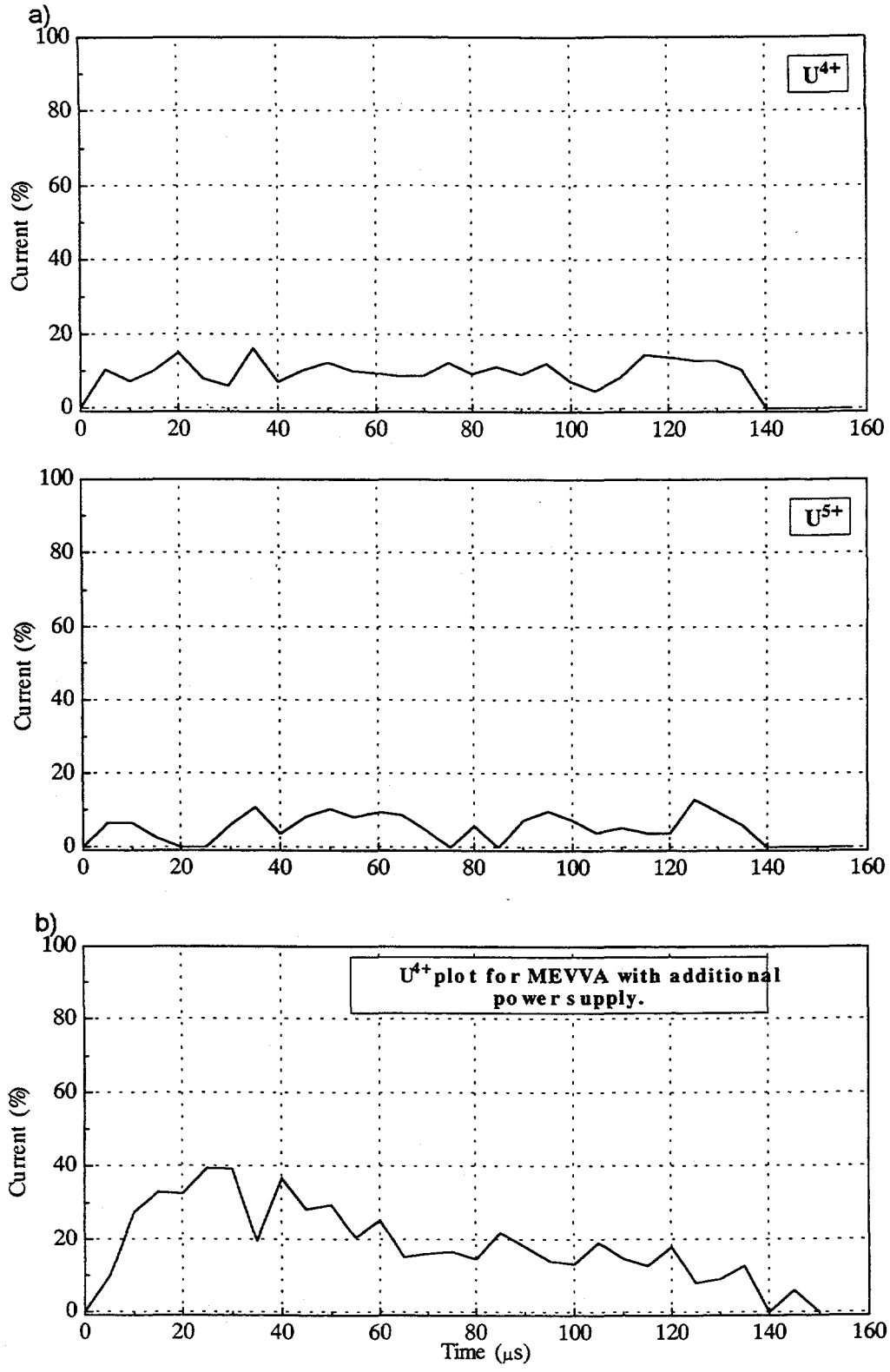

Fig.9. TOF CSD during the beam pulse a) for MEVVA operation without additional power supply for U^{4+} and U^{5+} components, and b) for MEVVA operation with additional power supply for U^{4+} component.

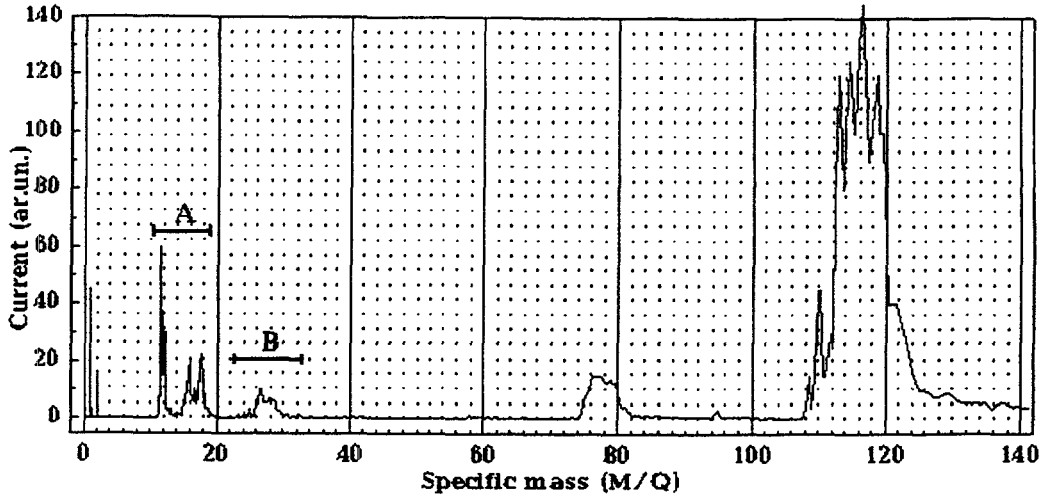

Fig10. MA CSD for e-MEVVA operation without e-beam

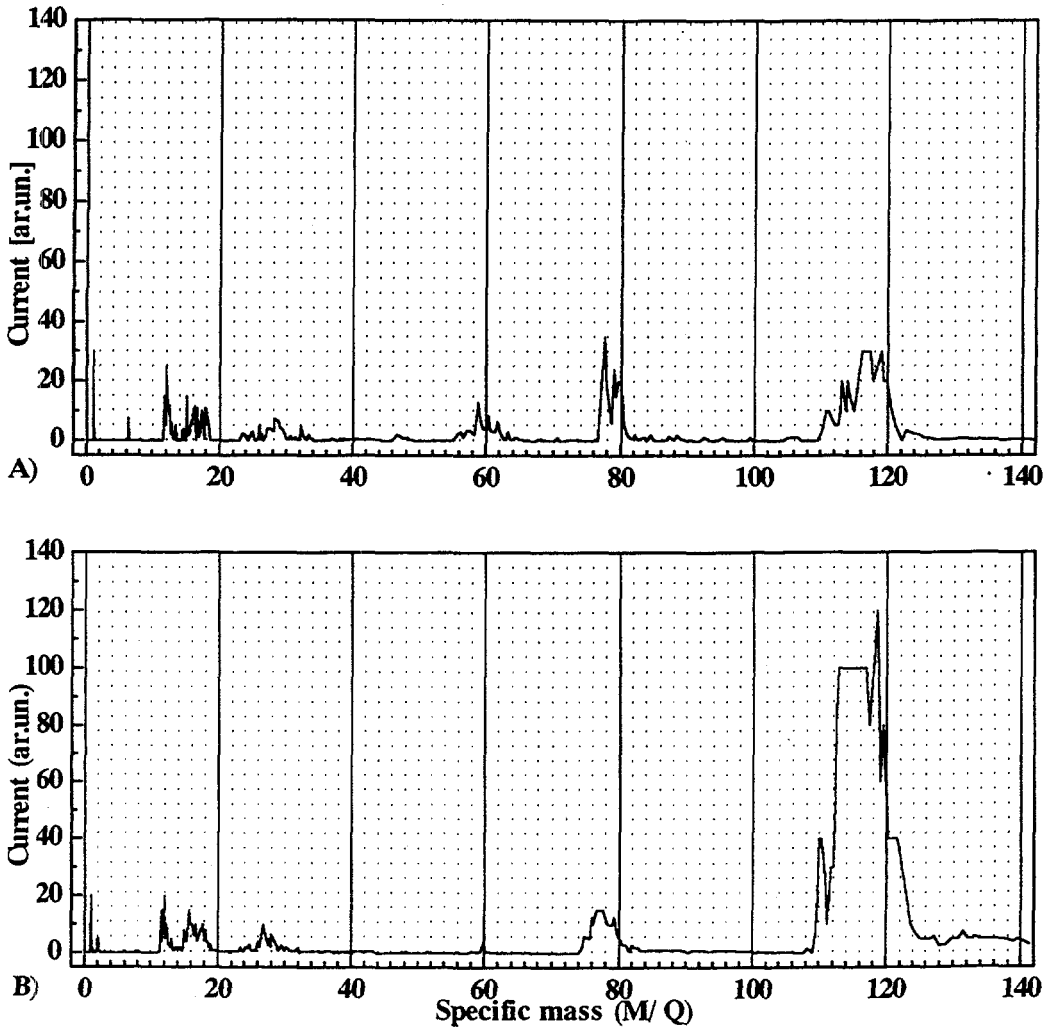

Fig.11. MA CSD for e-MEVVA operation with e-beam. At a) trigger pulse, b) before e beam.

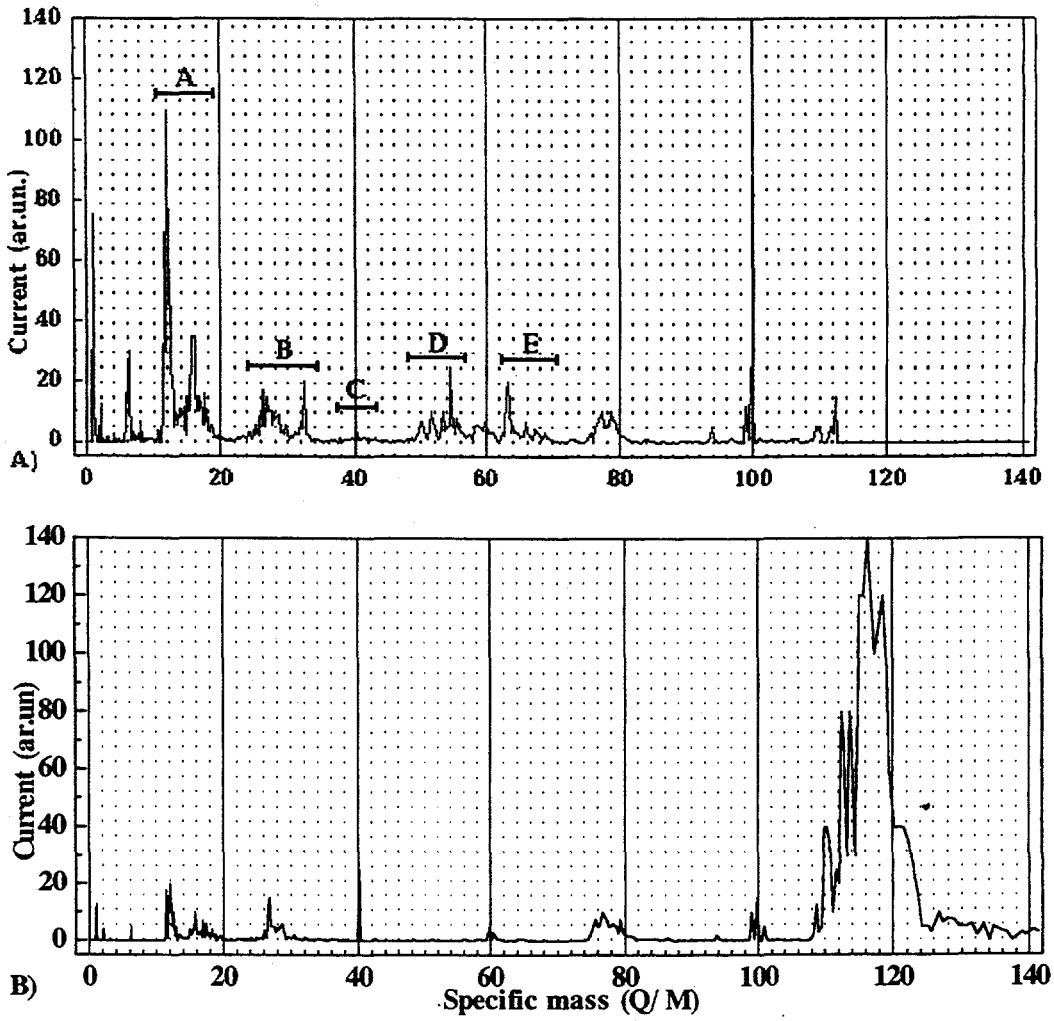

Fig.12. MA CSD for e-MEVVA operation with e-beam. At a) for e-beam, b) after e-beam time points.

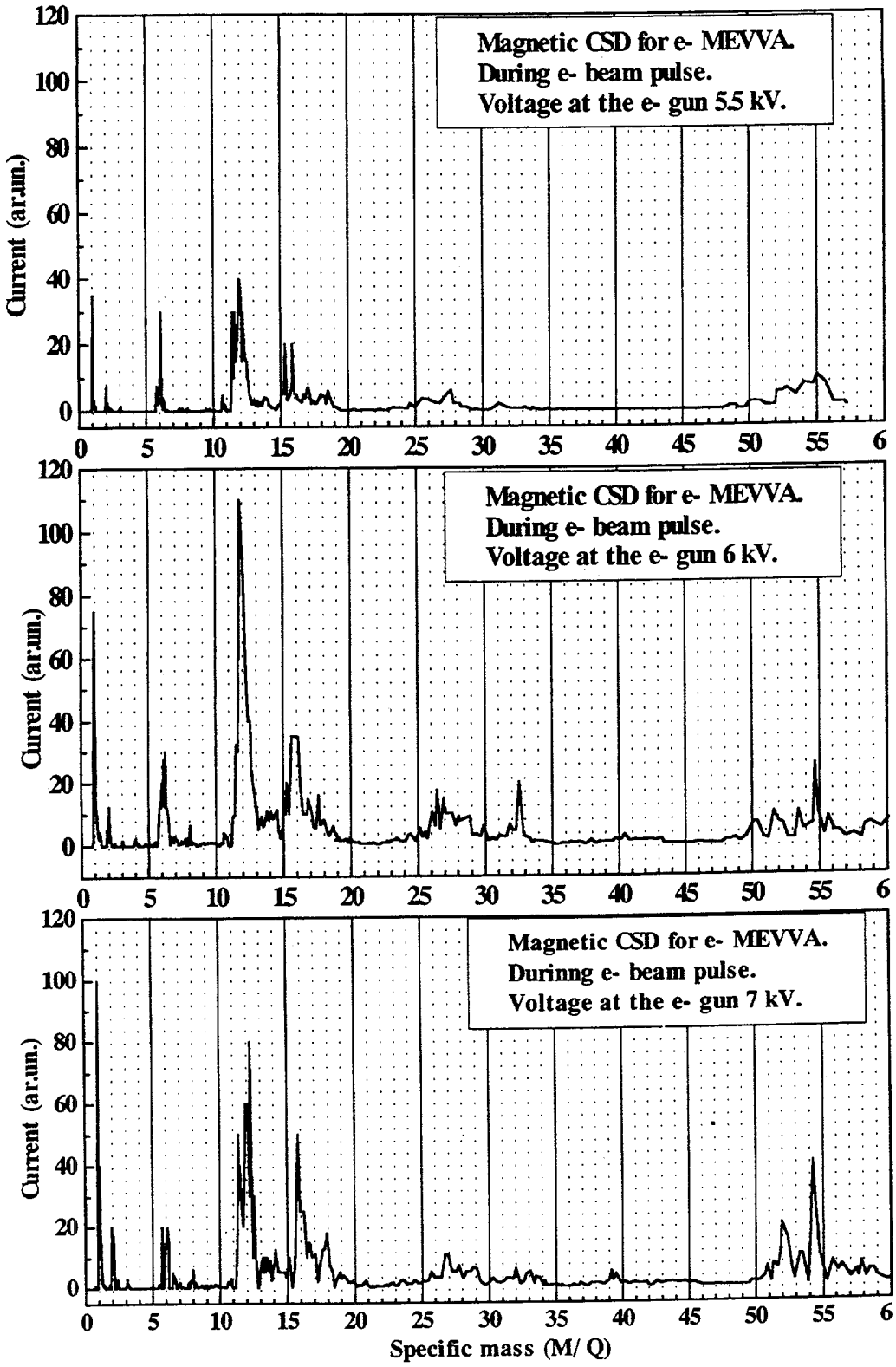

Fig 13. MA CSD for e-MEVVA operation with e-beam, accelerating voltage at the e-gun: 5.5, 6 and 7 kV.

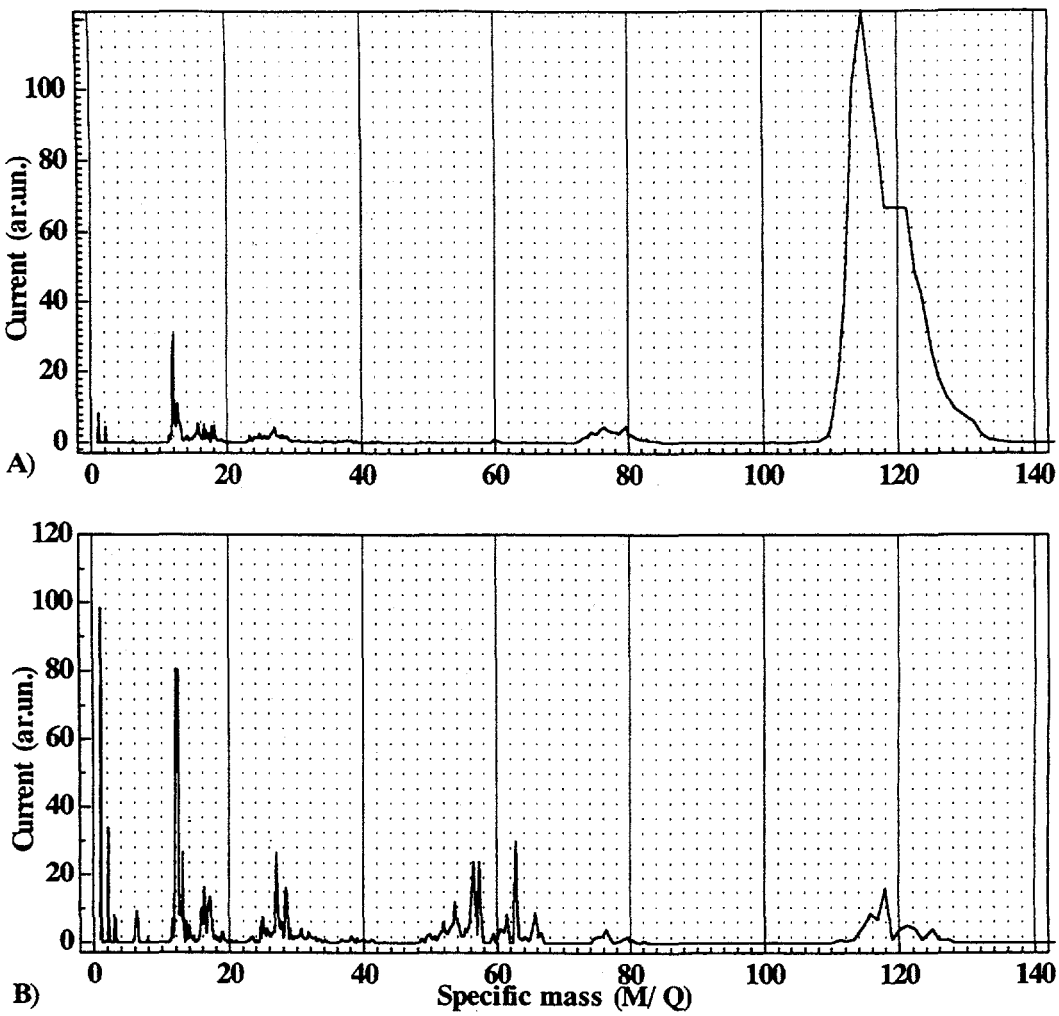

Fig.14. MA CSD for e-MEVVA operation a)without and b) with e-beam. E-beam accelerating voltage 7 kV.

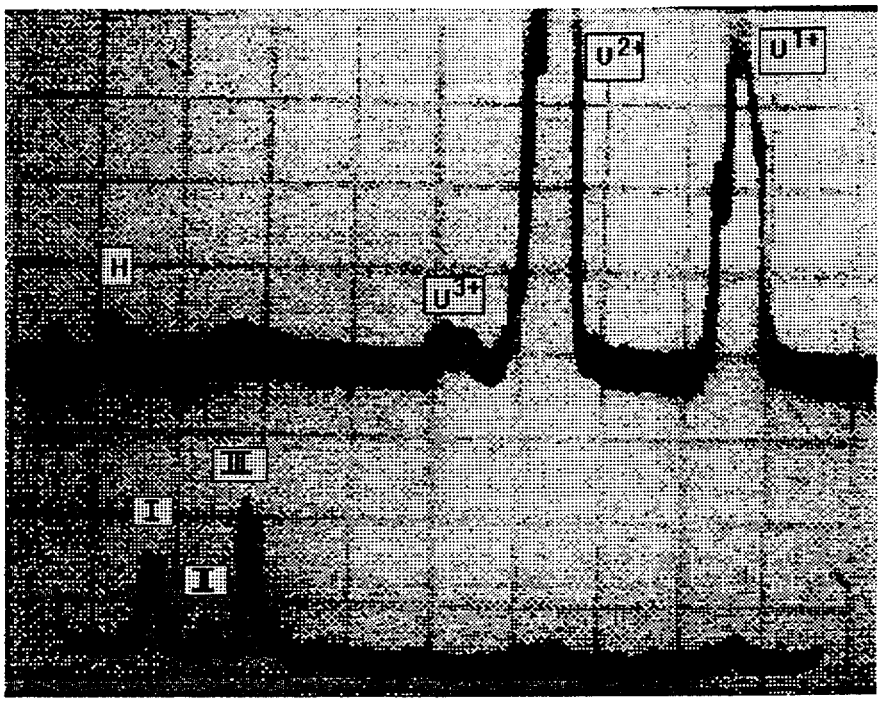

Fig.14. TOF CSD for e−MEVVA operation regime without (upper one) and with e−beam (down one).

A REVIEW OF VACUUM ARC ION SOURCE RESEARCH AT ANSTO.

P. J. Evans, J. T. Noorman and G. C. Watt.
Physics Division, ANSTO, Private Mail Bag No.1, Menai, NSW 2234, Australia.

My talk today will briefly describe the history and current status of vacuum arc ion source research at the Australian Nuclear Science and Technology Organisation (ANSTO). In addition, I shall make some mention of the important role of previous Vacuum Arc Ion Source Workshops in fostering the development of this research field internationally.

During the period 1986 - 89, a type of plasma centrifuge known as a vacuum arc centrifuge was developed at ANSTO as part of a research project on stable isotope separation. In this device, a high current vacuum arc discharge was used to produce a metal plasma which was subsequently rotated in an axial magnetic field. The high rotational speeds (10^5 - 10^6 rad sec^{-1}) achievable with this method produce centrifugal separation of ions with different mass:charge ratios such as isotopic species. The first portent of things to come occurred in 1985 when Dr. Ian Brown visited ANSTO's Lucas Heights Research Laboratories and presented a talk on the metal vapour vacuum arc (MEVVA) ion source which had only recently been invented by Brown and co-workers, J. Galvin and R. MacGill, at Lawrence Berkeley Laboratory. For those of us involved in vacuum arc centrifuge research, this was an exciting development primarily because the metal vapour vacuum arc plasma source was common to both devices. Thus, a type of arc, which had since the 1930's been extensively investigated as a means of switching high current loads, had found wider application as a useful plasma source.

While research activities on the vacuum arc centrifuge continued at ANSTO until 1989, interest in vacuum arc ion sources continued to grow culminating in the decision to commence fabrication of a MEVVA II ion source. Following a review of operations in late 1988, metal ion implantation research emerged as a project in its own right with the initial objective of developing an ion implantation system which incorporated a metal vapour vacuum arc ion source. This phase of the project was completed in 1990 and was followed by a series of studies on applications of ion implantation. Even though the modification of metal surfaces has been a main feature of the latter research, the first major investigation to be undertaken was the ion implantation of glassy carbon, a low density graphitic material, with tungsten and titanium. This work provided the basis for a successful collaboration between ANSTO and LBL researchers which evolved from discussions that took place at the 1st Workshop on Vacuum Arc Ion Sources. Specifically, the growth of diamond thin films on ion implanted glassy carbon was investigated as a function of surface treatment and deposition time.

Subsequently, we have conducted a number of research projects in which ion implantation has been utilised to modify the surface properties or structure of metals and ceramics. In particular, the corrosion resistance of type 2011 aluminium alloy; the surface hardness of several steels and Ti-6Al-4V surgical alloy; and, more recently, the formation of titanium aluminide phases under high dose conditions. In addition,

alumina specimens have been implanted with Mg ions to determine the effectiveness of this treatment for biomedical applications.

Concurrent with these applied studies has been work aimed at improving the reliability and performance of the vacuum arc ion source and versatility of the implantation system. In particular, we developed a trigger power supply which has proved suitable for most cathode materials and operated reliably for more than 2 years. We have also experimented with several arc discharge power supplies of different design. While the effects of the latter on ion source performance were not great, it did lead to some design features that subsequently formed the basis of a power supply module which combined both the trigger and arc power supplies in a single unit. Other developmental work performed in conjunction with that on the ion source system has included specialised target holders for the controlled heating, cooling or rotation of samples during implantation.

ANSTO, as an Australian Government research organisation, serves the national scientific community by providing access to some of its research facilities. Much of this access takes place under the auspices of the Australian Institute of Nuclear Science and Engineering (AINSE) which awards annual grants to university researchers for this purpose. Since 1993, a yearly average ~ 60 days of machine time have been devoted to such activities with demand steadily increasing. Furthermore, many external users of the ion implanter also make use of ANSTO's two accelerators for the characterisation of their ion beam modified surfaces. A 3 MV Van de Graaff linear accelerator is available for routine ion beam analyses, such as Rutherford backscattering (RBS) and nuclear reaction analysis (NRA), while heavy ion time-of-flight elastic recoil spectrometry is performed on an 8 MV Tandem.

The experience gained over the past few years, from both our own research programs and through the support provided to external users, has yielded certain insights into the use of MEVVA ion sources for surface modification studies. These will now be briefly discussed with specific examples from recent work at ANSTO and elsewhere.

MEVVA ion sources are simple, robust devices capable of generating ion beams of most metal species. A typical system comprising ion source and associated power supplies is shown schematically in Fig. 1. The most common design in use today is the repetitively pulsed version with typical duty cycles of less than 5%. Long term stable operation depends primarily on the reliability of the triggering mechanism and the properties of the cathode material. Each trigger event removes some of the film of cathode material deposited on the surface of the alumina insulator in previous discharges of the main arc. It is this continual process of deposition and removal which prevents the surface resistance between the trigger electrode and cathode from becoming too low or too high; neither of which is conducive to producing an adequate burst of plasma to initiate the main discharge. As might be expected, the properties of the cathode material play an important role in achieving surface resistivities in the right range to ensure prolonged operation of the source. Generally, cathodes of lower melting point

metals such as aluminium and tin do not perform as well as their higher temperature counterparts (e.g. Ti and Cr). This is attributed to a more rapid net build-up of deposits on the insulator surface due to the relatively larger amounts of material removed from the cathode in each discharge. Thus, for low melting point cathodes, a short circuit condition (i.e. non-triggering) is reached in a shorter time. While this limitation usually poses no problem for low and medium dose implants, it may result in the need to refurbish the cathode assembly prior to the completion of a high dose implant. For the most part, the latter difficulty is circumvented in multi-cathode vacuum arc ion sources by changing to a fresh cathode and continuing with the irradiation. Nevertheless, triggering problems do occur during extended operation with some low melting point cathodes. Whether or not these can be overcome by alternative designs of the cathode-trigger assembly has yet to be determined as there would appear to be no previous, systematic study of this aspect of MEVVA ion source technology.

The cathode-trigger geometries utilised in most MEVVA type ion sources described in the literature show considerable similarity. This particular design has proved very suitable for most higher melting point, metallic elements and alloys, and satisfactory for some non-metals (e.g. C), semiconductors (e.g. Si) and inorganics (e.g. LaB_6). However, greater variability in performance has been encountered with the latter groupings of materials which is most probably due to their different structure and properties. For example, graphite rod cathodes are commonly used for the generation of carbon ion beams. The resulting arc, while capable of extended operation, tends to be less stable in comparison with better performing metals such as titanium. In addition, macroparticle formation appears to be more pronounced with graphite cathodes, at least for the type used in our experiments.

Vacuum arc discharges are sustained by material eroded from the cathode surface. Operation of a MEVVA source usually entails repetitive discharging of the arc, often for extended periods, during which time, the front surface of the cathode gradually recedes causing the arc geometry to change. In severe cases, the latter may lead to source failure though in reality, an attendant deterioration in the trigger insulator may also be an important contributing factor in any failure. Two methods of overcoming changes in cathode geometry have been developed. With multi-cathode sources such as the MEVVA V, a non-operating cathode assembly is easily replaced with another similar one from the carousel; after which the implantation can be continued. An alternative, which is suitable for single cathode sources, has been developed by researchers at Beijing Normal University. In their design, a drive mechanism, attached to the cathode, provides a means of compensating for changes in geometry resulting from arc erosion. Both approaches have been successfully used to increase the time between cathode replacements requiring a break in vacuum. In both cases, the methods have been applied to comparatively small diameter cathodes. Whether a similar gain could be achieved by using larger diameter cathodes does not appear to have been examined in any detail.

Vacuum arcs with larger cathodes have certainly operated successfully in other applications. However, the trigger electrode arrangement used in most MEVVA ion sources does not usually result in uniform erosion of the cathode surface. Instead, erosion for many materials of interest occurs predominantly in the region adjacent to the trigger insulator, at least during the initial period of operation. Thus, increasing the cathode diameter may lead to individual discharges being localised rather than distributed over most or all of the circumference. Consequently, the extracted beam under such conditions might exhibit some non-uniformity which would make it less suitable for ion implantation studies. Further research is required to assess the viability of using larger diameter cathodes in MEVVA ion sources.

The preceding discussion has focused on how the properties and dimensions of the cathode might influence MEVVA ion source performance. Several specific problems associated with this part of the source were identified and it was suggested that further research is necessary to find satisfactory solutions. Another feature of MEVVA sources of importance to those users engaged in ion implantation studies is the ion beam characteristics. In particular, beam duration, size and uniformity may all affect the nature and quality of the implanted surface. A pulse forming network design is often used as the basis for the vacuum arc power supply in MEVVA systems. This type of design provides an output current pulse with an approximately rectangular waveform which supplies power to the vacuum arc for a pre-determined time. Since plasma is only produced during the discharge, the latter also governs the duration of the ion beam current pulse. Beam pulse lengths in the range several hundred microseconds to more than one millisecond have been adopted by various researchers. While longer pulse lengths generally result in shorter processing times, they can also influence the properties of the implanted surface in several ways. In particular, for a given pulse repetition frequency and ion beam current, the temperature rise of the sample will increase in proportion to the arc discharge time. This may produce a variety of effects including phase formation or diffusion of species out of the implant layer. An example of such behaviour is provided by recent work at ANSTO and the University of Wollongong in which the high dose implantation of aluminium with Ti was studied over a range of substrate temperatures. At ambient temperatures (<150 °C), the implant profile was approximately Gaussian and $AlTi_3$ was the predominant phase observed in X-ray diffraction analysis. In contrast, temperatures of ~ 400 °C yielded a broader implant distribution with significantly lower peak concentration. The X-ray spectrum showed Al_3Ti to be the preferred phase under these conditions. Longer discharge times also place constraints on the high voltage extractor power supply which must be capable of maintaining the selected voltage setting throughout the discharge. Failure to so will result in a drop in voltage and a corresponding decrease in ion energies during each discharge pulse. Thus, the spread in energy will be greater than that obtained if the accelerating voltage remained at its pre-set value.

Macroparticle formation in vacuum arcs was mentioned briefly above. These are molten or solid particles of cathode material which are eroded from the cathode surface during the discharge. Many are deposited on adjacent surfaces in the ion source and do not

play any part in the implantation process. However, some fraction are projected through the extractor grids in the general direction of the target. As a consequence, macroparticles are commonly observed in microscopic examination of surfaces implanted by means of MEVVA ion sources. The gradual build-up of such particles during implantation results in small areas of the target surface being shadowed from the ion beam and hence receiving less than the full implant dose. This phenomenon would not appear to be a major problem in laboratory studies provided it is recognised as a possible source of localised failure in tests of the implanted surface. However, it may limit the beneficial effects of MEVVA ion implantation in specific applications and hence reduce the attractiveness of the treatment to potential end users of the technique. A method of removing macroparticles from the extracted ion beam has been demonstrated by the Berkeley group and reported in their paper at the Second MEVVA Workshop in Beijing. The use of a 90° magnetic filter, similar to that developed for thin film deposition studies, in conjunction with a MEVVA ion source provided an effective means of preventing particles from impinging on the implantation surface. Despite this advance, the particle-free MEVVA ion source has not been widely adopted by practitioners in the field who, for the most part, continue to use earlier models for their research.

The development and utilisation of MEVVA ion sources has expanded rapidly since the first paper on the subject by Brown *et al* in 1985. In the past decade, sources of this type have been extensively used for the metal ion implantation of a wide variety of surfaces including those of many technologically important materials. The expanding literature on the subject testifies to the many significant successes achieved to date. Inevitably, problems have been encountered in the continuing effort to increase the performance or find new applications of MEVVA ion sources. The present report has endeavoured to document some of these problems in light of experience gained at ANSTO during the past 5 years. This experience has entailed both the development of MEVVA sources and their subsequent use for metal ion implantation research. Generally, we have found the MEVVA ion source to be an inherently simple, robust and versatile tool for the modification of surfaces. Furthermore, the problems discussed above have, for the most part, not been an impediment to the use of MEVVA generated ion beams for a large number of successful laboratory studies, both here and elsewhere, involving most types of materials. In the longer term however, solutions to these problems must be found especially if the technology is to find application in areas where high quality, cost effective surface treatments are required. There is little doubt that this is possible in most cases discussed above. Thus, the prospects for commercial treatment processes based on MEVVA ion implantation appear to be promising and point to an optimistic future for this technology.

Previous Workshops at Berkeley and Beijing made a valuable contribution to our understanding and appreciation of vacuum arc ion sources. They provided a useful forum for discussing problems of the type described above and for exploring possible solutions. In addition, these meetings enabled researchers in the field to view, at first

hand, developments in other laboratories. The present 3rd Workshop has returned to Berkeley which was considered the most convenient location on this occasion. It is hoped that the spirit and benefits of the current and earlier Workshops will serve as a stimulus for the organisation of similar meetings in the future, thereby maintaining a worthwhile tradition of communication on MEVVA ion sources.

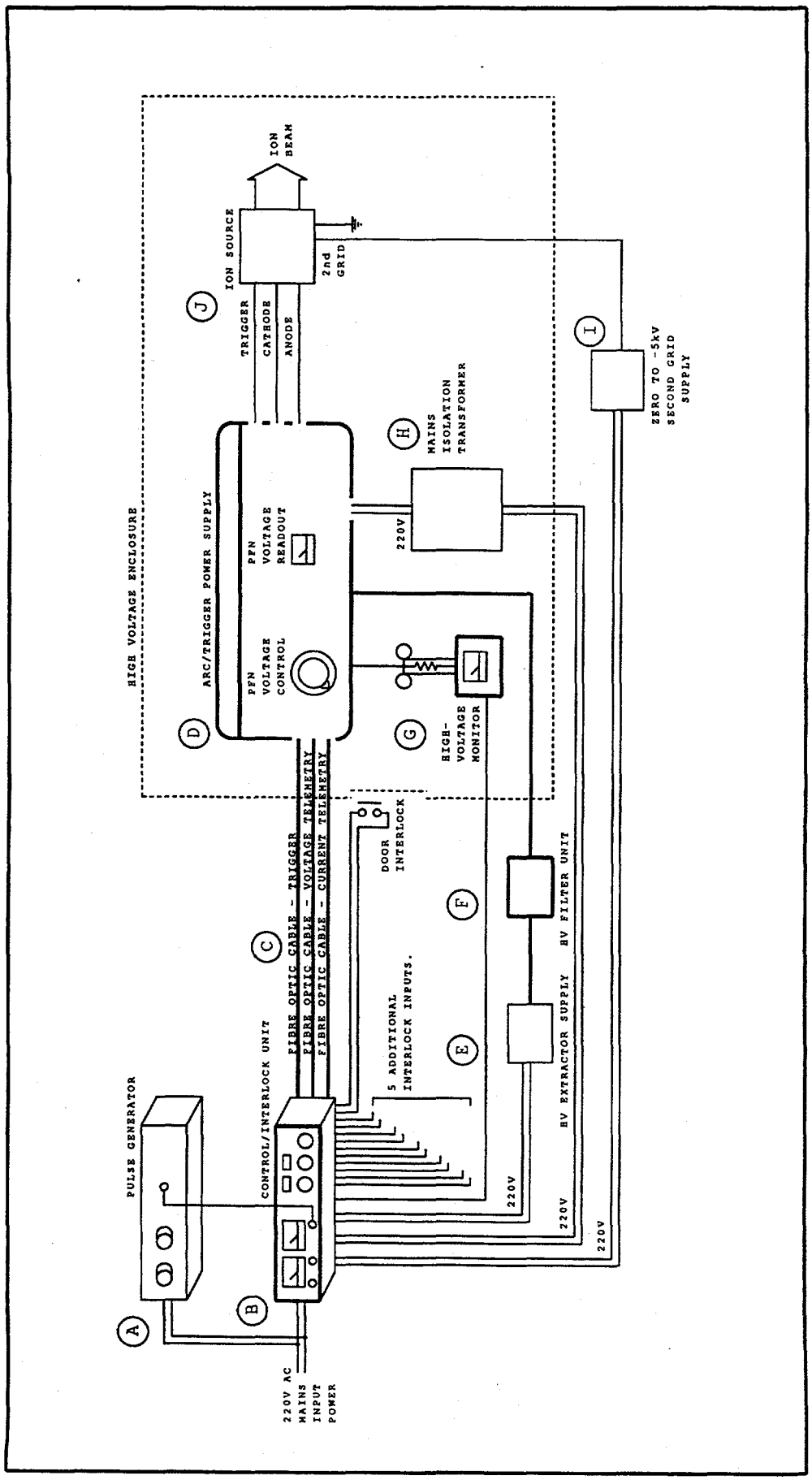

Figure 1 - Schematic layout of typical vacuum arc ion source system.

Abstract submitted to :
Workshop on Vacuum Arc Ion Source,
University of California, Berkeley California

September 18 - 20, 1995

A HIGHLY RELIABLE TRIGGER FOR VACUUM ARC PLASMA SOURCE

Henri Bernardet, Xavier Godechot, François Jarjat.

SODERN
20 avenue Descartes, 94451 Limeil-Brevannes cedex, FRANCE.

We have developed a reliable electrical trigger and its associated circuitry to fire vacuum arc plasma or ion source. We tested different embodiments of the trigger device in order to get a highly reliable one, which is able to perform over than 1.2 10^6 shots at 60 A and 6.5 µs pulse length. The evolution of the ion current emitted has been recorded as a function of the number of shots. We have also investigated in which direction the plasma jet is emitted : axially or radially. This device can be used to fire a vacuum arc plasma or ion source by plasma injection [1]. It has obvious advantage to be placed outside the cathode and therefore would ease maintenance of vacuum arc devices.

1 "Investigation of Firing Properties of a Vacuum Arcs Triggered by Plasma Injection", Henri Bernardet, Xavier Godechot and Christophe Riviere, paper presented at this workshop

A HIGHLY RELIABLE TRIGGER FOR VACUUM ARC PLASMA SOURCE

Henri Bernardet, Xavier Godechot, François Jarjat.

Schematic representation of vacuum arc fired by plasma injection

CHARACTERISTICS :

4 electrodes device

ADVANTANGES :

Easy to maintain

AIMED PERFORMANCES :

High reliability, over 10^6 shots

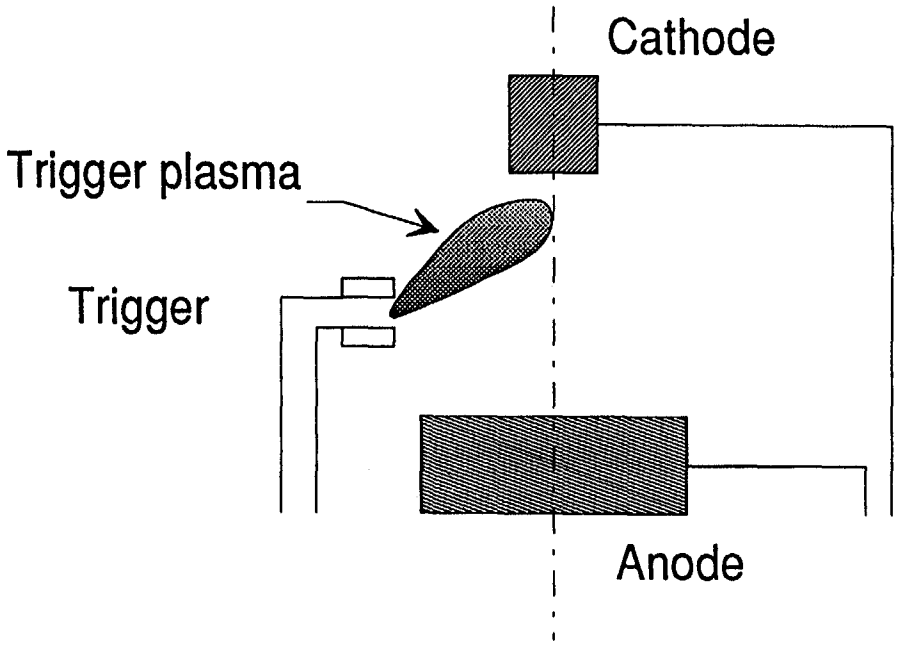

Schematic representation of the experimental setup

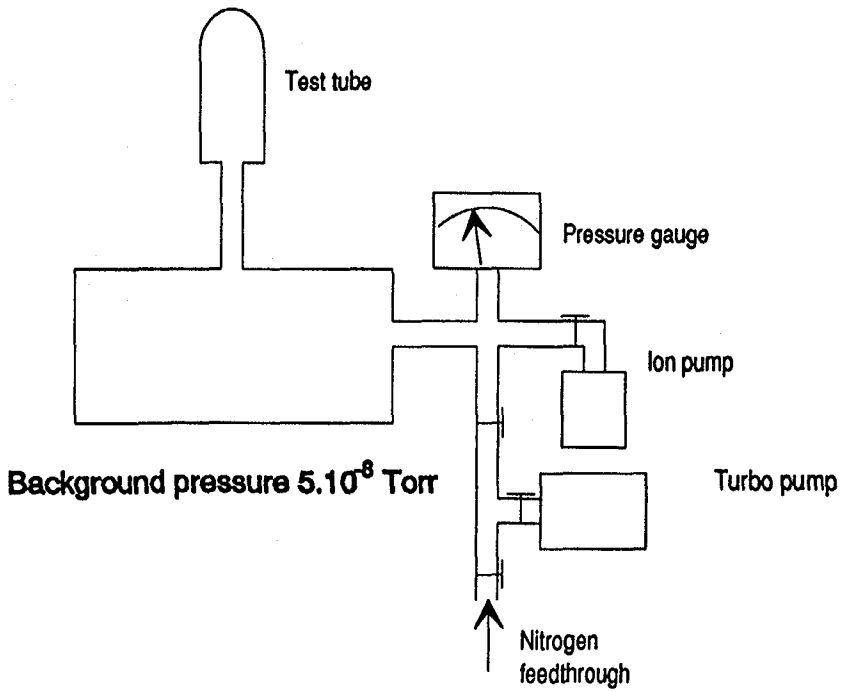

Background pressure 5.10^{-8} Torr

Vacuum equipment

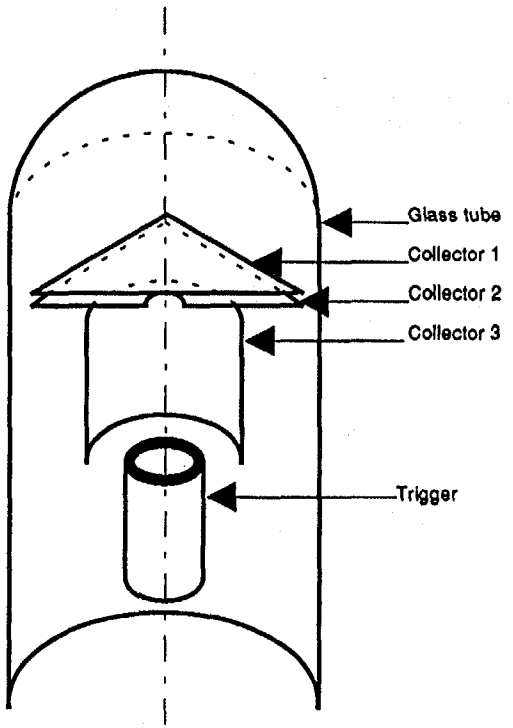

Detail view of the test tube

Schematic of the electrical configuration

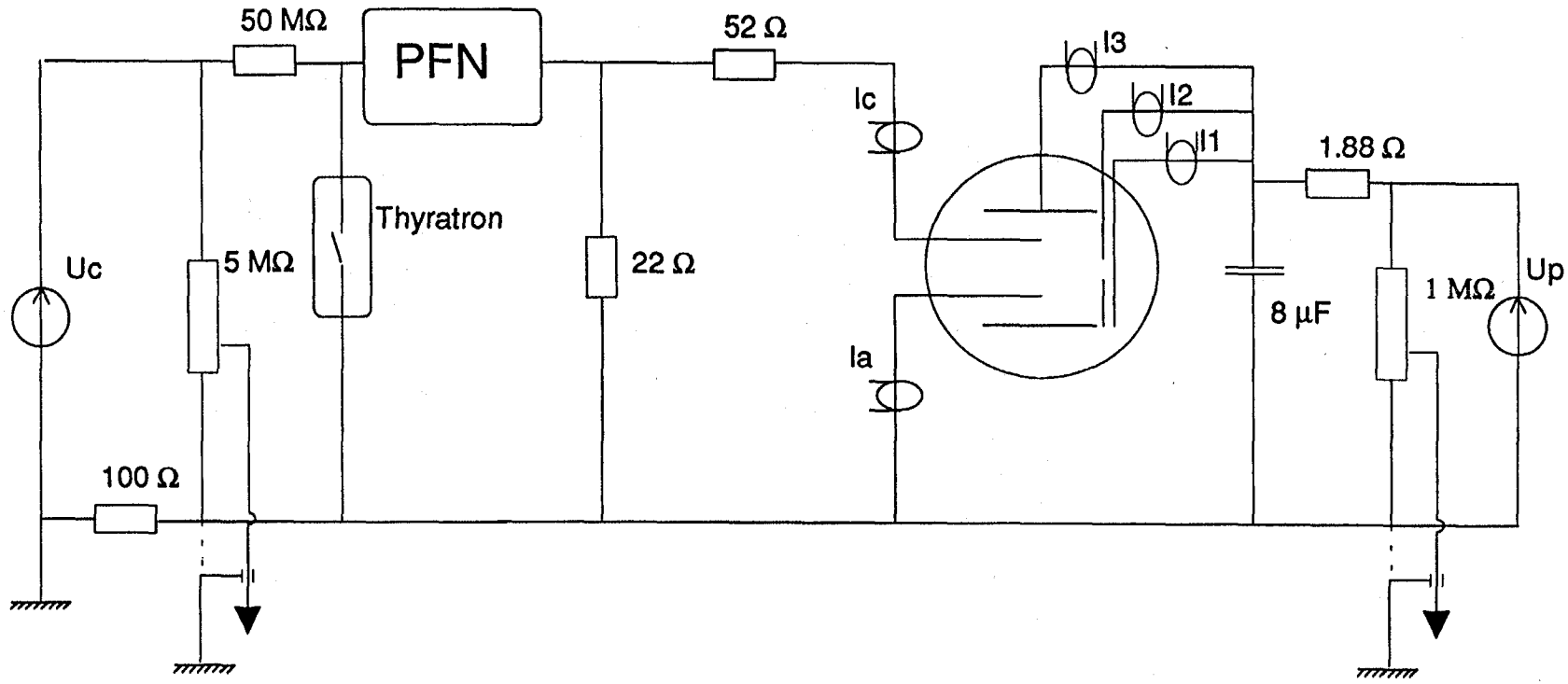

PFN : pulse forming network 15Ω
Uc : voltage (0 to 20 kV)
Up : collectors biasing
(0 to -1000 V)

Ia : Anode current
Ic : Cathode current

I1 : Collector 1 current
I2 : Collector 2 current
I3 : Collector 3 current

Recording of the arc and collectors currents

. Typical operating currents : Iarc 60 A, I1=0. 0.5 A, I2=2 A, I3=2.5 A

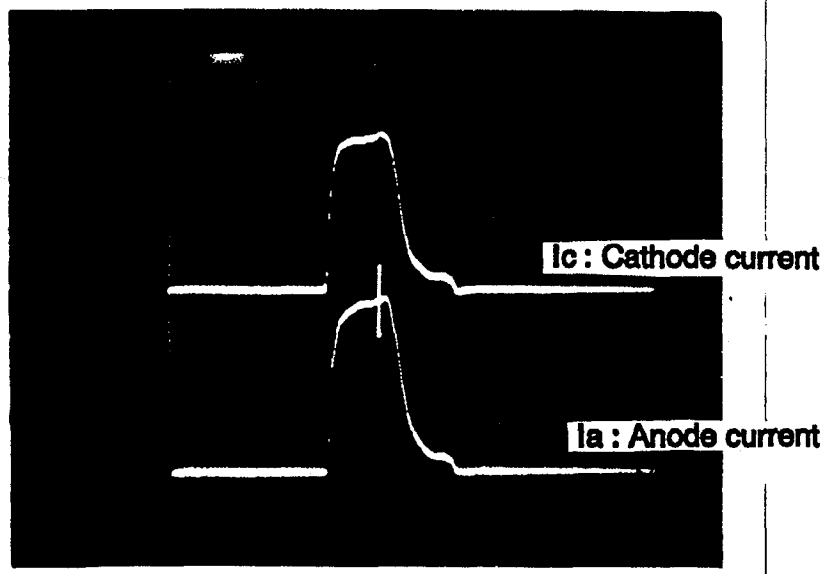

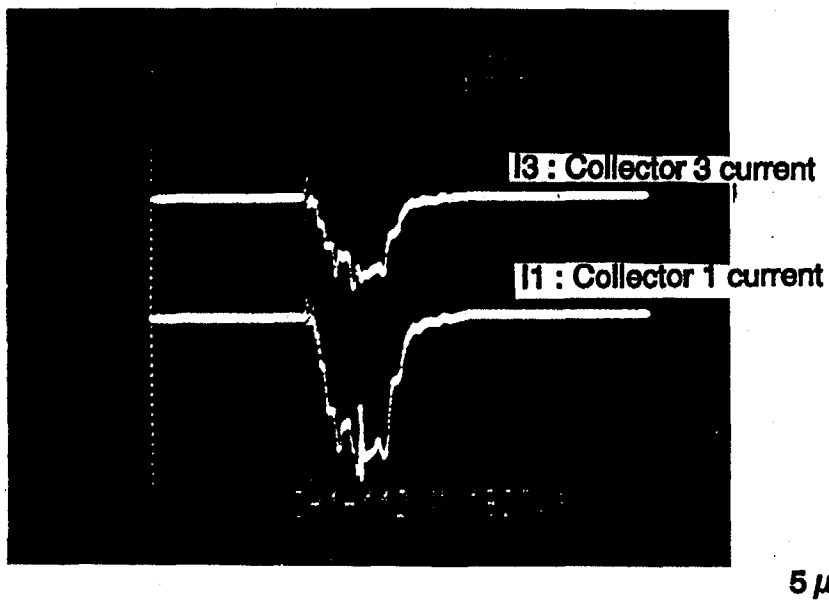

Trigger type A

. Reliability : 15000 to 45000 shots

. Firing voltage : 6 to 8 kV

. Current intensity : 80 to 100 A

. Pulse length : 6.5 μs

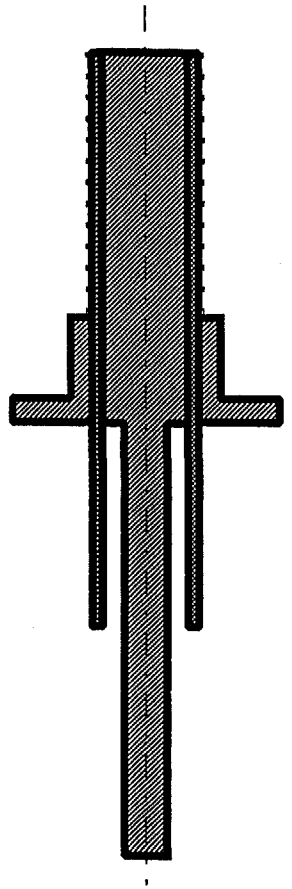

: Mo Mn metal coating

: Dilver P (Kovar)

: Alumina

Alumina and Dilver P parts are brazed with Ag-Cu

Trigger type B

. Reliability : 6000 shots

. Firing voltage : 6 to 8 kV

. Current intensity : 80 to 100 A

. Pulse length : 6.5 μs

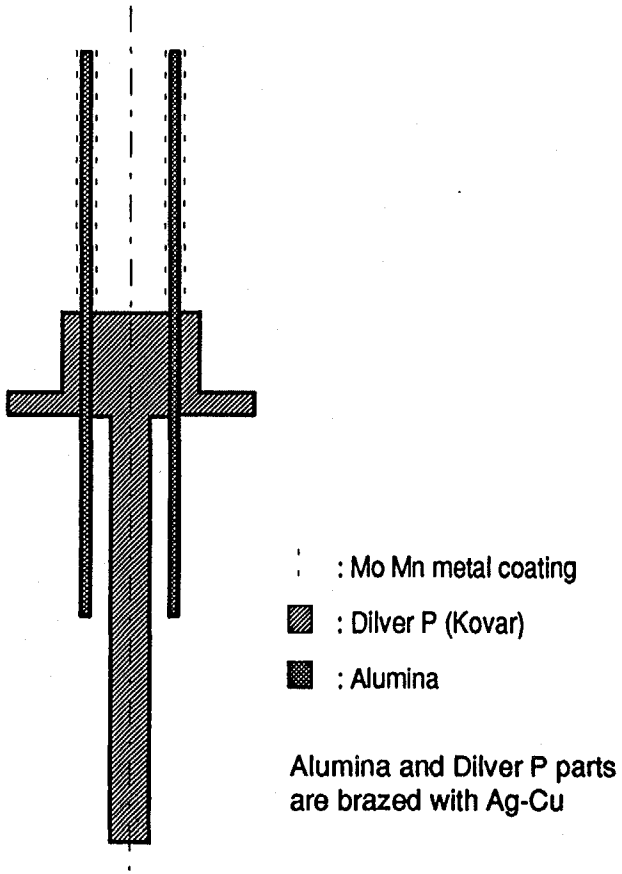

Problems during operation with trigger A and B

. Breakdowns through alumina

. Destruction of the metal coating

. Firing voltage increases with number of shots

Trigger type C

. Reliability : more than 10^6 shots

. Firing voltage : 5.6 kV

. Current intensity : 60 A

. Pulse length : 6.5 μs

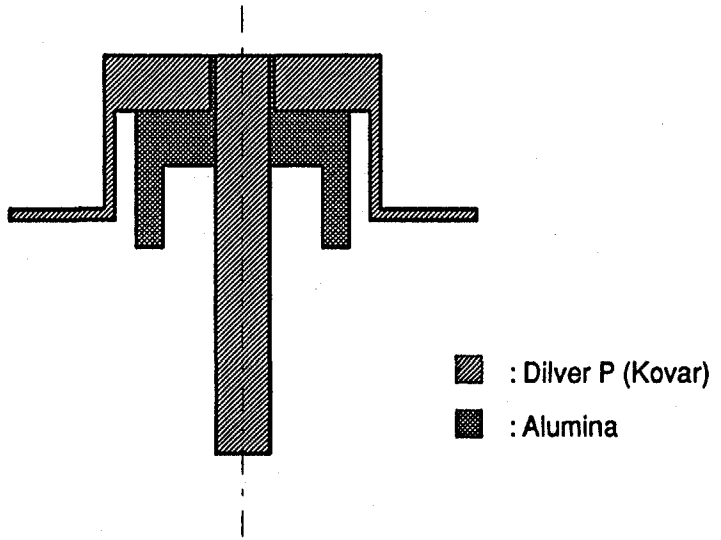

Alumina and Dilver P parts are brazed with Ag-Cu

. Has been succesfully tested to trigger vacuum arc with stainless steel, molybdenum, copper and carbon cathode.

. Operates with trigger current up to 1000 A

Evolution of the Performances during 1.2 million shots

. Total Ion saturation current measured by the three collectors

. A noticable decrease after 800,000 shots

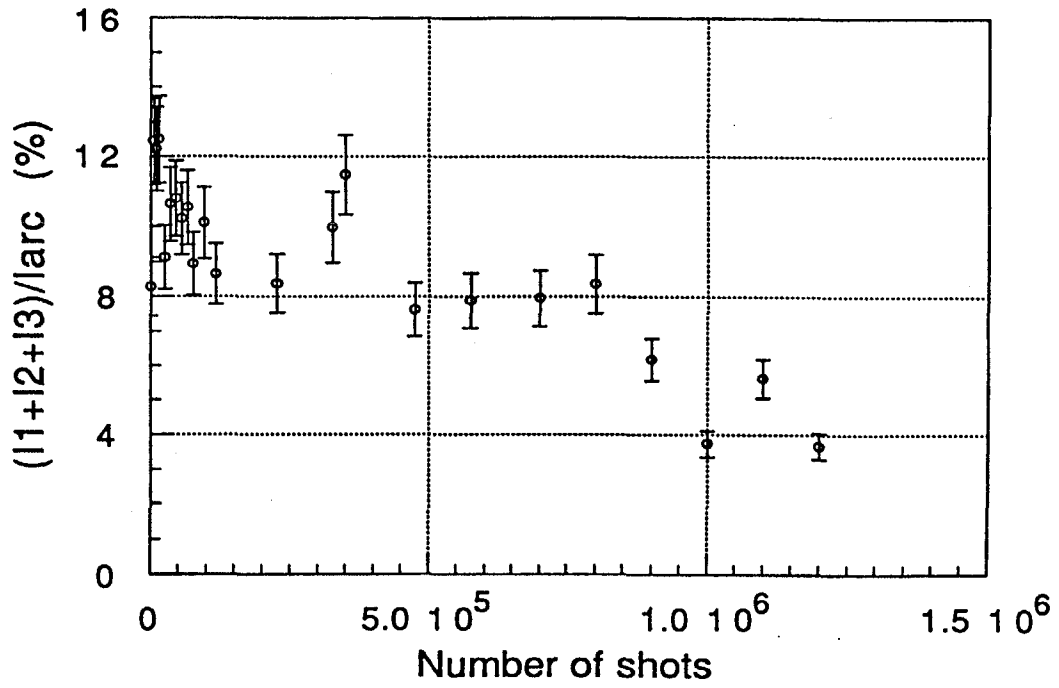

Evolution of the performances during 1.2 million shots

. Relative ion saturation current measured by each collector

. No or little evolution with the number of shots

. The results approximately fits a cosine law :
from computations : I1= 5.9 %,
I2=37.5 %
I3=56.6 %

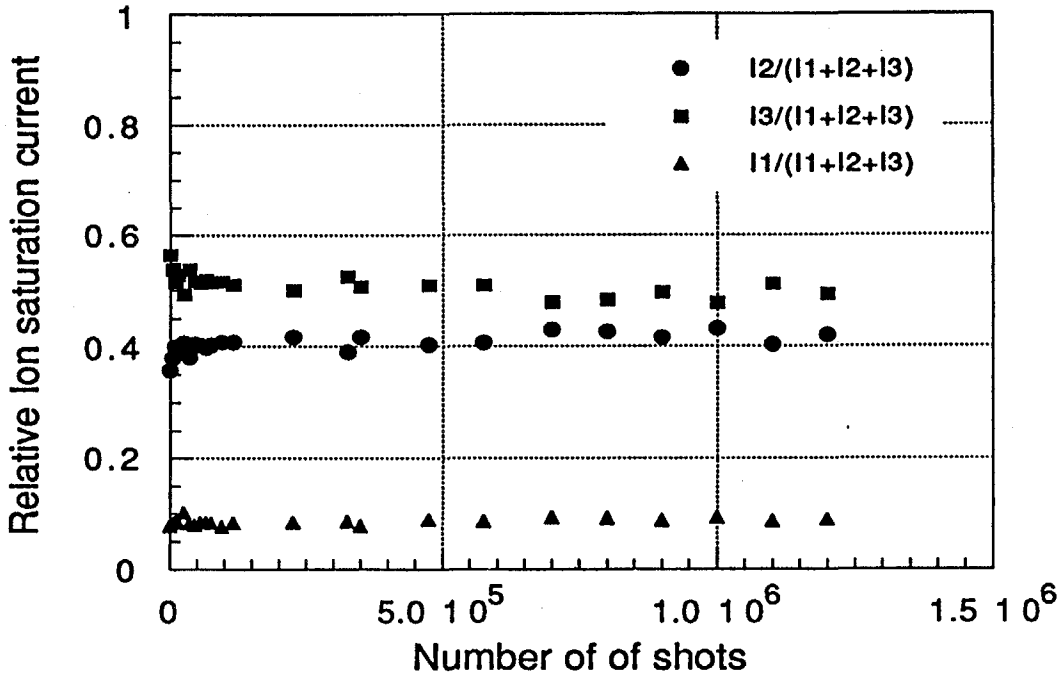

Aspect the central part of the trigger type C after 1.2 million shots

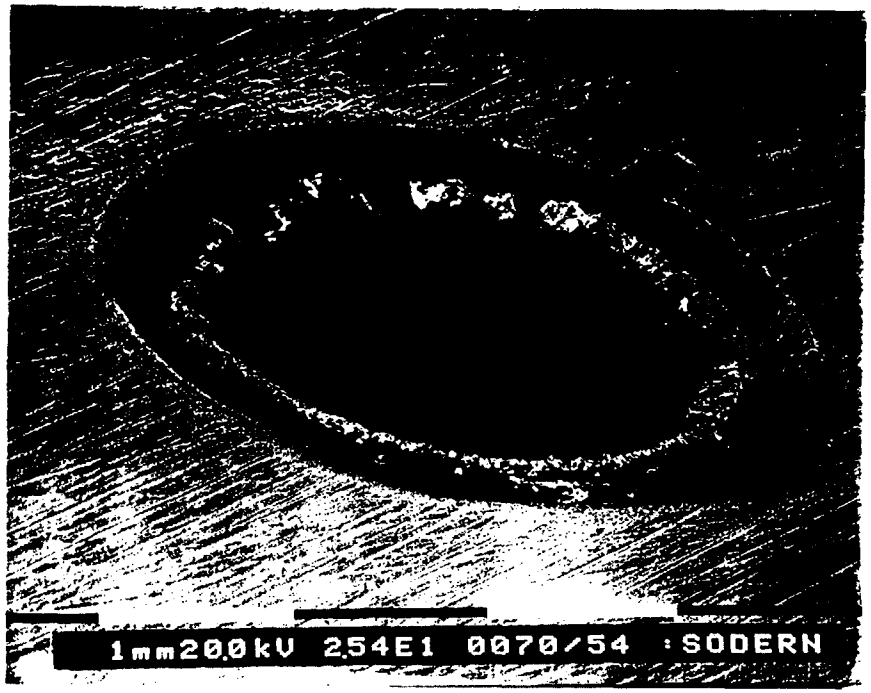

General view

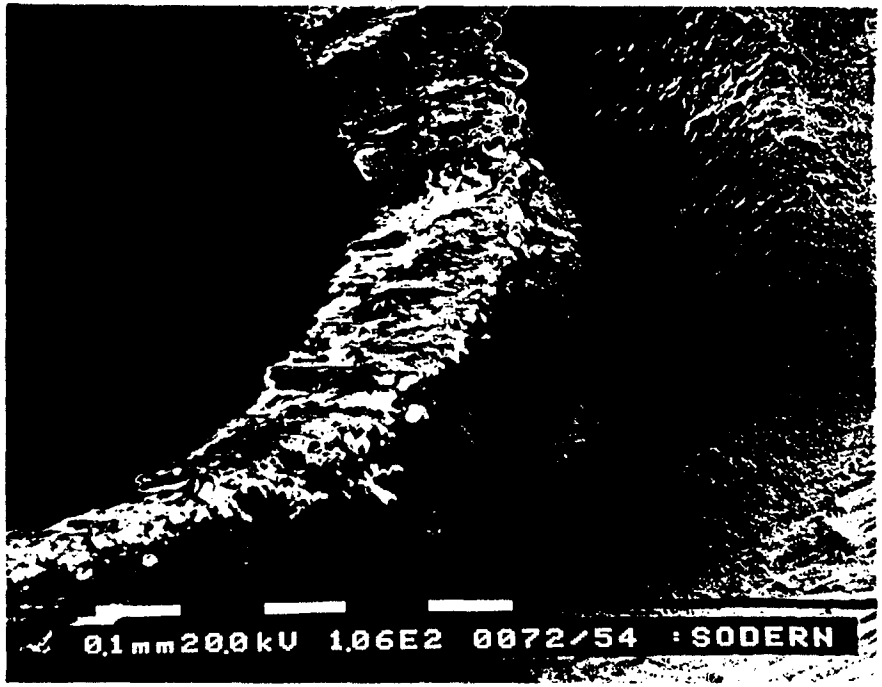

Detailed view

Conclusions

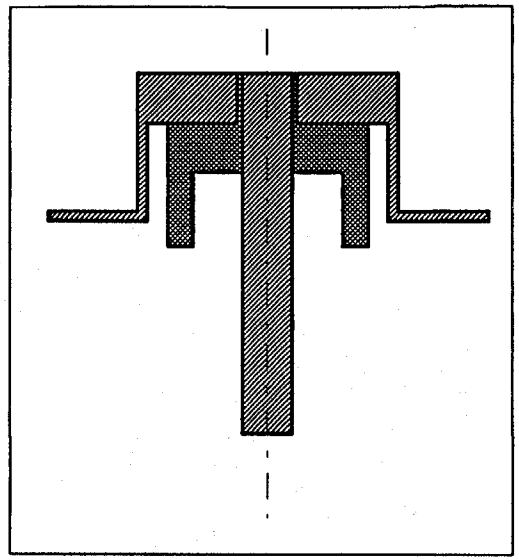

. To fire a vacuum arc by plasma injection

. Designed and tested 3 types of trigger

. Reliable trigger (type c) : more than 1.2 million shots (60 A, 6.5 μs)

. Plasma emission approximatly follows a cosine law

. Has been succesfully tested to trigger vacuum arcs with stainless steel, molybdenum, copper and carbon cathodes.

. Operates with trigger current up to 1000 A

Abstract submitted to :
Workshop on Vacuum Arc Ion Source,
University of California, Berkeley California

September 18 - 20, 1995

INVESTIGATION OF FIRING PROPERTIES OF A VACUUM ARCS TRIGGERED BY PLASMA INJECTION

Henri Bernardet, Xavier Godechot, Christophe Riviere.

SODERN
20 avenue Descartes, 94451 Limeil-Brevannes cedex, FRANCE.

The firing characteristic of a vacuum arc, by means of plasma injection, is described. In this method, a plasma, created from a trigger device, plumes away to the space between the cathode and anode. As the plasma is quasi-neutral, the electrostatic field is concentrated across the sheath at the surface of the cathode, thus, creating a high electrical field. As a result, a vacuum arc fires between the cathode and anode. We have investigated the firing rate as a function of the trigger-cathode distance, trigger current, the anode-cathode distance and voltage. We found a firing rate between 90 to 100% for a trigger current in the range of 400-1200 A, the trigger pulse length was 4 μs, and the trigger-cathode distance was 1.6 to 3.6 cm. The anode cathode gap length changes the firing rate to a low extent for values between 2 to 5 cm. The anode cathode voltage do not change the firing rate. The effect of a magnetic field applied axially over the trigger have also been investigated. Using a version of a highly reliable trigger [1], we were able to deposit stainless steel, copper, carbon and molybdenum, thin films.

1 "A Highly Reliable Trigger for Vacuum Arc Plasma Source", Henri Bernardet, Xavier Godechot and François Jarjat, paper presented at this workshop.

INVESTIGATION OF THE FIRING PROPERTIES OF VACUUM ARC TRIGGERED BY PLASMA INJECTION

Henri Bernardet, Xavier Godechot, Christophe Riviere.

Firing vacuum arc with plasma injection

. Characteristic
  4 electrodes device

. Applications
  plasma surface modification
  ion sources

. Advantage
  easy to maintain

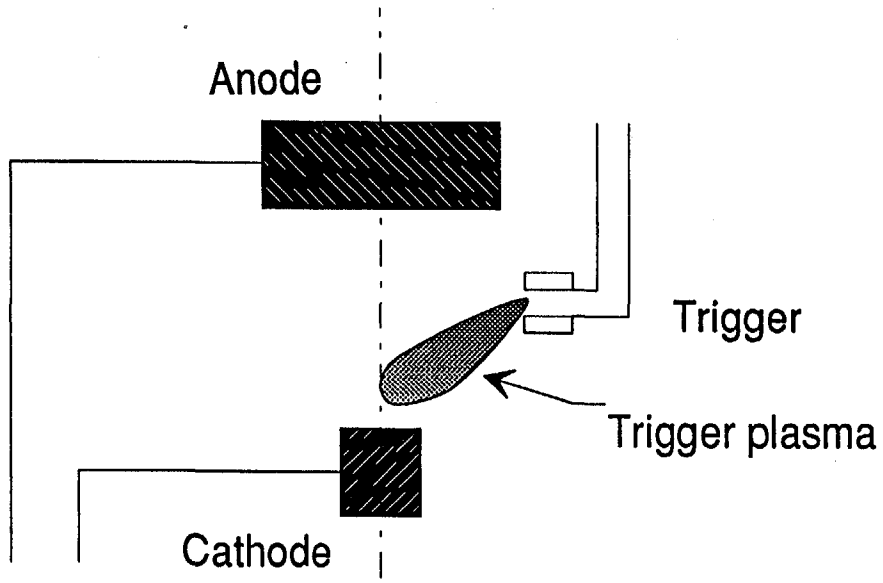

Schematic representation of the firing of a vacuum arc by plasma injection

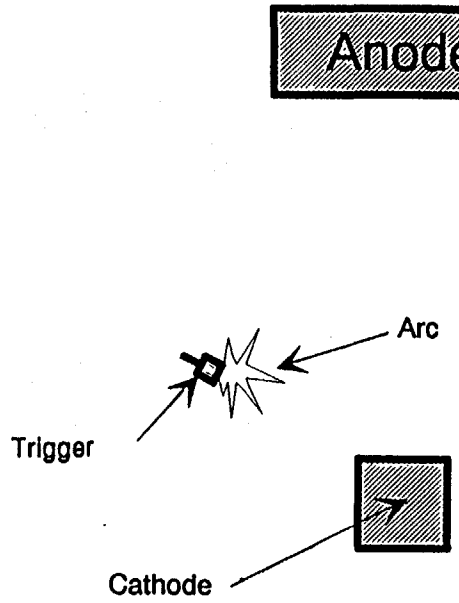

a/ Trigger arc

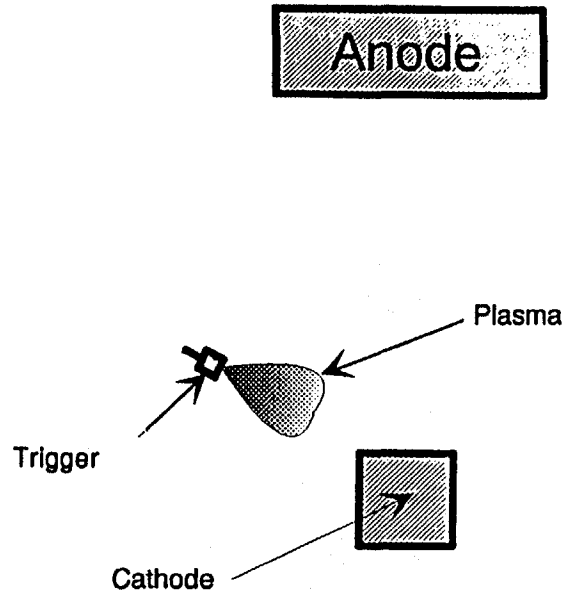

b/ Injection of the plasma in the interelectrode space

Schematic representation of the firing of a vacuum arc by plasma injection

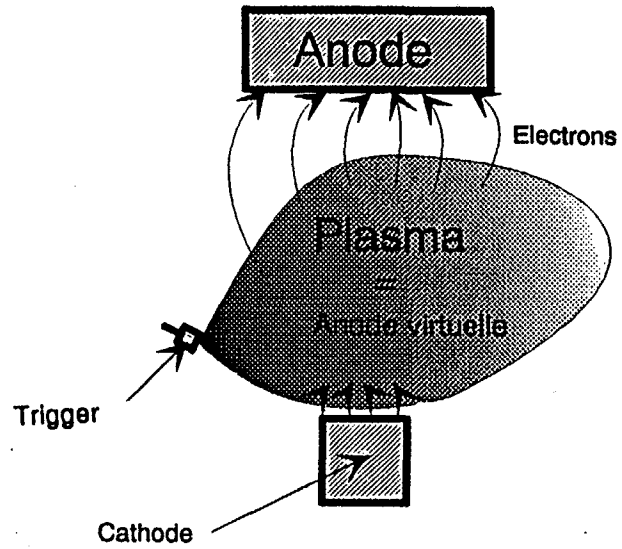

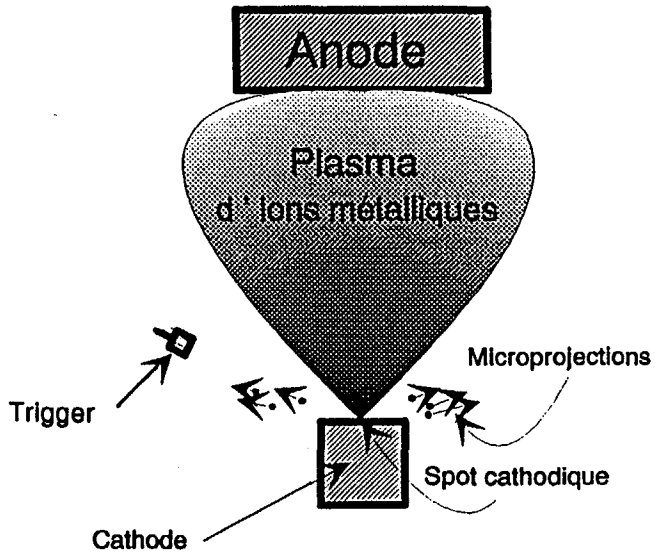

c/ Creation of a high electrical field between the plasma and the cathode

d/ Vacuum arc between the cathode and the anode

Schematic of the experimental configuration

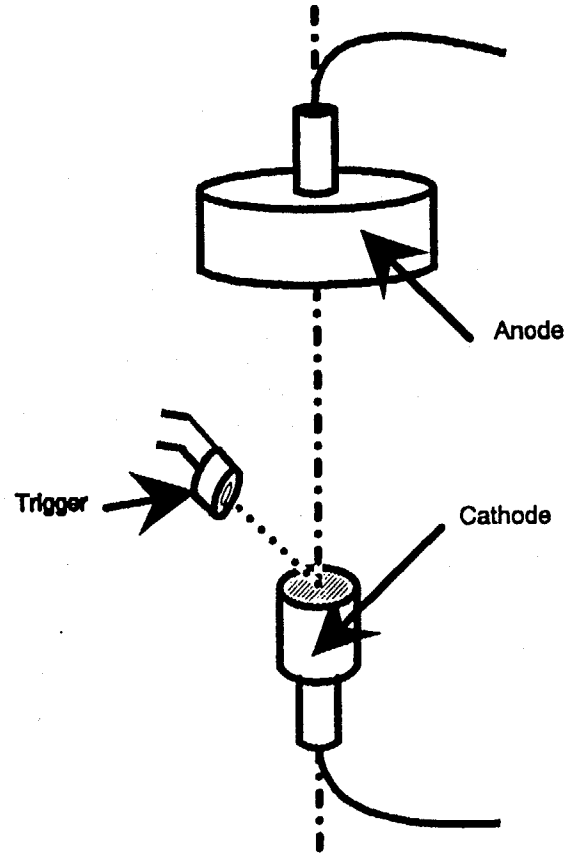

Photograph of the experimental setup

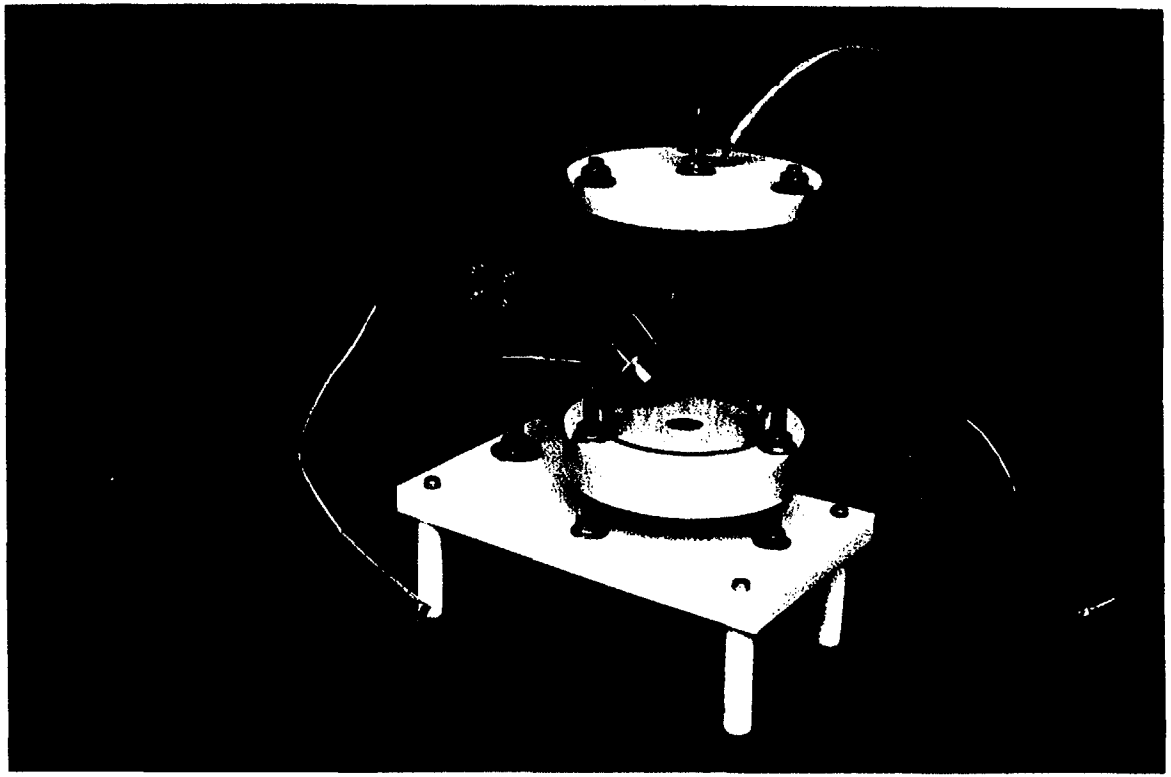

Schematic representation of the trigger

Reliability : approximatly 1000 shots
refurbishment by polishing

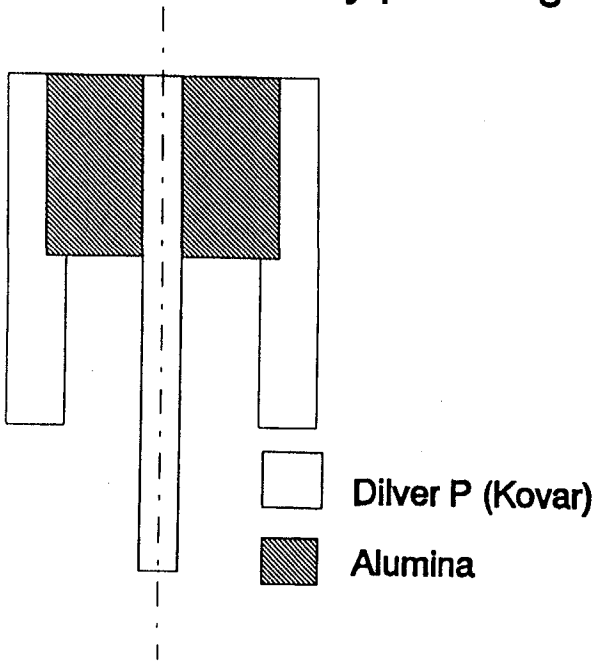

Alumina and dilver P parts
are brazed with Ag-Cu

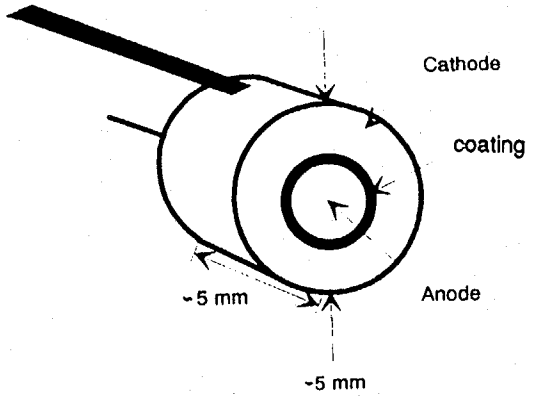

. Front view

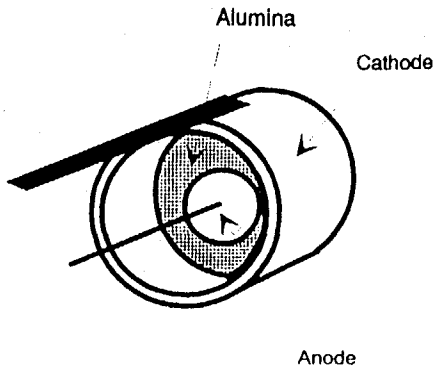

. Back view

Schematic of the electrical configuration

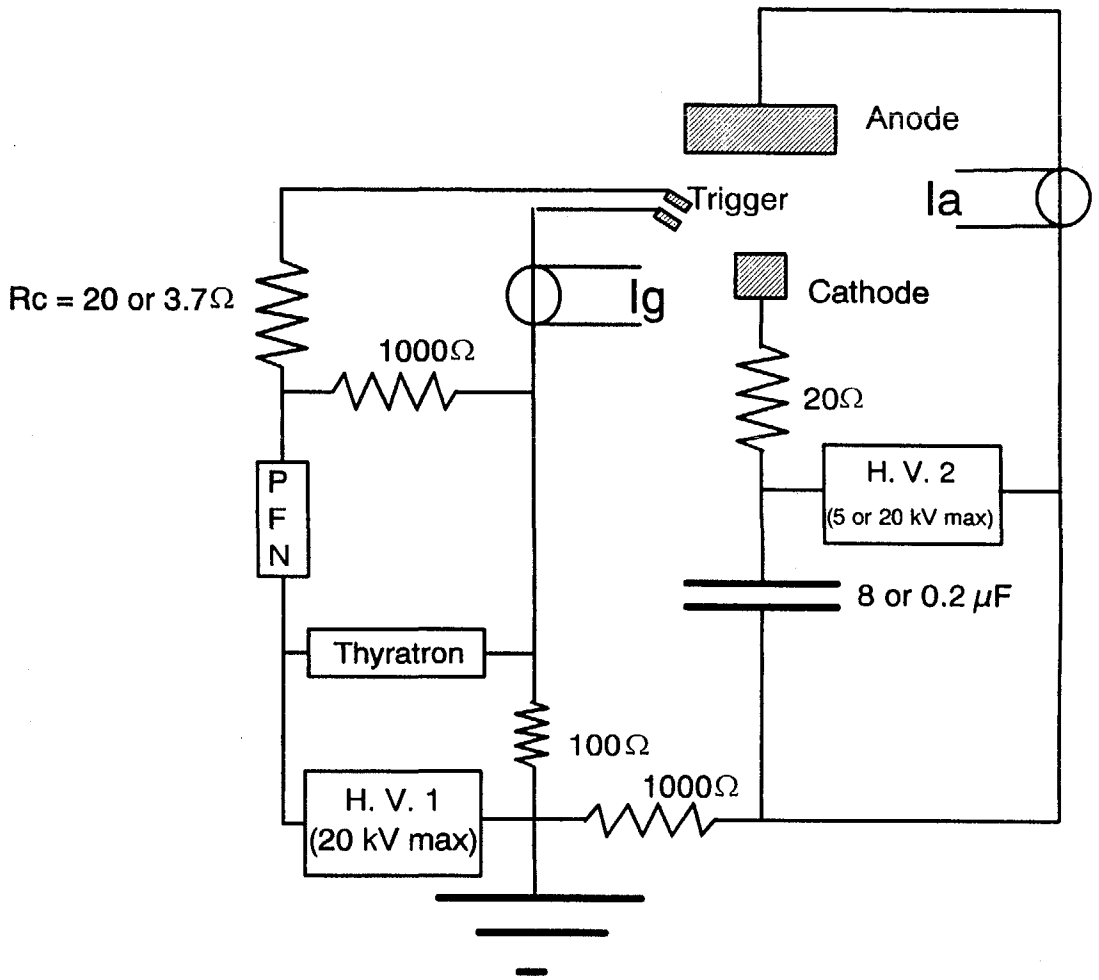

Trigger and arc pulse

Typical values : trigger : 300-1400 A, 4 μs, arc : 250A, 60 μs

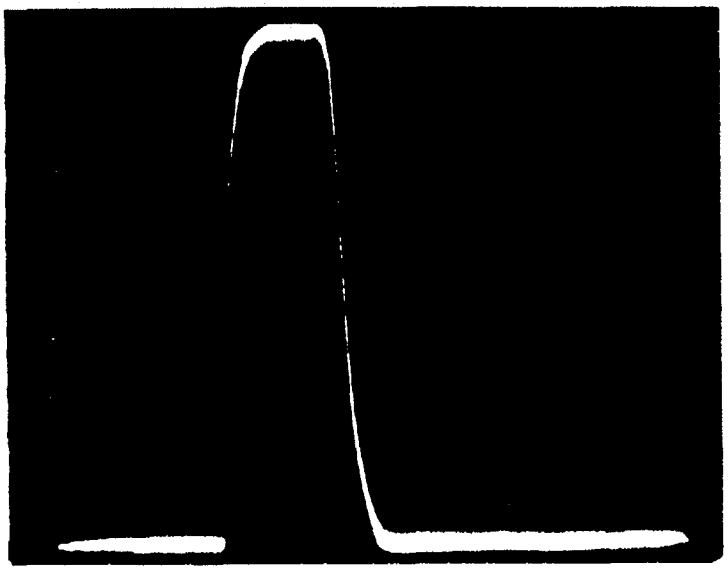

Trigger 2 μs/cm

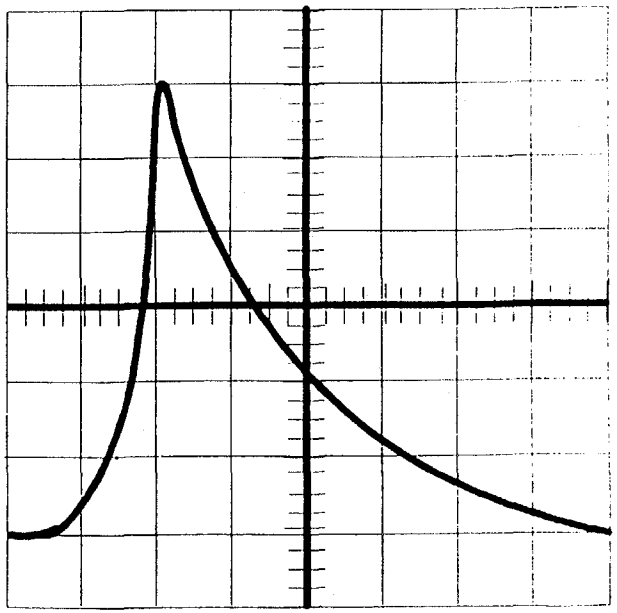

Arc 20 μs/cm

Trigger and arc pulse

Typical values :

trigger : 300-1400 A, 4 μs

arc : 200A, 60 μs

---- : Trigger

——— : Arc

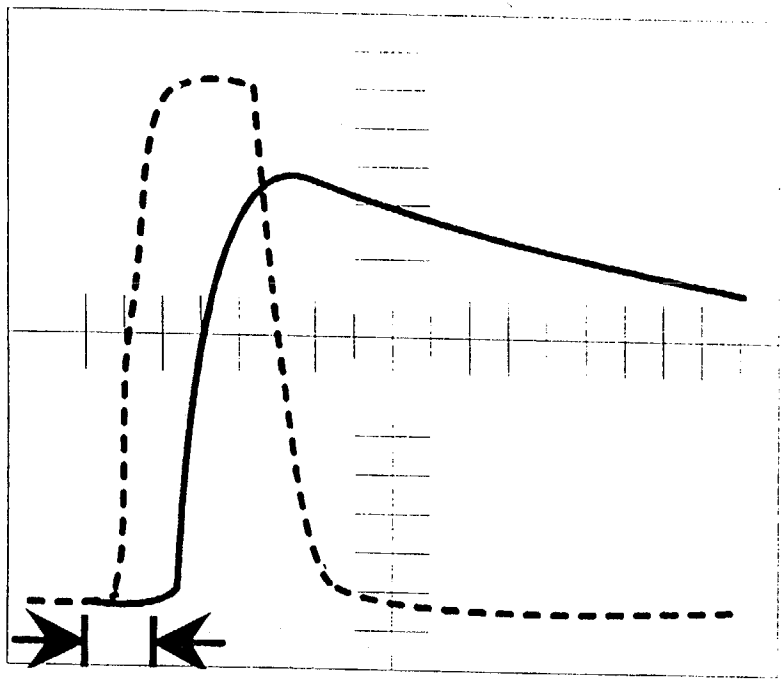

Firing delay

1 μs/cm

Parameters

. Anode-cathode gap length

. Anode-cathode voltage

. Trigger current

. Trigger-cathode gap length

. Firing rate = $\frac{\text{number of anode-cathode arc}}{\text{number of trigger arc}}$

Firing rate for 2 anode-cathode distances versus trigger current.

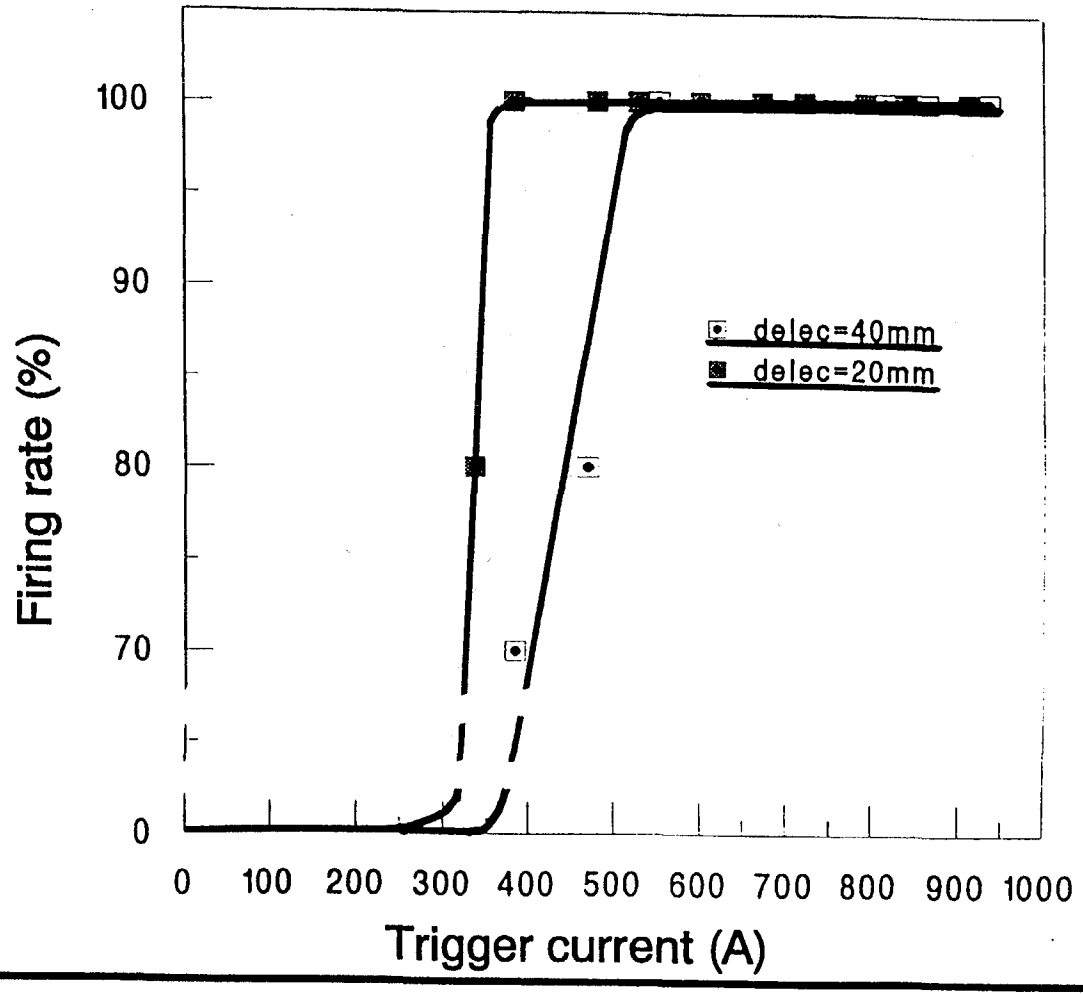

Trigger current to get a 90-100 % firing rate versus anode-cathode gap length

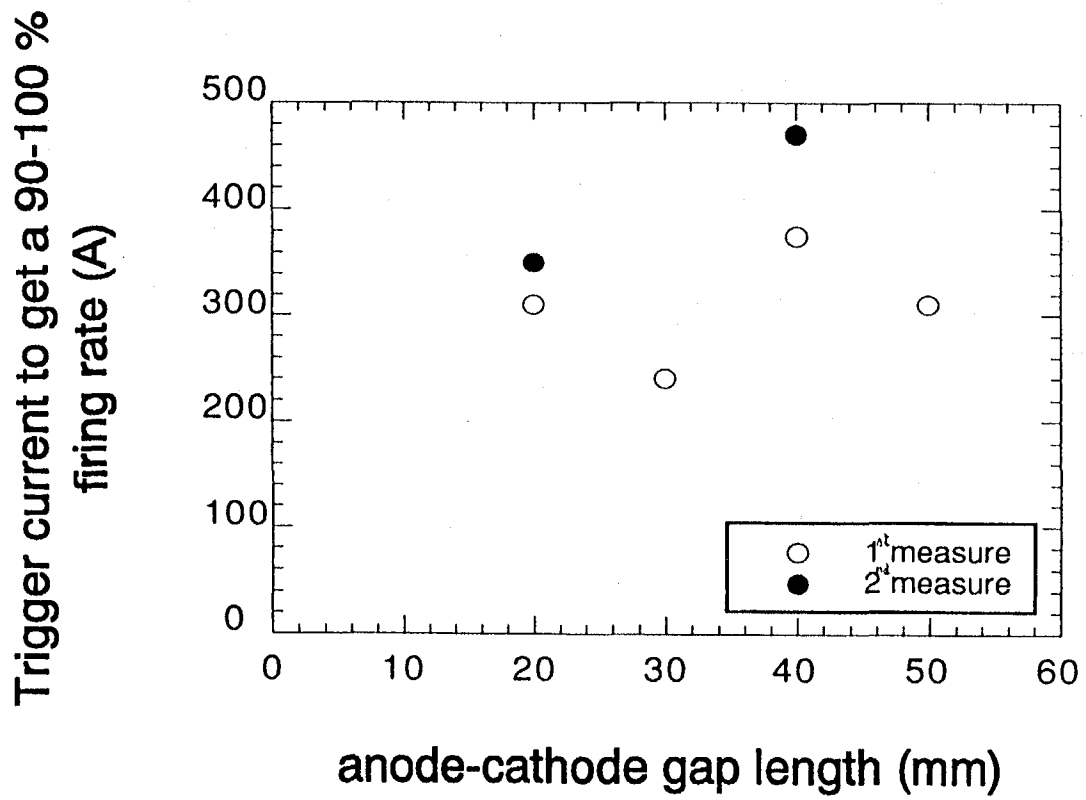

Firing rate versus trigger current for different anode-cathode voltage

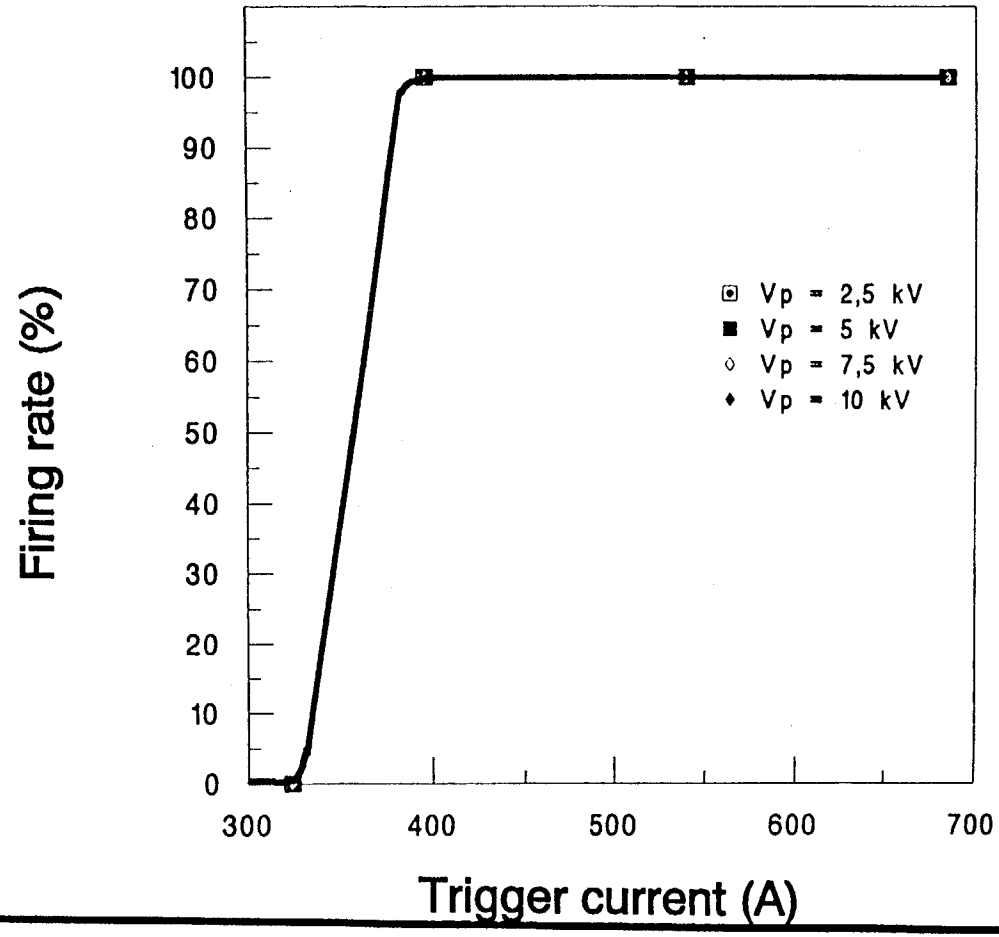

Firing rate versus trigger current for different trigger-cathode gap length

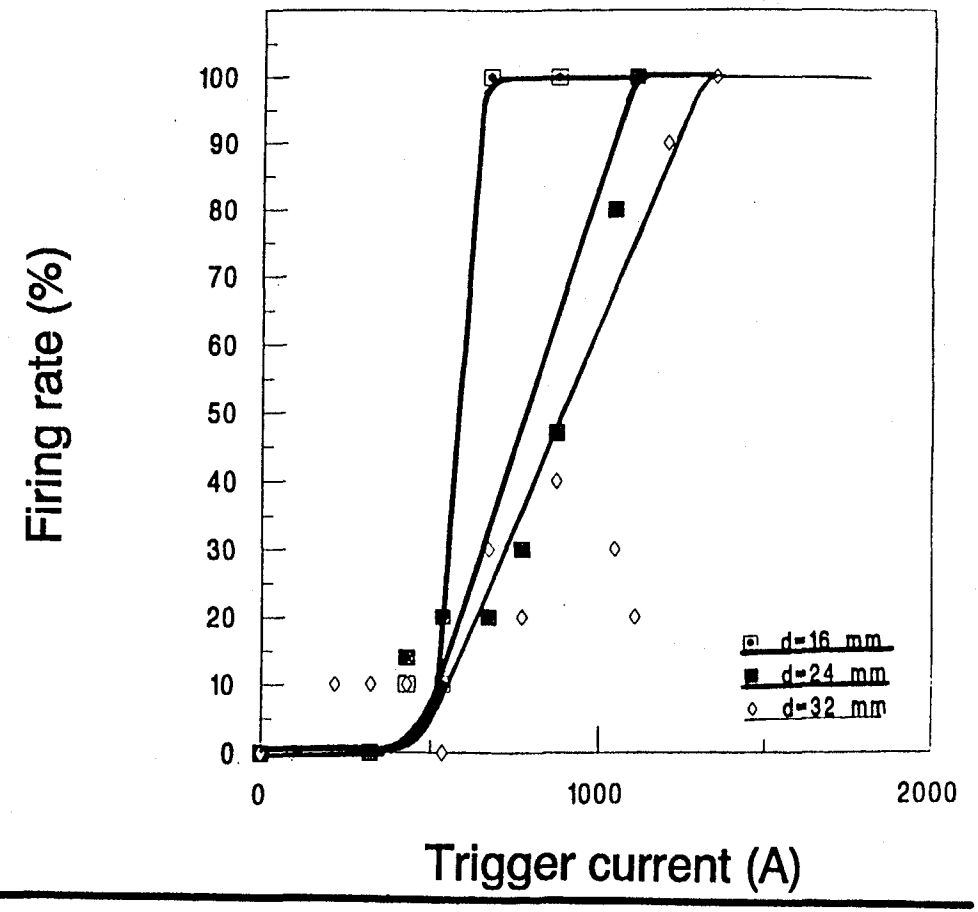

Trigger current to get 90-100 % firing rate, for different trigger-cathode gap length

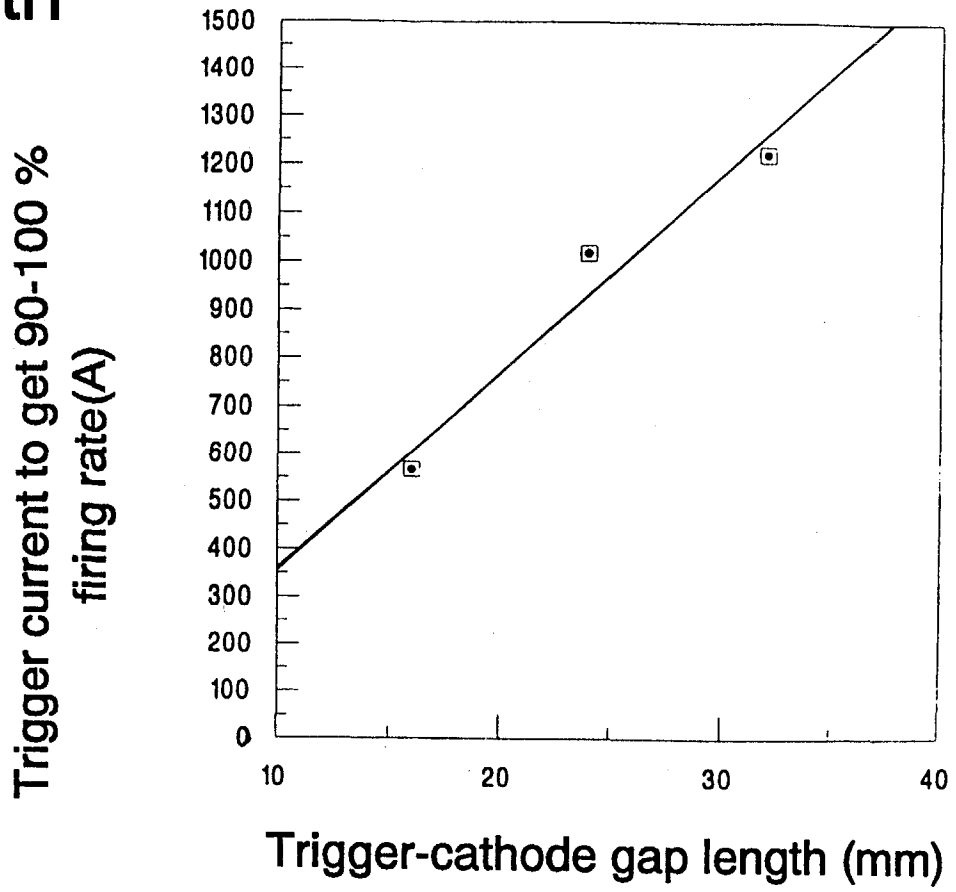

Schematic representation of the magnetic field applied over the trigger

It was tested to enhance triggering rate at low current.

Magnetic field approximately 1000 Gauss

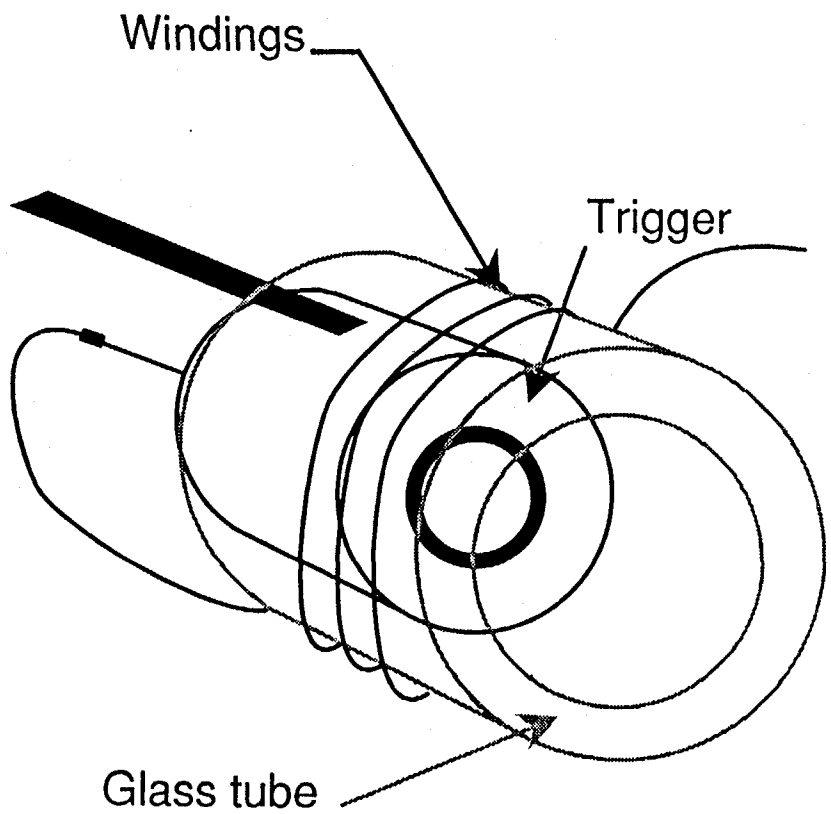

Firing delay with and with no magnetic field

Trigger-cathode gap length 40 mm.

---- : Trigger

——— : Arc

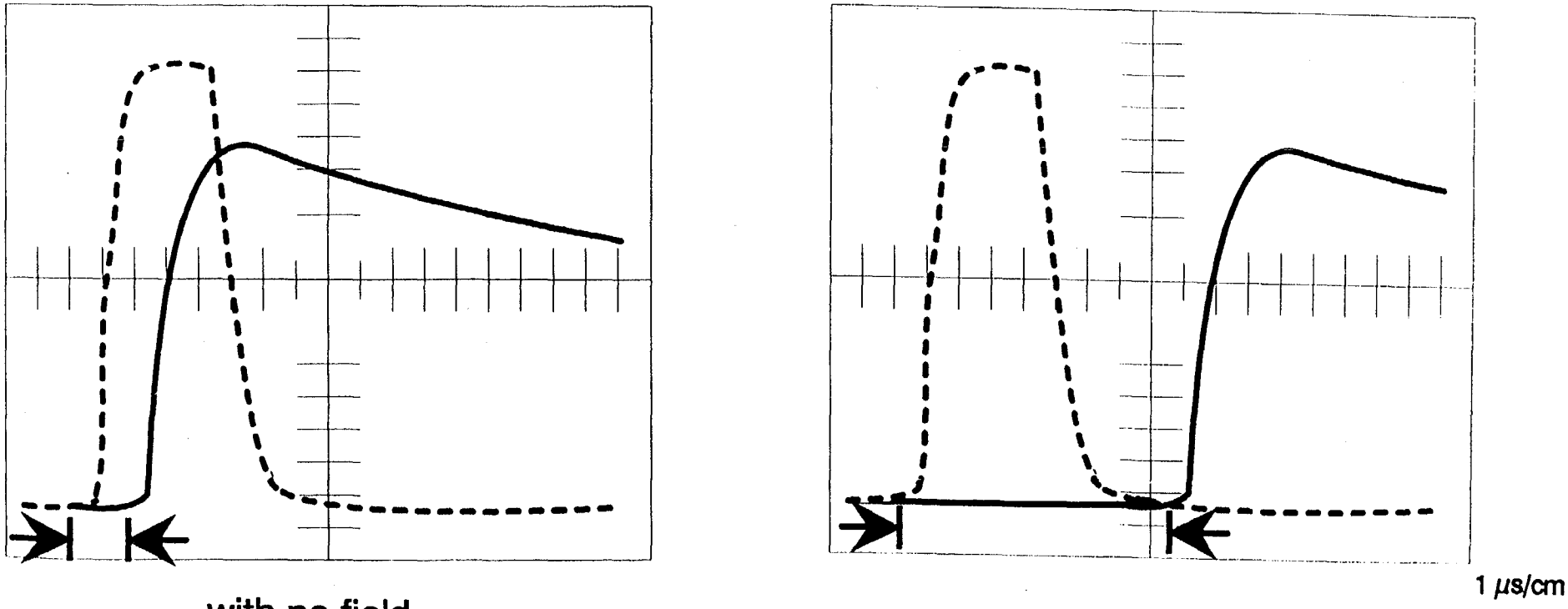

with no field

with field

Effects of the magnetic field

. Firing rate for 2 anode-cathode distance.

. Results are scattered

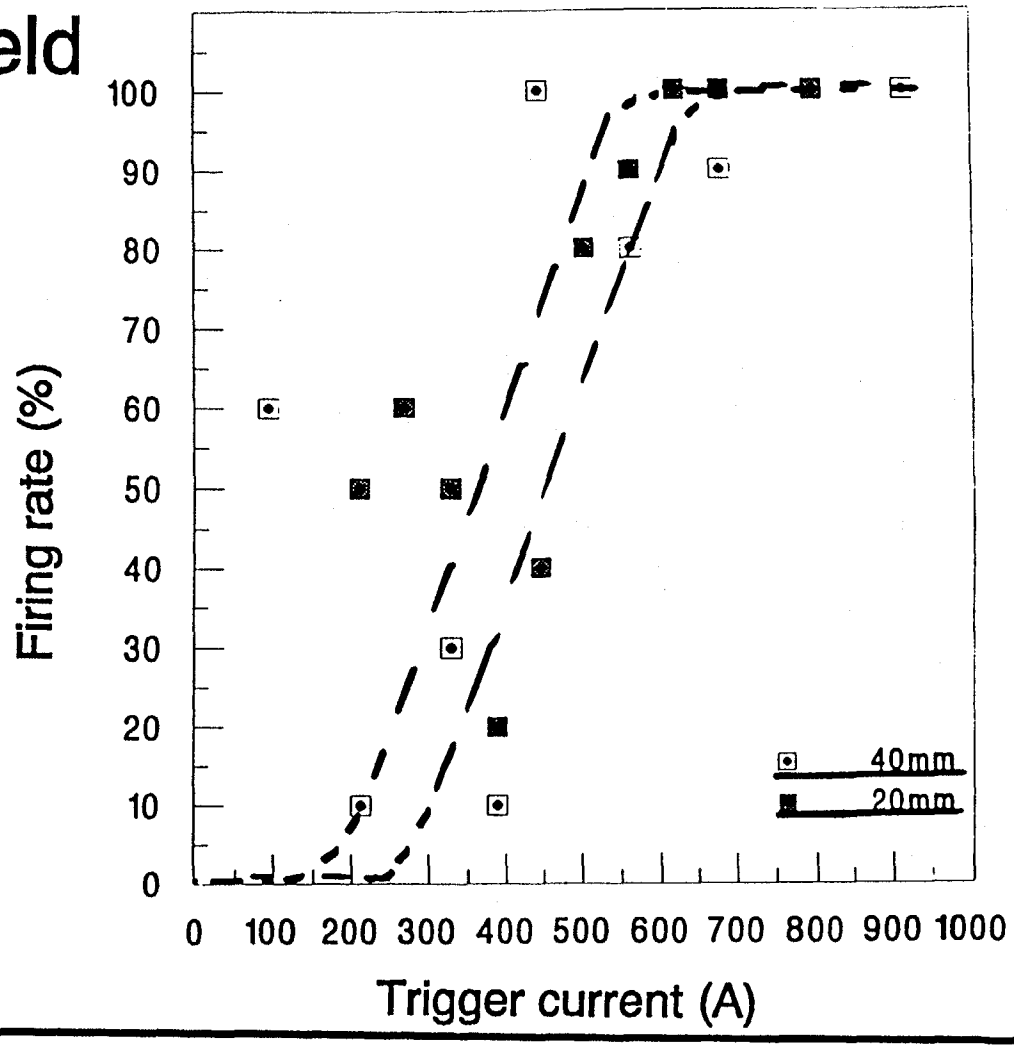

Conclusions

. we investigate the firing rate versus various paramaters :

  . trigger-cathode gap length has an important effect

  . anode-cathode gap length has a little effect

  . anode-cathode voltage has no effect

  . application of a magnetic field over the trigger scatters the results and enhance the triggering delay.

. we were able to fire arcs operating with stainless steel, copper, molydbenum and carbon cathodes.

Gas and Metal Ion Sources

Efim Oks*† and George Yushkov*

*High Current Electronics Institute,
Siberian Division of the Russian Academy of Sciences,
4 Akademichesky Ave., 634055 Tomsk, Russia.
†State Academy of Control System and Radioelectronics,
40 Lenin Ave., 634050 Tomsk, Russia.

I Inroduction

The positive ion sources are now of interest owing to both their conventional use, e.g., as injectors in charged-particle accelerators and the promising capabilities of intense ion beams in the processes related to the action of ions on various solid surfaces[1]. For industrial use, the sources of intense ion beams and their power supplies should meet the specific requirements as follows: They should be simple, technologically effective, reliable, and relatively low-cost. Since the scanning of an intense ion beam is a complicated problem, broad ion beams hold the greatest promise. For the best use of such beams it is desirable that the ion current density be uniformly distributed over the beam cross section. The ion beam current density should be high enough for the treatment process be accomplished for an acceptable time. Thus, the ion sources used for high-current, high-dose metallurgical implantation should provide for gaining an exposure dose of $\sim 10^{17}$ cm^{-2} in some tens of minutes. So the average ion current density at the surface under treatment should be over 10^{-5} A/cm^2. The upper limit of the current density depends on the admissible heating of the surface under treatment. The accelerating voltage of an ion source is dictated by its specific use; it seems to lie in the range from $\sim$ 1 kV (for the ion source used for surface sputtering) to $\sim$ 100 kV and over (for the ion sources used for high-current, high-dose metallurgical implantation).

The above requirements are met by mevva-type metal-ion sources depending for their operation on a vacuum arc[2]. The successful development of this type of ion source is testified both by the growing number of research groups that develop and use such sources and by the buildup of relevant publications (see Ref. 2). Metal ion beams can be produced by a variety of methods[3,4], among which the concept harnessed in the mevva-type sources, the extraction of an ion beam from the plasma produced by the cathode spots of a vacuum arc, is distinguished by a number of fundamental advantages[4–6]. The cathode spots of a vacuum arc eject directed plasma jets consisting of the cathode material. Therefore it is possible to produce a plasma medium for the generation of a beam of ions of any conducting material, composite materials included. The ion current fraction in the plasma is rather high, 6–10% of the vacuum arc current. Despite the high temperature in cathode spots, they operate on the cathode surface being cool as a whole; so such a discharge system possesses all advantages of a cold emitter. A vacuum arc can operate at residual gas pressures as low as is wished and at any currents exceeding the threshold current for

the existence of a cathode spot. With the fact that this method is simple to realize, the reasons for the intense development of this type of source are obvious.

Both metal and gas ion beams can be used for surface treatment, and it is not clear now which of these two types of ion beams will find preferred use.

A well-developed application of ion sources is the production of intense beams of positive gas ions. As a rule, for the generation of plasma a type of low-pressure discharge is used. The ion sources based on an arc discharges in a magnetic field[7], with their constructional features, show the highest energy efficiency and gas economy. The replacement of the hot emitter by the plasma of a vacuum arc will eliminate the energy consumption for heating and prevent the cathode from contamination and blowout at an abnormally increased pressure.

II A gas/metal ion source

(a) The principle of operation

We have developed a gas/metal ion source named TITAN[8,9] where a metal ion beam

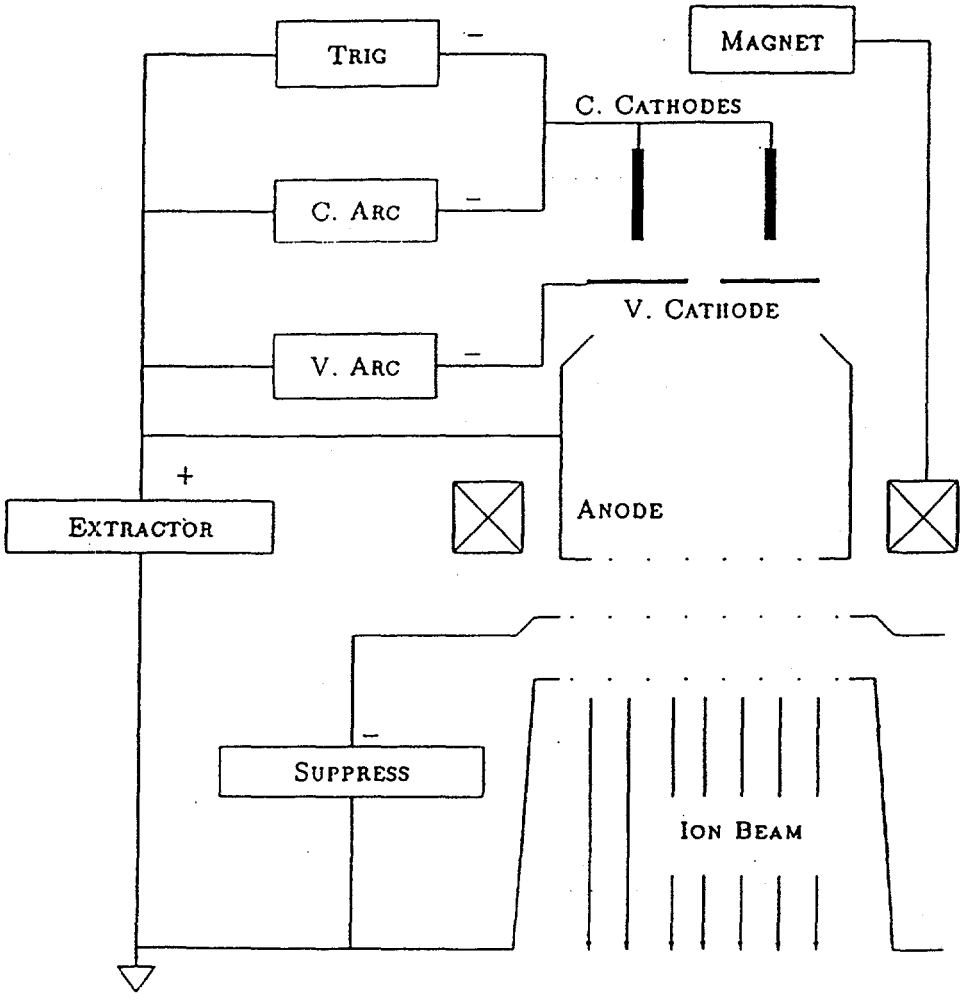

Fig. 1. The electrode system of the TITAN ion source.

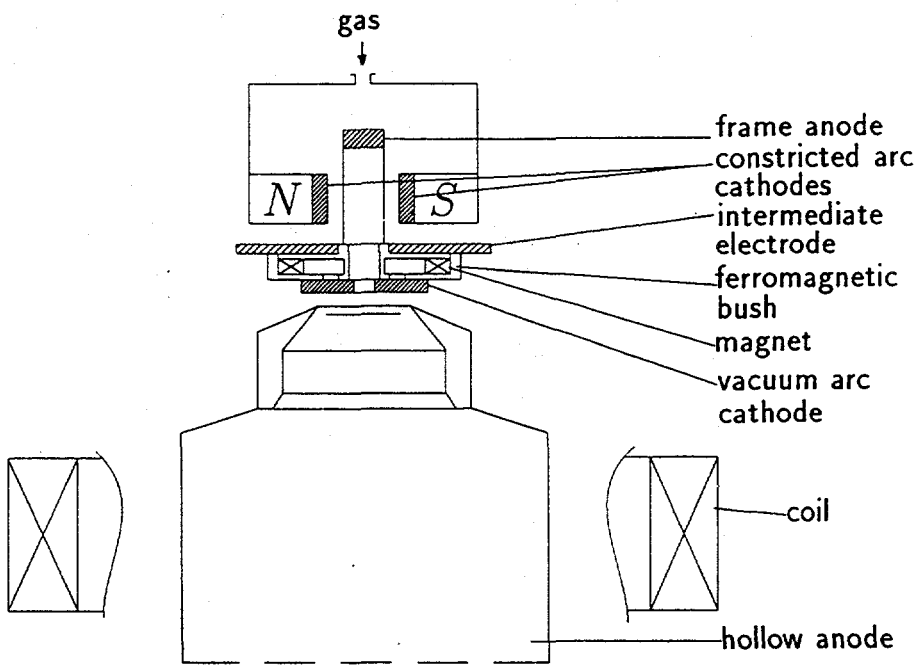

Fig. 2. The discharge chamber of the TITAN ion source.

is generated like in a mevva source and a gas ion beam like in a cold-cathode duoPIGatron with a common hollow cathode (Fig. 1). For the production of gas ions a constricted arc is ignited between the cold cathodes and the hollow anode; it is constricted by a hole in an intermediate electrode (Fig. 2). The constricted arc cathodes are placed in a Penning discharge chamber where plasma-forming gas is supplied. Making the working gas flowing and the discharge operating in one path through the constriction hole allows efficient ionization of the gas by the electrons having passed through the double layer to produce in the hollow anode a gas-discharge plasma necessary for the generation of an ion beam. The vacuum arc powered from an independent power supply is initiated between the vacuum arc cathode and the hollow anode. When the arc operates, the cathode material plasma fills the hollow anode producing the ion-beam-generating medium. With combined operation of the discharges, it is possible to produce an ion beam containing both gas and metal ions. The extraction system consists of three grids. The first one is a plasma grid being at the potential of the hollow anode. Two other grids made of metallic W-Re filaments stretched in parallel form an acceleration-deceleration system. The ion beam formed is transported onto a collector placed at a distance of 0.2–1.5 m from this system. We have developed two basic version, pulsed and dc, of the ion source.

(b) The pulsed ion source

For the pulsed version, the accelerating voltage in various ion sources varies from 10–60 kV to 20–100 kV and the beam cross-sectional area from 200 to 300 cm^2. The constricted arc and vacuum arc pulse duration is $\sim$ 400 μs at a pulse repetition rate of 1–50 pps.

The peak current of gas and metal ion beams is 0.1–1 A depending on the constricted arc current (10–50 A) and vacuum arc current (20–200 A). The fraction

of gas and metal ions in the ion beam was controlled by varying the constricted arc and vacuum arc currents. The control limits were found indirectly using RBS analysis of the irradiated target and for a Ta/Ar pair they were from 0.05/99.5 at.% to 90/10 at.%, respectively. Beams of He, Ne, Ar, Xe, Kr, N, C, Mg, Al, Ti, Cu, Nb, Cr, Fe, Co, Ni, Zn, Zr, Sn, Sm, Ta, W, Re, Y, Bi, Pb, and Mo ions were produced. This source version was used for high-dose implantation and ion-beam assistance.

(c) The dc ion source

We do not think that the best way to increase the average ion beam current is to increase the frequency and/or the peak pulse current since this would complicate the power supply system and involve additional problems with stable discharge initiation and an increase in the ion current density in the beam is limited by the capabilities of the extraction system used. The simplest method of increasing the average beam current is realization of the dc mode of operation of the ion source. We were able to realize the dc mode having modernized the discharge system of the ion source by making the construction more heatproof and using additional cooling. The accelerating voltage (10 kV) and the arc currents (10 A) were limited by the power (10 kW) of the power sources used for this ion source version. Beams of Ar, Xe, N, O, Mg, and Al ions have been produced with currents of 0.2–0.3 A, which is more than an order of magnitude higher than the average beam current for the pulsed version. We used the dc ion beam sources in experiments on surface sputtering and on thin-film deposition by reactive ion sputtering.

(d) The magnetic field effect

A magnetic field of up to 0.01 T produced by a solenoid, when applied to the discharge system of the ion source, increases the current extracted from the arc plasma. Measurement of the plasma parameters (n, T_e, φ) performed with the use of Langmuir and thermal emission probes have made it possible to find the mechanism for the effect of a magnetic field on the emission of ions. On application of a magnetic field, the plasma potential φ with respect to the anode and to the constricted and the vacuum arcs changes from positive to negative. Under these conditions the plasma ions are kept from going to the anode by the electrostatic field of the charged plasma.

For the gas ions of the constricted arc that go away to the anode or plasma electrodes, a potential barrier of negative anode fall $U = Ze\varphi$ appears. If the mesh size l of the emission grid is smaller than the thickness of the negative anode fall layer l_1, the barrier prevents the ions to go out beyond the grid, and the increase in ion current is insignificant. If $l > 2l_1$, the barrier can be partially eliminated by the field of the acceleration gap. When l is further increased, the emission of ions occurs from an open plasma surface; the ion current density reaches its maximum determined by the Bohm formula and becomes independent of l.

For the directed flow of the vacuum arc metal ions, a change in φ results in that some ions whose radial velocity is too low to overcome the potential barrier reflect from the latter. The condition that an ion of charge Z having escaped from the cathode spot with energy E_i at the angle α to the system axis travels through the

anode cavity is $\alpha \leq \arcsin\sqrt{Ze\varphi/E_i}$. So, the ion flow is constricted by the action of the radial electric field in the plasma. The ion current onto hollow anode walls decreases, while the emission current correspondingly increases. Since for most of the ions emitted by the cathode spot which comply with the travelling condition the inequality $E_i \cos^2\alpha > Ze\varphi$ is valid, the effect of the l value on the ion emission current is not so strong. It should be noted that the applied magnetic field does not influence on the generation of ions in the cathode spot; it is responsible only for the changes in the anode plasma of the vacuum arc.

The magnetic field applied to the hollow anode region increases the densities of both the "gas" and the "metal" plasmas at the axis of the discharge system. In this case the condition that the plasma emission surface is stabilized by the grid,

$$d < \frac{2}{3}\left(\frac{\varepsilon_0}{0.4}\right)^{1/2}\left(\frac{2}{q_i k T_e}\right)^{1/4}\frac{U_{ac}^{3/4}}{n^{1/2}}$$

can be violated, and the plasma will penetrate into the acceleration gap. The plane plasma boundary will transform into a convex boundary, and the accelerating field will become defocusing for the ion beam in its center. A partial defocusing of the ion beam makes the current density distribution over the beam cross section more uniform. The current density distribution can be varied, with the acceleration gap geometry and the accelerating voltage being fixed, by varying not only the discharge currents but also the magnetic field strength. Since the accelerating and the cutoff electrodes have a high geometrical transparency and the defocusing of the ion beam increases the ion losses at these electrodes only slightly, this effect can be harnessed to produce a more uniform distribution of the ion current density over the beam cross section.

III Transverse extraction of an ion beam from the anode cavity

The ion source described in Refs. 8 and 9 utilize axial extraction of a cylindrical ion beam from the anode cavity plasma. Being wide-spread, this technique for the formation of ion beams seems not to be the best. Cathode spots are "point" plasma sources; so the plasma density distribution near the emission boundary, and hence the ion current density distribution over the beam cross section, are nonuniform. Owing to the circular beam cross section, a nonuniformity in the embedded atom dose distribution appears in both the longitudinal and the radial scanning of the surface under treatment by the beam. These difficulties are also substantial for the extraction of a gas ion beam from the constricted discharge plasma, since the ionization occurs in the main near the constriction channel.

An alternate method is to fill the anode cavity with the plasma produced by several sources and to extract rectangular-cross-section beams through an emission window made in the side wall of the hollow anode. Preliminary experiments were carried out on a setup shown schematically in Fig. 3. Used as a plasma source was the discharge chamber of the source dc version. A rectangular emission window

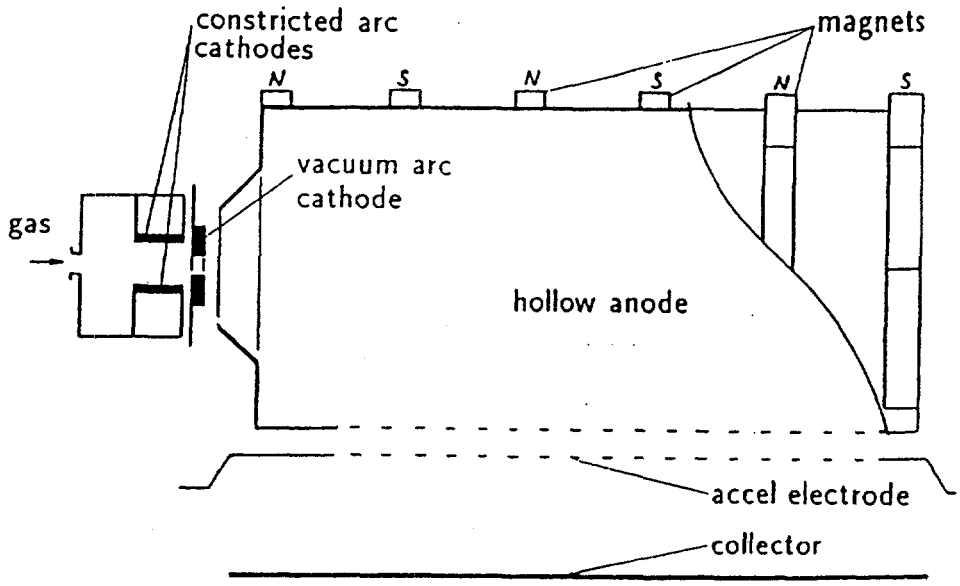

Fig. 3. The electrode system of the ion source with transverse extraction of the beam from the anode cavity.

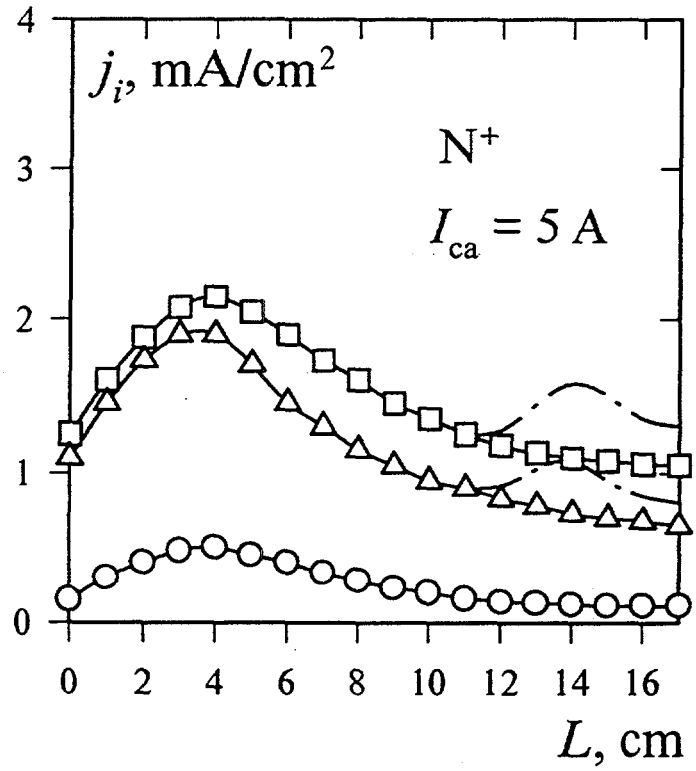

Fig. 4. The nitrogen ion beam current density profiles for constricted arc current of 5 A. o – zero magnetic field; △ – linear and □ – azimuthal configuration of magnets. Dashed lines – magnets at the anode end.

4×17 cm^2 in size was made in the anode side wall of length 19 cm and diameter 11 cm.

To keep the plasma charged particles from going to the anode cavity walls, a 0.2-T multipole magnetic field was used that was produced by Sm-Co constant magnets placed on the external side of the anode cavity. Two positions of the magnets on the anode cylinder were utilized: a linear position with evenly spaced 11 rows of magnets placed along the hollow anode cylinder and an azimuthal position with evenly spaced 6 rows of magnets placed in a circle around the hollow anode cylinder. 12 magnets were placed radially on the end of the hollow anode. The nitrogen ion current density distribution over the ion beam longitudinal section obtained for a constricted arc current of 5 A is given in Fig. 4. The use of a "magnetic wall" results in a 3–5 fold increase in ion current. The increase in ion current is a maximum for the azimuthal arrangement of magnets. Application of a magnetic field to the anode end results in the appearance of the second maximum in the ion current density distribution.

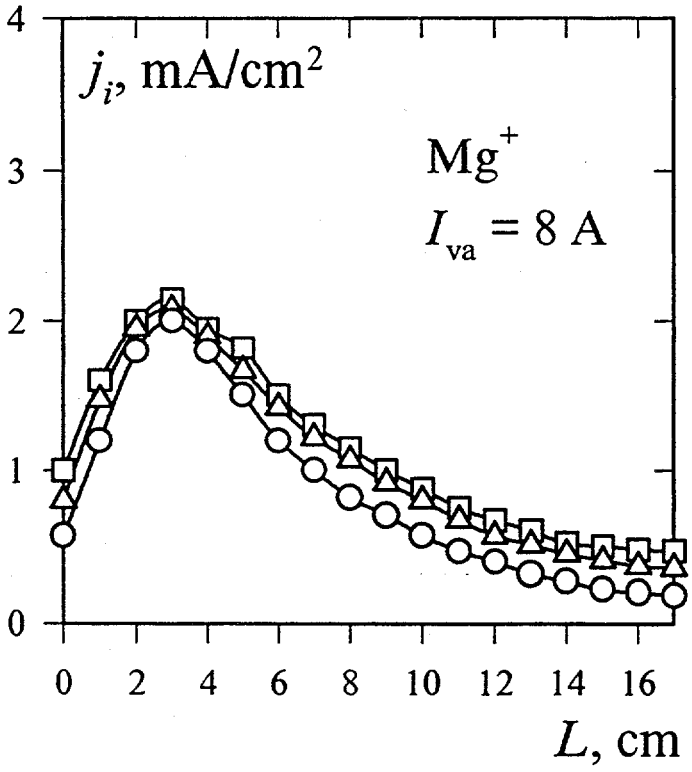

Fig. 5. The magnesium ion beam current density profiles for vacuum arc current of 8 A. o – zero magnetic field; △ – linear and □ – azimuthal configuration of magnets.

The magnesium ion current density distributions over the beam cross section measured for two configurations of the applied magnetic field and with no magnetic field at a vacuum arc current of 8 A are given in Fig. 5. The run of the $j = f(L)$ curves corresponds to the cosine curve that describes the density distribution for the plasma coming into the anode cavity from the cathode region of the vacuum arc. In this case, since the magnetic field is localized near the anode cavity walls, it would affect this distribution only slightly. This weak, compared to the case of a constricted arc, effect of the applied magnetic field on the beam current seems to

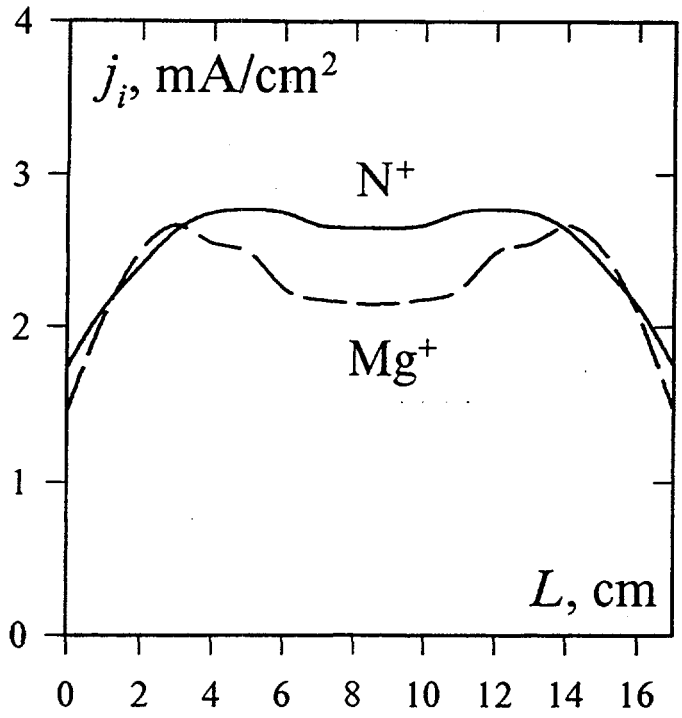

Fig. 6. Expected ion beam current density profiles for the discharge chambers used and the azimuthal configuration of magnets.

be due to the high velocities of the ions emitted by the cathode spots. According to estimates, for Mg^+ ions of energy ~ 40 eV [6] the Larmor radius near the anode cavity walls is over 1.5 cm, while for a constricted discharge it is ~ 0.1 cm. The slight increase in ion current on the application of a magnetic field is perhaps related to the reflection of only low-energy plasma ions from the potential barrier.

The obtained current density distributions for the ions extracted from the vacuum arc and constricted arc plasmas are substantially nonuniform; however, the cross-sectional uniformity of the ion beam can be improved by placing two discharge chambers at the ends of the hollow anode. In this case, owing to the superposition of the plasma flows, more uniform distributions are anticipated, such as those shown in Fig. 6. In view of the similarity laws, it is possible to obtain similar distributions for broader beams.

IV Gas-discharge plasma initiation of a vacuum arc

For stable operation of a pulsed ion source it is necessary to provide stable initiation of the vacuum arc cathode spots. The gas-discharge ignition of a vacuum arc in the TITAN ion sources has made the cathode lifetime as long as over 10^7 shots. We currently perform a research work aimed at the development of a mevva-type ion source with a gas-discharge-initiated vacuum arc. To ignite the initiating gas discharge at low pressures, a pulsed ($\tau = 1$ ms) magnetic field of up to 3 T is used.

In the experimental setup (Fig. 7) the Penning discharge cell is formed by a

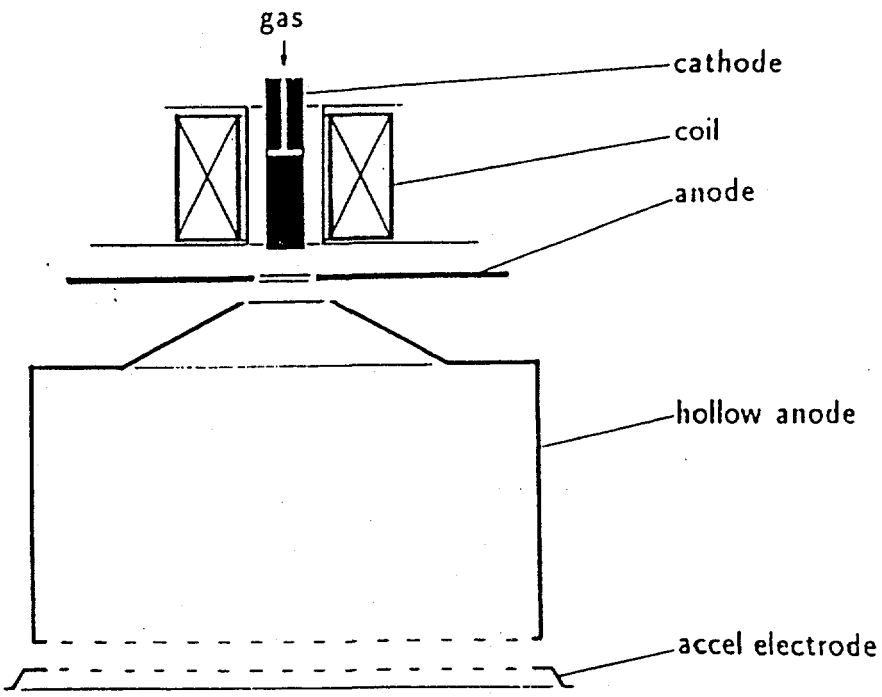

Fig. 7. The electrode system of the source with a vacuum arc initiated by a Penning discharge in a strong magnetic field.

titanium cathode, a hollow anode, and an anode. The first two electrodes serves as cathodes and the third one is the anode of the Penning initiating discharge powered from a dc voltage source producing 3–7 kV of voltage. A capacitor of capacitance 0.25 μF charged from this source is connected between the cathode and the anode. When the solenoid produces a magnetic field pulse and a 3–7-kV voltage is applied to the Penning cell, a Penning initiating discharge is ignited in the discharge gap. The Penning initiating discharge plasma fills the cathode-anode gap where the initiating arc discharge is ignited due to the discharge of the capacitor. The current therewith reaches 100–200 A, which exceeds the threshold current for the formation of cathode spots, in less than 1 μs. At the cathode end cathode spots appear, and the cathode material plasma produced by the cathode spots fills the cathode–hollow anode gap. This plasma in turn gives rise to the initiation between the cathode and the hollow anode, of a vacuum arc that is sustained for 150 μs by the discharge of the LC circuit. On ignition of an initiating arc discharge, stable initiation and operation of a vacuum arc with a current of 50–300 A is observed during the pulse. The vacuum arc initiation voltage is 100–350 V. The least gas pressure at which the vacuum arc initiation ensured decreases with increasing magnetic field. For $B = 3$ T the required gas pressure in the hollow anode can be reduced to $8 \cdot 10^{-5}$ Torr. This allows the conclusion that this technique for the initiation of vacuum arc cathode spots can be used successfully at lower, compared to the ion source, pressures. The beam current of Ti ions of all multiplicities extracted from the device was 0.2–1.5 A depending on the vacuum arc current. This research work is supported by the US

Department of Energy through Lawrence Berkeley Laboratory under the contract 4602410.

V A gas ion source based on a hollow-cathode discharge

A glow discharge with a hollow cathode can be used to produce broad beams of gas ions. However, the minimum pressure at which a discharge can still stably operate in the low-pressure mode is high enough ($\sim 10^{-3}$ Torr) in order that an intense ion beam could be produced and transported to a large distance.

Reducing the pressure results in that the primary electrons produced at the cathode as a result of ion-electron emission, oscillating in the cathode cavity, have no time to spend their energies in ionizing collisions with working gas atoms, and the discharge goes over into its high-voltage form. The decrease in anode area that increases the number of oscillations of the primary electrons in the cathode cavity is limited by the value of $S_a = S_c\sqrt{m_e/m_i}$ at which a double layer is formed near the anode[10]. It is possible to ensure the discharge operation at a lower pressure by providing an income of fast, capable of ionizing electrons from an external source into the anode cavity.

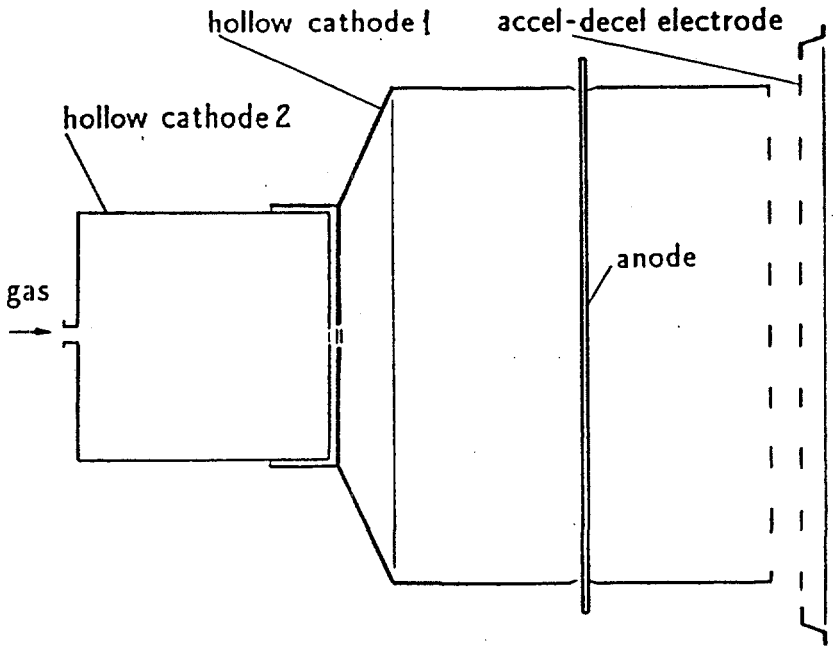

Fig. 8. The electrode system of the gas ion source based on a hollow-cathode discharge.

The design of the device is shown schematically in Fig. 8. The main discharge operated between cylindrical hollow cathode *1* and an anode. This discharge was

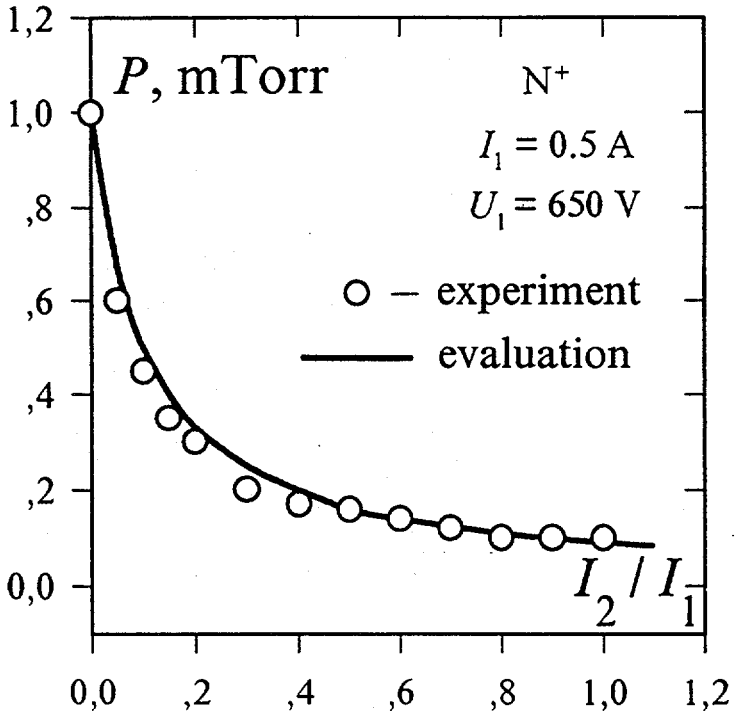

Fig. 9. Low limit pressure p of the hollow-cathode *1* discharge versus the auxiliary-to-main discharge current ratio I_2/I_1. The main discharge operating voltage U_1 = 650 V and current $I_1 = 0.5$ A. Nitrogen.

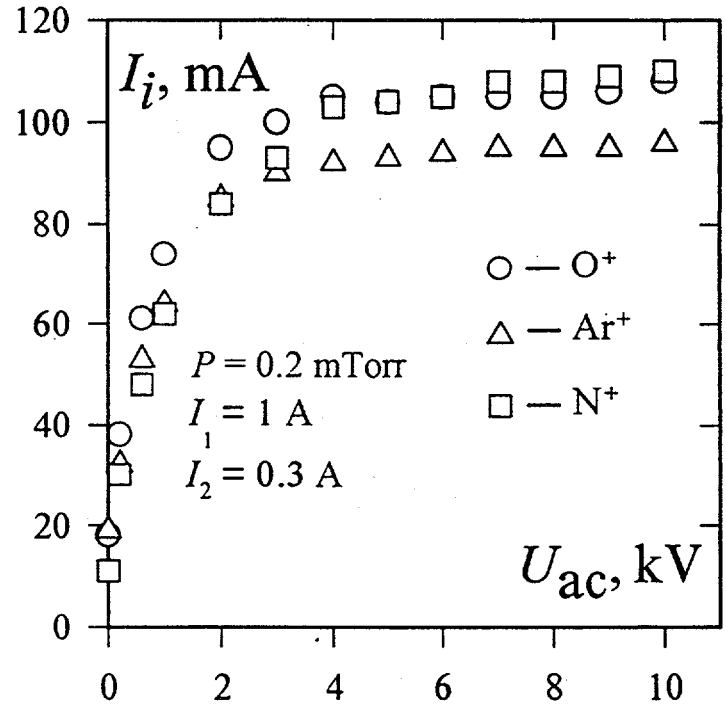

Fig. 10. Ion beam current as a function of accelerating voltage for ions of various gases.

initiated and sustained by an auxiliary discharge with hollow cathode *2*. Cathode *1* served as an anode for axiliary discharge. The working gas was fed into the cavity of cathode *2*. The gas pressure difference at the diaphragm separating the cathodes ensured an elevated pressure in hollow cathode *2* (over $5 \cdot 10^{-3}$ Torr) at which the auxiliary discharge was stably initiated and operated. The auxiliary discharge afforded the electron emission into the cavity of cathode *1*. In cathode *1* a gas-discharge plasma was produced from which an ion beam was extracted. The discharges were powered from two dc voltage sources (1 kV, 1 A).

As a rough approximation, it can be shown that the pressure at which the discharge operation voltage remains constant depends on the auxiliary-to-main discharge current ratio as $p \propto (\gamma + I_2/I_1)^{-1}$. The dependence of p on I_2/I_1 obtained in accordance with this estimation (for the secondary ion-electron emission coefficient $\gamma = 0.1$ electron/ion) and that measured for the main discharge operation voltage $U_1 = 650$ V and current $I_1 = 0.5$ A for nitrogen are given in Fig. 9. Thus, injection of additional electrons into the plasma of a hollow-cathode discharge reduced the working pressure from 10^{-3} to 10^{-4} Torr.

With the accelerating voltage of 2–10 kV, beams of various gases, oxygen included, with currents of up to 0.1 A have been produced (Fig. 10). The beam cross-sectional area was $\sim$ 140 cm^2. The ion current from the plasma onto the whole surface of the hollow cathode is the Bohm current. So, the beam-to-discharge current ratio is proportional to the emission area to the total area of the hollow cathode, and the beam current can be increased by increasing the latter ratio. The highly simple design of the ion source and its stable parameters offer promise for its application in future.

References

[1] See, for instance, Proc. of the Conference on Ion Beam Modification of Materials, published in Nucl. Instrum. Methods.

[2] I.G. Brown, Rev. Sci. Instrum. **65**, 30611 (1994).

[3] L. Valyi, *Atom and Ion Sources* (Wiley, New York, 1977).

[4] *The Physics and Technology of Ion Sources*, ed. by I.G. Brown (Wiley, New York, 1989).

[5] I.G. Kesaev, *Cathode Processes in Electrical Arcs* (Nauka, Moscow, 1968).

[6] *Vacuum Arcs: Theory and Applications*, ed. by J.M. Lafferty (Willey, New York, 1980).

[7] A.T. Forrester, *Large Ion Beams* (Willey, New York, 1988).

[8] S.P. Bugaev, A.G. Nikolaev, E.M. Oks, P.M. Schanin, and G.Yu. Yuskov, Rev. Sci. Instrum. **63**, 2422 (1992).

[9] S.P. Bugaev, A.G. Nikolaev, E.M. Oks, P.M. Schanin, and G.Yu. Yuskov, Rev. Sci. Instrum. **65**, 3119 (1994).

[10] A.S. Metel', Zh. Tekh. Fiz. **54**, 241 (1984).

VACUUM ARC ION SOURCES — ACTIVITIES & DEVELOPMENTS AT LBL

Ian Brown
Plasma Applications Group
IBT/AFRD/LBL

Lawrence Berkeley Laboratory
University of California
Berkeley

The Team ('95)

Ian Brown
Andre Anders
Simone Anders
Mike Dickinson
Bob MacGill
Othon Monteiro
Sebastien Raoux
Zhi Wang
Efim Oks (guest scientist from Tomsk)
Gera Yushkov (guest scientist from Tomsk)

Vacuum Arc Ion Source (& plasma) Developments

- Spark source / high charge state work
  - A vacuum spark, not arc. For very high charge states.
- High charge states in magnetic field
- Hybrid metal / gas operation
- Multipole work, for plasma profile flattening
- Workhorse Mevva V for many implantation applications
- Broad beam work
  - 50 cm embodiment made and used for implantation
- Macroparticle removal
  - Plasma duct installed and demonstrated

Vacuum arc ion source & beam characteristics

Extraction voltage		~ 10 – 100 kV
Ion beam energy		~ 10 – 300 keV
Beam current		~ 10 mA – 20 A
"	diameter	~ 0.1 – 50 cm
"	divergence	$\geq 3^{o}$
"	emittance	$\geq 0.05\ \pi$ cm.mrad.
"	length	~ 10 μs – dc
Ion charge state		~ 1 – 6
Ion species		Li, C, Mg, Al, Si, Ca, Sc, Ti, V, Cr, Mn, Fe, Co, Ni, Cu, Zn, Ge, Sr, Y, Zr, Nb, Mo, Pd, Ag, Cd, In, Sn, Sb, Ba, La, Ce, Pr, Nd, Sm, Gd, Dy, Ho, Er, Tm, Yb, Hf, Ta, W, Ir, Pt, Au, Pb, Bi, Th, U

Ion implantation

- Broad-beam mode (as opposed to scanned spot)
- Typical implantation parameters
  - Energy ~ 50 – 150 keV
  - Dose ~ 10^{12} – 10^{18} cm^{-2}
  - Range ~ 1000 Å
  - Straggling ~ 500 Å

Ion implantation research applications

Some examples of research done

- High temperature oxidation inhibition
- Corrosion resistance
- Hardening of ceramics
- Buried conducting layers in Si ($IrSi_3$)
- Buried strained layers in Si ($Si_{1-x}Ge_x$)
- Hi-T_c film compositional "tuning": Y, Cu into YBaCuO
- Fundamental study of implantation ranges in C
- Effect of implantation on diamond nucleation
- Rare earths into III-V's for luminescence, etc
- ....

Very broad beam, high current, DC embodiment

- DC plasma tests
  - 5 Amps of Ti plasma
- DC extracted ion beam
  - 600 mA of Ti ions @ 18 keV (power supply limited)
  - 18 cm diameter extractor
- Very large extractor
  - 7 Amperes of Ti ions @ 100 keV (20A peak)
  - 50 cm diameter extractor

☞ ☞ "Bigger" beams (current and size) by orders of magnitude

Macroparticle contamination

- Small metal globules formed along with plasma
  - ~ 0.1 to 10 μ in size
  - initially molten and rapidly solidified in flight
  - less, in general, for cathode materials of higher melting point
  - natural separation; flux is peaked close to parallel to thesurface
  - In general, not a problem
- But nevertheless it is in principle desirable to remove the macroparticles completely from the ion beam
- A plasma duct consisting of a bent solenoid field can do this

☞ ☞ Macroparticle-free beams have been produced

Charge state enhancement

- Vacuum arc ions are in general multiply stripped
  - Q = 1+ to 6+
  - Q = 1+ to 3+
- Ion energy can be increased by increasing the charge state rather than by increasing the implanter operating voltage
- Some recent work has shown that the application of a strong magnetic field to the arc region can provide such upward charge state control
- New high charge states created; Q increased by a factor up to 2X
  - mean ion energy can be about doubled without change in voltage

☞ ☞ Upward control of ton charge states can be effected
The effect is significant for implantation application

Hybrid metal / gaseous beams

- Vacuum arc is basically a metal ion device
- By adding gas to the discharge, gaseous species can be formed
- Allows for mixed metal / gas ion beams
- Can form buried compound layers such as oxides and nitrides
- Versatility of the source is enhanced by this capability
- Serendipitous triggering advantage
  - Arc initiated by gaseous breakdown; no high voltage pulse needed
  - No erosion of the triggering system
  - The ion source can be operated for millions of repetitive pulses before the cathode needs to be changed.

☞ ☞ Gaseous / metallic ion beams can be produced

PLASMA DISTRIBUTION OF CATHODIC ARC DEPOSITION SYSTEM

Simone Anders, Sébastien Raoux, Kannan Krishnan, Robert A. MacGill and Ian G. Brown

Lawrence Berkeley National Laboratory, Berkeley, CA 94720

ABSTRACT

The plasma distribution using a cathodic arc plasma source with and without magnetic macroparticle filter has been determined by depositing on a transparent plastic substrate and measuring the film absorption. It was found that the width of the distribution depends on the arc current, and it also depends on the cathode material which leads to a spatial separation of the elements when an alloy cathode is used. By applying a magnetic multicusp field near the exit of the magnetic filter, it was possible to modify the plasma distribution and obtain a flat plasma profile with a constant and homogeneous elemental distribution.

I. INTRODUCTION

Cathodic arc deposition is an established technique for the formation of thin films [1,2]. Cathodic arc plasma sources of various designs can be operated in vacuum for the deposition of metal films[3], films of amorphous hard carbon [4-11] or amorphous semiconductors [12], and in a gaseous atmosphere to form metal oxide [13-16] or metal nitride thin films [14, 17-20]. Cathodic arc deposition is a high rate deposition method because the cathodic arc discharge which is used to transform the cathode material into the plasma state is typically a high-current discharge of one hundred to several hundred amperes, and the ion current, which determines the amount of metal plasma available for deposition, is around 10% of the arc current [21]. This results for certain sources of specific design in deposition rates as high as 3000 Å/s [3]. A problem for cathodic arc deposition is the formation of droplets of the cathode material (solid debris in the case of carbon) along with the plasma. This has been addressed by applying bent magnetic macroparticle filters which separate plasma and particles [5-14, 22-25]. All these filters lead to a certain loss of plasma which is deposited at the filter walls, and effective filters transport about 25% of all ions injected into the filter [25].

The plasma distribution of a cathodic arc deposition system is given by the "natural" plasma distribution of the cathodic arc which is influenced by the anode and cathode geometry, and it can be modified by magnetic fields. The plasma distribution determines the spatial profile of the deposition and is therefore an important parameter for film homogeneity and maximum sample size.

In the present paper we describe a number of experiments investigating the plasma distribution of various deposition systems - plasma source without additional magnetic field, and plasma source with additional magnetic field and with magnetic macroparticle filter. We also demonstrate the successful application of a magnetic multicusp configuration to homogenize and flatten the plasma profile for high quality deposition.

II. CATHODIC ARC DEPOSITION SYSTEMS

For all the experiments described in the following sections we used a pulsed cathodic arc plasma source consisting of a 6 mm diameter cathode surrounded by a cylindrical anode [26]. The discharge was triggered by a high-voltage spark over a ceramic insulator around the cathode. The arc current was 50-300 A, the arc duration 5 ms and the repetition

rate 1 Hz. The source could be equipped with a solenoid of 10 turns around the anode to focus the plasma. The arc current was used to feed the solenoid, and the maximum magnetic field at the position of the cathode surface was 75 mT. The source could also be connected to a 90° bent magnetic macroparticle filter which consisted of a free-standing coil of 25 turns with a minor radius of 4 cm and a major radius of 12 cm. The maximum magnetic field in the filter was 50 mT when the solenoid was operated electrically in series with the arc discharge and the focusing solenoid.

A magnetic multicusp arrangement, as is often used in gaseous plasma sources to homogenize and flatten the plasma distribution [27-29], could be attached to the exit of the magnetic macroparticle filter. We explored two different sizes of multicusp "homogenizer". The small multicusp (or "magnetic bucket") consisted of a steel tube of 8 cm length and 13 cm diameter, the large one of 8 cm length and 22 cm diameter to the inside wall of which SmCo magnets were arranged to form a multicusp magnetic field configuration, 10 magnets for the small multicusp, 30 magnets for the large one. Fig. 1 shows the plasma source with solenoid, magnetic macroparticle filter, the large homogenizer, and the substrate location.

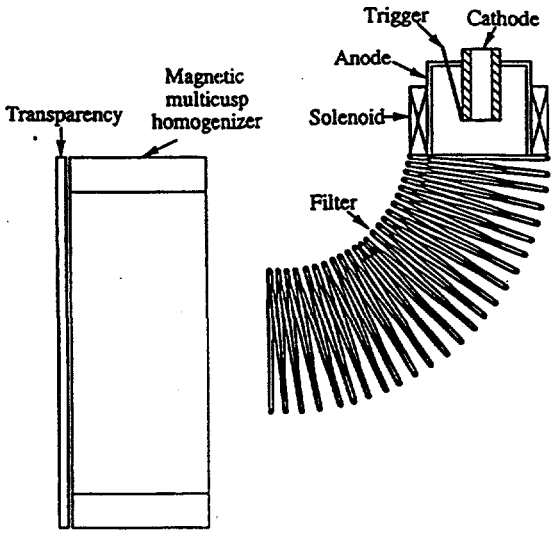

Fig. 1: Deposition arrangement showing the plasma source with focusing solenoid, the magnetic macroparticle filter, the large magnetic multicusp and the substrate (transparency).

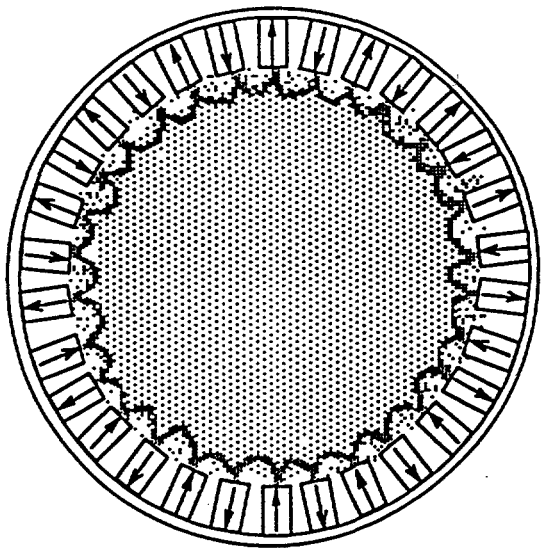

Fig. 2: End view of the large magnetic multicusp with schematic plasma distribution.

Fig. 2 shows an end view of the large homogenizer and schematically the distribution of the plasma in it. The magnets were 2 cm thick, and the region of the strong magnetic field reached about 2.5 cm into the plasma region. This results in an almost field-free inner region for the small multicusp of 4 cm and for the large multicusp of 13 cm diameter.

III. DETERMINATION OF THE DEPOSITION RATE

The deposition rate is proportional to the plasma distribution for cathodic arc discharges because the vacuum arc plasma is fully ionized and the neutral component in the plasma is typically only a few percent [30]. If a magnetic filter is used even this small fraction is removed and only ionized species are emitted from the filter [31]. The deposition profile which is given by the plasma distribution was determined by depositing semitransparent metal films on a transparent substrate (polyester transparency, 125 μm thick). Using a HeNe laser absorption set-up the transmitted light as a function of position was determined. The thickness of the deposited film was determined using the optical constants of the film material and of the dielectric substrate [32]. Assuming

a two layer system and taking transmission, absorption and reflection into account, the film thickness was calculated from a numerical solution of the Fresnel equations [33].

The absorption method is a reliable determination of the deposited film thickness if the optical constants don't vary too much over the range of film thickness deposited on the substrate. To test the reliability of this method we have measured for one case the plasma profile by the absorption method and compared it to a measurement of the plasma distribution using a Langmuir probe. A pulsed cathodic arc plasma source with a cobalt cathode was used for deposition on a transparency, and the film thickness was determined by the absorption method. In a second experiment a Langmuir probe with an area of 10 mm^2 at a negative bias voltage of -100 V was used to measure the ion saturation current during the arc discharge. The probe was at the same distance as the transparency (9 cm from the cathode surface) and moved perpendicular to the discharge axis. From the ion saturation current the plasma density profile was calculated. Fig. 3 shows the normalized deposition rate determined by the absorption method (empty dots) and by the probe method (full dots). The agreement is very good.

IV. PLASMA DISTRIBUTION FOR CATHODIC ARC SOURCE

The plasma distribution of a cathodic arc discharge has been investigated by a number of authors. In earlier papers [21, 30, 34-36] the research interest came from the field of vacuum current interrupters, and this origin explains the electrode geometry which was in most cases two disc shaped electrodes opposed to each other. The distribution was determined to be anisotropic, peaked towards the anode, and described by cosine or exponential functions. More recent papers describe systems closer in geometry to cathodic arc deposition devices with annular or cylindrical anodes [26, 37, 38]. A deviation from the cosine distribution was found, and axial magnetic fields are often used to influence the plasma distribution and form a distribution more peaked on the discharge axis.

We have measured the plasma distribution using the absorption method for a number of cathode materials and arc currents. No additional magnetic field was applied, and the substrate (transparency) was at a distance of 9 cm from the cathode surface. Fig. 4 shows the normalized distribution of the deposition for various cathode materials.

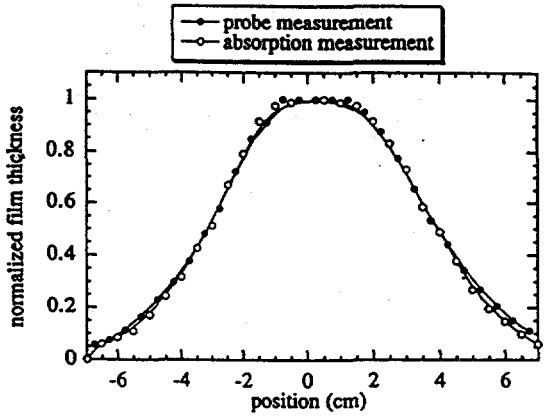

Fig. 3: Normalized film thickness as a function of position in the substrate plane. Co cathode, plasma source without solenoid, filter and multicusp, distance cathode surface - substrate 9 cm, 160 A arc current. The rate was measured using the probe method (full dots) and the absorption method (empty dots).

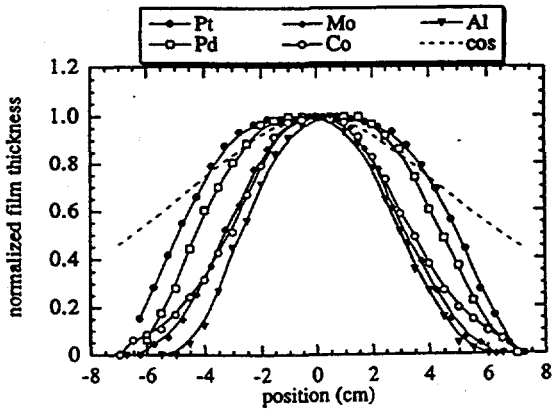

Fig. 4: Normalized distribution of the film thickness for various cathode materials. Plasma source without solenoid, filter and multicusp, distance cathode surface - substrate 9 cm, 160 A arc current. The rate was measured using the absorption method.

We found that the distribution deviates considerably from the cosine, and the full width at half maximum (FWHM) is a function of the cathode material. Fig. 5 shows that the FWHM of the distribution varies considerably with cathode material, and there is a tendency for materials with higher mass to have a broader distribution.

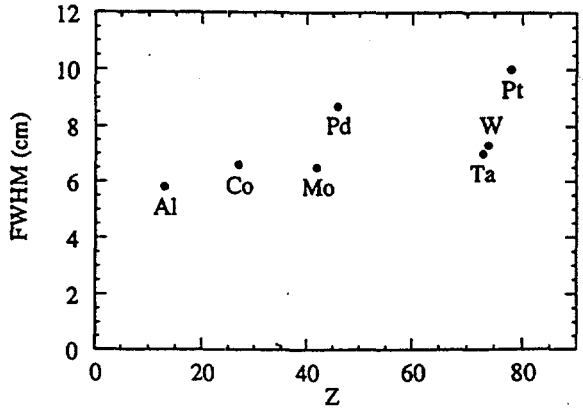

Fig. 5: FWHM of the film thickness profile taken from Fig. 4 for various cathode materials as a function of atomic number.

In another series of experiments we measured the FWHM of the distribution as a function of the discharge current. Fig. 6 shows the FWHM of the distribution for Pt in the current range between 50 and 300 A.

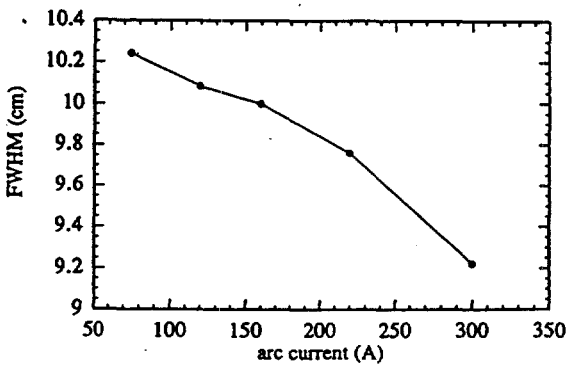

Fig. 6: FWHM of the film thickness profile for a Pt cathode as a function of the arc current. Plasma source without solenoid, filter and multicusp, distance cathode surface - substrate 9 cm. The rate was measured using the absorption method.

The distribution is more peaked on the discharge axis at higher arc currents. This effect was found also for other cathode materials (Al, Ta). This could be due to the fact that with increasing arc current more plasma is produced and ejected along the discharge axis but due to the geometry of the anode there is a shading effect for plasma emitted to the side.

V. PLASMA DISTRIBUTION FOR CATHODIC ARC SOURCE WITH MAGNETIC MACROPARTICLE FILTER

Magnetic macroparticle filters are typically 90° bent magnetic field arrangements with the magnetic field produced by external solenoids [5, 7, 12, 13, 14, 37], or by solenoids within the vacuum system which can be driven by the arc discharge current itself [6, 25, 26]. Other bending angles have also been tested for macroparticle filtering such as straight filters [4, 6, 39], 20° [9], or 45° [24, 40].

In bent magnetic field arrangements the plasma undergoes complex transport processes best described by a fluid model for a partially magnetized plasma [25, 41]. The models predict a shift of the plasma toward the outer torus wall [41], which has also been observed experimentally [25]. A shift perpendicular to the plane of symmetry has also been found [25], the direction of which changed with the direction of the toroidal magnetic field. Other papers report on a symmetric plasma distribution [5], or a distribution which is shifted toward the inner or outer torus wall depending on the magnetic field strength, and also shifted perpendicular to the plane of symmetry [42]. Possibly, the motion of the plasma column in the filter can be described by a spiral motion, and depending on the geometry, field strength, and plasma properties, all kinds of shifts can be observed.

We have measured the deposition profile using the plasma source with focusing solenoid and attached macroparticle filter. The profile was measured at a distance of 9 cm from the filter exit. Fig. 7 shows, for the examples of Ta and Al depositions at a current of 300 A, that the profiles were shifted to the outer wall of the filter in our case, and that they

were asymmetric. We observed the same effect as for the plasma source without solenoid and filter, namely a different width of the plasma distribution for different elements.

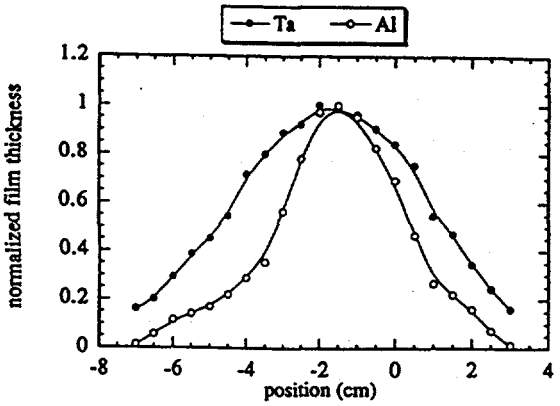

Fig. 7: Normalized film thickness as a function of the position in the substrate plane. Ta (full dots) and Al (empty dots) cathode, plasma source with solenoid and filter. Distance filter exit - substrate 9 cm, 300 A arc current. The rate was measured using the absorption method.

The last observation has an important consequence. The problem of the deviation of the deposition maximum from the filter axis can be solved by simply placing the substrates at the deposition maximum, or by using additional coils at the filter exit to change the position of the deposition maximum. But a different width of the distribution for various elements means that if a deposition is performed using an alloy cathode the different elements will be separated spatially, and a different ratio of the elements will be found at each radial location. We have observed this effect when depositing a film using an alloy cathode of composition $Nd_{1.0}Fe_{7.0}$. The plasma source with solenoid and filter was used, the substrate was a silicon wafer located at a distance of 5 cm from the filter exit, and the arc current was 300 A. The ratio of Nd and Fe in a film of 3000 Å thickness was determined by Rutherford Backscattering Spectrometry (RBS) over a range of 1.5 cm from the sample center. Over this small range the ratio varied from $Nd_{1.0}Fe_{10.0}$ at the center of the sample to $Nd_{1.0}Fe_{9.0}$ at 0.5 cm distance from the center, $Nd_{1.0}Fe_{7.2}$ at 1 cm distance, up to $Nd_{1.0}Fe_{6.7}$ at 1.5 cm distance. The increase of the heavy element Nd toward the edge of the sample reflects the fact that heavier elements have broader distributions.

VI. APPLICATION OF A MAGNETIC MULTICUSP HOMOGENIZER

In order to overcome this problem we have used an approach well known in other domains of plasma physics - the use of a magnetic multicusp field to homogenize the plasma distribution.

The magnetic multicusp is a magnetic field configuration established by alternatively polarized magnets as shown in Fig. 2, which produces a strong field at the border of the multicusp but an almost field-free in the inner region. Diffusion in the plasma leads to a flat plasma profile in the inner region, but transverse diffusion is greatly reduced by the strong magnetic field at edge thus confining the plasma within the multicusp.

We can estimate the diffusion in the plasma by calculating the drift velocity of ions and comparing it to the directed velocity of ions in a vacuum arc plasma. The diffusion in the field-free case is given by the ambipolar diffusion coefficient $\mathscr{D}_a$ which is for ion-ion collisions in the hard sphere approximation [43]

$$\mathscr{D}_a = 2\,\mathscr{D}_i = \frac{6}{8}\frac{1}{n_i r_i^2}\sqrt{\frac{kT_i}{\pi m_i}} \qquad (1)$$

where $\mathscr{D}_i$ is the ion diffusion coefficient, n_i is the ion density, r_i is the ion radius, m_i is the ion mass, T_i is the ion temperature, and k is Boltzman's constant. The plasma density in the magnetic multicusp can be estimated from the deposition rate at the multicusp exit plane and is of order 10^{19} m^{-3}. The ion temperature (not to be confused with the directed ion velocity) is comparable to the electron temperature and is around 1 eV [44, 45]. We assume a ratio of the plasma density of about 2 for the plasma on axis to the plasma at 5 cm

distance from axis (see Fig. 4), and can estimate a plasma density gradient over the multicusp radius of 10 m^{-1}. In this case the ion drift velocity v_i^{drift} is [43]

$$v_i^{drift} = -\mathscr{D}_a \frac{\nabla n_i}{n_i} \qquad (2)$$

and we obtain for Al ions an approximate value of the drift velocity of $v_i^{drift} = 5x10^4$ m/s and for Pt ions $v_i^{drift} = 2x10^4$ m/s. This should be considered only as a rough estimate, but it shows that the drift velocity and directed velocity of ions which is typically 10^4 m/s are of the same order of magnitude and thus a magnetic multicusp with an aspect ratio of about 1 should be long enough to provide a flat plasma profile if the plasma is trapped in the multicusp. We can also estimate the cross-field drift velocity at the border of the multicusp by the Bohm diffusion coefficient [43]

$$\mathscr{D}_{Bohm} = \frac{1}{16}\frac{kT_e}{eB} \qquad (3)$$

where T_e is the electron temperature, e the elementary charge, and B the magnetic field strength. Assuming a magnetic field strength of 410 mT (SmCo magnets) and an electron temperature of 1 eV, we obtain ion drift velocities perpendicular to the magnetic field of order 1 m/s. This is four orders of magnitude smaller than the directed ion velocity and drift velocity in the field-free region, and should be sufficient for highly effective confinement of the plasma in the magnetic multicusp interior region.

Fig. 8 shows the deposition profile for a number of elements obtained at the exit plane of the multicusp. The deposition was performed using the plasma source with solenoid, filter and small multicusp in a distance of 6 cm from the filter exit. The profiles are quite different from profiles obtained without multicusp. They are flat over a range of about 4 cm, and they are very similar for all elements.

In order to enlarge the area of homogeneous deposition we used a multicusp with the same length but a larger diameter (22 cm instead of 13 cm) and a larger number of magnets (30 instead of 10).

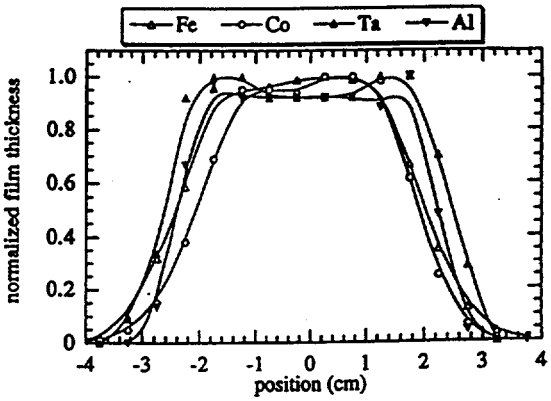

Fig. 8: Normalized film thickness for Fe, Co, Ta, and Al. Plasma source with solenoid, filter and small multicusp, distance filter - multicusp 6 cm, transparency in exit plane of multicusp, 300 A arc current. The rate was measured using the absorption method.

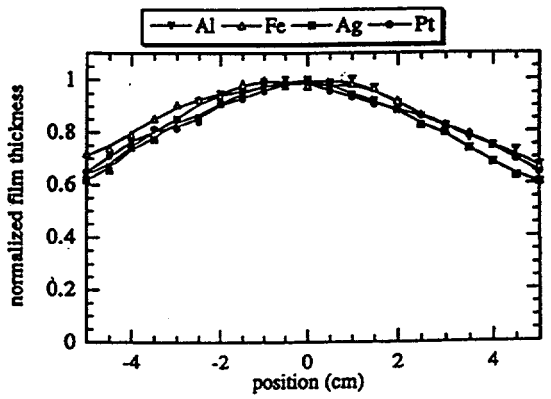

Fig. 9: Normalized film thickness for Fe, Ag, Pt, and Al. Plasma source with solenoid, filter and large multicusp, distance filter - multicusp 6 cm, transparency in exit plane of multicusp, 300 A arc current. The rate was measured using the absorption method.

Fig. 9 shows the profiles for different elements using the plasma source with solenoid, filter and large multicusp. The transparency was at the multicusp exit plane and the multicusp entrance plane at a distance of 6 cm from the filter exit. The discharge current was 300 A. Almost identical profiles were obtained for various elements, but the profiles are not as flat as with the small multicusp. It is probably necessary to use a longer multicusp field region as its diameter is increased so as to produce effective homogenization of the plasma distribution. This observation is in agreement with the estimation above.

When we replaced the SmCo magnets with ferrite magnets which have a much lower field strength, the multicusp had almost no effect and the profile is very close to the profile obtained without multicusp. The maximum field strength at the magnet surface for the SmCo magnets was 430 mT, for the ferrite magnets 40 mT. Fig. 10 shows the profiles for an Fe deposition using the plasma source with solenoid, filter and large multicusp for the two different types of magnet. For comparison the profile after removing the multicusp but leaving the transparency in the same position is shown also.

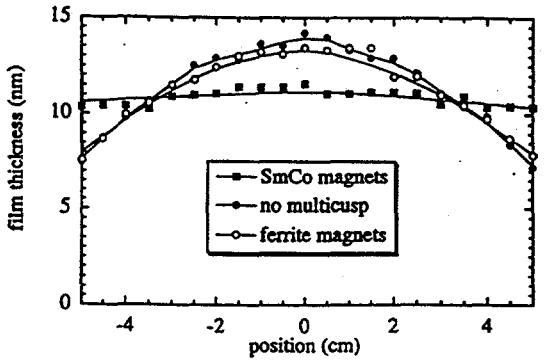

Fig. 10: Normalized film thickness for Fe; plasma source with solenoid, filter and large multicusp with SmCo and ferrite magnets, distance filter - multicusp 6 cm, transparency in exit plane of multicusp, 300 A arc current. For comparison deposition with same set-up but multicusp removed. The rate was measured using the absorption method.

In this case the profiles were not normalized, so as to compare deposition rates. The rate with multicusp is slightly lower in the center because the plasma is spread out over the multicusp diameter. The integrated rate over a substrate diameter of about 15 cm is comparable with and without multicusp.

In order to test the results for the deposition profiles obtained with the magnetic multicusp for an alloy deposition application we have repeated the deposition of a film very similar to the one described in the previous section. An alloy cathode with a composition $Nd_{1.0}Fe_{4.4}$ was used in the plasma source with solenoid, filter and the small magnetic multicusp 5 cm away from the filter exit. The Si wafer substrate was located in the exit plane of the multicusp, and the arc current was 300 A. The film composition of the 1800 Å thick film was determined by RBS over a range of 2.5 cm from the sample center, and the composition was found to vary only between $Nd_{1.0}Fe_{4.4}$ and $Nd_{1.0}Fe_{4.5}$ over this area. This demonstrates the successful application of the multicusp to a film deposition using an alloy cathode.

VII. SUMMARY

The plasma distribution for our cathodic arc plasma source was measured by an absorption method which was demonstrated to be a simple and reliable way of determining the plasma profile. It is more peaked at higher currents which is possibly a geometric effect of our source design. The width of the profile varies with the cathode material, and this effect occurs for the source without and with macroparticle filter. This leads to a spatial separation of the elements when a deposition is performed using an alloy cathode. If the plasma is ejected from the filter into a magnetic multicusp of appropriate design, however, the plasma profiles are flattened and show the same shape for various elements. Depositions using an alloy cathode demonstrated that the compositional homogeneity of the thin film is greatly improved by the application of a magnetic multicusp plasma homogenizer.

ACKNOWLEDGMENTS

We wish to thank Mike Rubin, Lawrence Berkeley Laboratory, for his advice regarding the optical measurements. This work was supported by the Electric Power Research Institute under Award number 8042-03, the U.S. Department of Energy, Division of Advanced Energy Projects, and the Center for Excellence in Synthesis and Processing, under contract No. DE-AC03-76SF00098.

REFERENCES

[1] D. M. Sanders, D. B. Boercker, and S. Falabella, IEEE Trans. Plasma Sci. **18**, 883 (1990).

[2] R. L. Boxman and S. Goldsmith, IEEE Trans. Plasma Sci. **17**, 705 (1989).

[3] R. L. Boxman and S. Goldsmith, Surface & Coatings Technol. **43/44**, 1024 (1990).

[4] B. F. Coll, P. Sathrum, R. Aharonov, and M. A. Tamor, Thin Solid Films **209**, 165 (1992).

[5] I. I. Aksenov, S. I. Vakula, V. G. Padalka, V. E. Strel'nitskii, and V. M. Khoroshikh, Sov. Phys. Tech. Phys. **25**, 1164 (1980).

[6] J. Koskinen, A. Anttila, and J.-P. Hirvonen, Surface and Coatings Technol. **47**, 180 (1991).

[7] D. R. McKenzie, D. Muller, B. A. Pailthorpe, Z. H. Wang, E. Kravtchinskaia, D. Segal, P. B. Lukins, P. J. Martin, G. Amaratunga, P. H. Gaskell, and A. Saeed, Diamond and Related Mater. **1**, 51 (1991).

[8] S. Falabella, D. B. Boercker, and D. M. Sanders, Thin Solid Films **236**, 82 (1993).

[9] R. Lossy, D. L. Pappas, R. A. Roy, J. J. Cuomo, and V. M. Sura, Appl. Phys. Lett. **61**, 171 (1992).

[10] P. J. Fallon, V. S. Veerasamy, C. A. Davis, J. Robertson, G. A. J. Amaratunga, W. I. Milne, and J. Koskinen, Phys. Rev. B **48**, 4777 (1993).

[11] S. Anders, A. Anders, I. G. Brown, B. Wei, K. Komvopoulos, J. W. Ager III, and K. M. Yu, Surface & Coatings Technol. **68/69**, 388 (1994).

[12] D. Arbilly, R. L. Boxman, A. Rothwarf, and L. Kaplan, Thin Solid Films **253**, 62 (1994).

[13] A. Ben-Shalom, L. Kaplan, R. L. Boxman, S. Goldsmith, and M. Nathan, Thin Solid Films **236**, 20 (1993).

[14] P. J. Martin, R. P. Netterfield, T. J. Kinder, and L. Descôtes, Surface & Coatings Technol. **49**, 239 (1991).

[15] S. Anders, A. Anders, M. Rubin, Z. Wang, S. Raoux, F. Kong, and I. G. Brown, Surface & Coatings Technol., to be published.

[16] R. A. MacGill, S. Anders, A. Anders, R. A. Castro, M. R. Dickinson, K. M. Yu, and I. G. Brown, Surface & Coatings Technol., to be published.

[17] W. Olbrich, J. Fessmann, G. Kampschulte, and J. Ebberink, Surface & Coatings Technol. **49**, 258 (1991).

[18] A. Bendavid, P. J. Martin, R. P. Netterfield, and T. J. Kinder, Surface & Coatings Technol. **70**, 97 (1994).

[19] G. H. Kang, H. Uchida, and E. S. Koh, Surface & Coatings Technol. **68**, 141 (1994).

[20] R. R. Aharonov, Surface & Coatings Technol. **61**, 223 (1923).

[21] C. W. Kimblin, J. Appl. Phys. **44**, 3074 (1973).

[22] P. J. Martin, R. P. Netterfield, and T. J. Kinder, Thin Solid Films **193**, 77 (1990).

[23] J. Storer, J. E. Galvin, and I. G. Brown, J. Appl. Phys. **66**, 5245 (1989).

[24] S. Falabella and D. M. Sanders, J. Vac. Sci. Technol. A **10**, 394 (1992).

[25] A. Anders, S. Anders, and I. G. Brown, Plasma Sources Sci. Technol. **4**, 1 (1995).

[26] S. Anders, A. Anders, and I. G. Brown, J. Appl. Phys. **74**, 4239 (1993).

[27] K. N. Leung, Rev. Sci. Instrum. **65**, 1165 (1994).

[28] A. T. Forrester, *Large Ion Beams - Fundamentals of Generation and Propagation,* chapt. 8.9, Wiley-Interscience, New York 1988.

[29] I. G. Brown, ed., *The Physics and Technology of Ion Sources,* chapt. 7.1, Wiley-Interscience, New York 1989.

[30] D. T. Tuma, C. L. Chen, and D.K. Davies, J. Appl. Phys. **49**, 3821 (1978).

[31] Z. H. Wang, D. R. McKenzie, P. J. Martin, and R. P Netterfield, J. Vac. Sci. Technol. A **13**, 2261 (1995).
[32] American Institute of Physics Handbook, MacGraw-Hill Book Company, 1972.
[33] E. Hecht and A. Zajac, *Optics*, Addison-Wesley Publishing Company, Menlo Park 1974.
[34] J. Heberlein and D. Porto, IEEE Trans. Plasma Sci. **11**, 152 (1983).
[35] J. E. Daalder and P. G. E. Wielders, Proc. XIIth Symp. Phenomena in Ionized Gases (Eindhoven, Holland), 1975, p. 232.
[36] V. M. Lunev, V. D. Ovcharenko, and V. M. Khoroshikh, Sov. Phys. Tech. Phys. **22**, 855 (1977).
[37] I. I. Aksenov, V. G. Padalka, V. T. Tolok, and V. M. Khoroshikh, Sov. J. Plasma Phys. **6**, 504 (1980).
[38] Y. Cohen, R. L. Boxman, and S. Goldsmith, IEEE Trans. Plasma Sci. **17**, 713 (1989).
[39] K. Akari, H. Tamagaki, T. Kumkiri, K. Tsuji, E. S. Koh, and C. N. Tai, Surface and Coatings Technol. **43/44**, 312 (1990).
[40] D. A. Baldwin and S. Falabella, Soc. Vacuum Coaters Technical Proceedings of the 1995 Annual Meeting, to be published.
[41] I. I. Aksenov, A. N. Belokhvostnikov, V. G. Padalka, N. S. Repalov, and V. M. Khoroshikh, Plasma Phys. Control. Fusion **28**, 761 (1986).
[42] V. N. Zhitomirsky, L. Kaplan, R. L. Boxman, and S. Goldsmith, International Conference on Metallurgical Coatings and Thin Films, 1995, San Diego, to be published in Surface and Coatings Technol.
[43] A. Anders, *A Formulary for Plasma Physics,* Akademie-Verlag, Berlin 1990.
[44] G. A. Lyubimov and V. I. Rakhovskii, Sov. Phys. - Usp. **21**, 693 (1978).
[45] V. A. Ivanov, B. Jüttner, and H. Pursch, IEEE Trans. Plasma Sci. **13**, 334 (1995).

High Ion Charge States in a High-Current, Short-Pulse, Vacuum Arc Ion Source

André Anders, Ian Brown, Robert MacGill, and Michael Dickinson

Lawrence Berkeley National Laboratory, University of California, Berkeley, CA 94720

Abstract

Ions of the cathode material are formed at vacuum arc cathode spots and extracted by a grid system. The ion charge states (typically 1-4) depend on the cathode material and only little on the discharge current as long as the current is low. Here we report on experiments with short pulses (several μs) and high currents (several kA); this regime of operation is thus approaching a more vacuum spark-like regime. Mean ion charge states of up to 6.2 for tungsten and 3.7 for titanium have been measured, with the corresponding maximum charge states of up to 8+ and 6+, respectively. The results are discussed in terms of Saha calculations and freezing of the charge state distribution.

I. Introduction

Broad beams of multiply charged metal ions can be produced by vacuum arc plasma sources. They have been described in detail in [1, 2], and we give here only a brief description. An arc between metal electrodes in vacuum is usually initiated by applying a positive high voltage pulse to a trigger electrode. The arc burns in the plasma formed at non-stationary cathode spots. The cathodic plasma expands from the cathode spots into the vacuum and reaches the ion extractor system which is usually a three-grid system of the acceleration-deceleration type. It is common that ion sources of this type operate in a repetitively pulsed mode (arc duration of order 1 ms or less) with repetition rates of a few pulses per second, an arc current of 100-300 A, an ion beam current of order 100 mA (during pulses), and an extractor voltage in the range 20-100 kV. The ion charge state distribution (CSD) was investigated in a number of papers [1-4], and the most recent table is given in Ref. [1] for 50 cathode materials.

CSDs were found to be fairly reproducible in different embodiments of the vacuum arc ion source. However, it turned out that the CSDs do not only depend on the cathode material but also on the time elapsed since the arc pulse was started [5, 6], and on the presence and strength of an external magnetic field [6-9].

In the present paper we investigate the influence of the discharge current on the CSD. This is motivated by the fact that very high ion charge states have been observed spectroscopically in short-pulse, high-current vacuum spark experiments [10, 11]. High charge states are of interest for obtaining high ion energies at a given extractor voltage.

II. Experiments

For our experiments we used a vacuum arc ion source similar to what has been described previously [1, 12]. The arc was fed by a 7-stage LC-pulse line of 1.5 Ω impedance, resulting in pulses of 100-300 A amplitude, 5 μs rise time and 250 μs duration. The cathode spots burned on the front face of a water-cooled, cylindrical cathode of 6.2 mm diameter; the annular anode had an inner diameter of 20 mm and was 1 cm apart from the cathode surface (Fig. 1). The anode hole diameter was

reduced to 4 mm or 2 mm for discharge currents higher than 300 A and 3 kA, respectively, in order to avoid breakdown of the extractor voltage. The plasma leaving the arc discharge region expanded while streaming towards the extractor grids. The extractor grids had holes of 6 mm diameter and were placed 10 cm downstream the anode. The ion beam had a diameter of about 10 cm.

To achieve higher currents and shorter pulses, the LC pulse forming network was replaced by a fast high voltage capacitor (C = 12 μF or 100 μF in different experiments). The arc current was controlled by using various inductive loads (0.1-10 μH) and a 100 mΩ Ohmic resistor. In most experiments, the capacitor was located very close to the electrode arrangement to keep the circuit inductance relatively small (about 0.1 μH), and thus pulsed currents of several kiloamperes could be obtained even with the charging voltage not exceeding 600 V. The arc pulse length was in the range of 3-25 μs (FWHM). Ions of charge state z are accelerated to the energy $E_z = z\,U_{extr}$; the default extractor voltage was $U_{extr} = 50$ kV. Titanium and tungsten were used as cathode materials. The CSD was investigated by a time-of-flight (TOF) charge-to-mass spectrometer described elsewhere [12].

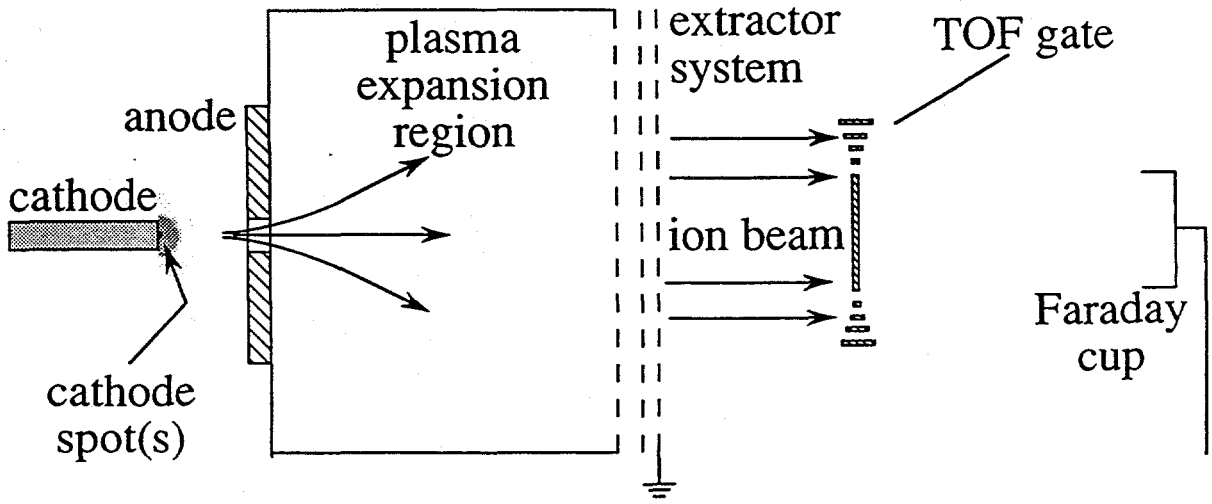

Fig. 1 Schematic of the source of multiply stripped metal ions and TOF diagnostics; (not to scale).

III. Results

Fig. 2(a) shows a typical TOF spectrum for Ti obtained by the "standard" low-current vacuum arc ion source. The arc current was 150 A, and the mean ion charge state was $\bar{z} = 2.2$, measured 100 μs after triggering. As a first step towards higher currents and shorter pulses we used a 100 μF capacitor and a circuit inductance of 3.6 μH. The titanium CSD at a peak current of 560 A (30 μs after triggering) is shown in Fig. 2(b); $\bar{z} = 2.4$ that is only slightly higher than at "standard" operation.

Higher discharge currents were achieved by reducing the inductive load. Figure 2(c) shows the titanium CSD at 1.8 kA peak current (12 μF capacitor, the FWHM of the current pulse was 6 μs) with $\bar{z} = 3.6$, i.e. significantly higher than at "standard" operation, and $\bar{z} = 3.75$ has been obtained at 3.4 kA.

It is known from previous work [3] that cathode materials of high boiling point tend to

have high charge states; the empirical law $\bar{z} = 0.38\left(T_{bp}(°C)/1000\right)+1$ was derived for discharge currents smaller than 200 A. To proof this rule at higher currents we replaced the titanium cathode ($T_{bp} = 3287$ °C) by a tungsten cathode ($T_{bp} = 5660$ °C). The mean ion charge state at "standard" operation (150 A, 100 µs after triggering) is $\bar{z} = 3.1$. Figs. 3(a) and (b) show TOF spectra of tungsten ion beams obtained with 12 µs pulses at a peak current of 3.4 kA with $\bar{z} = 5.8$ and 6.3. There is obviously a considerable shot-to-shot variation in the CSD but a clear increase of $\bar{z}$ with current (Fig. 4).

IV. Discussion

The formation of ions at cathode spots is associated with phase transitions and ionization of the cathode material. Although a number of papers have been published [13-19], a satisfying model has not yet been formulated. It has been shown that inhomogeneous heating of the cathode surface (mainly by ion bombardment) leads to local melting and the formation of a dense, non-ideal plasma of micron-size. This is the plasma of "microspots" which expands rapidly, driven mainly by the pressure gradient to the vacuum ambient. While local thermodynamic equilibrium is established close to the spot (within a distance of order 100 µm from the spot center), the expanding plasma quickly goes into non-equilibrium at low density.

As long as equilibrium conditions are fulfilled (the time between inelastic collisions is short compared to the characteristic expansion time), the plasma composition can be calculated by a set of Saha equations [15, 17, 19, 20]. Figs. 5-8 show calculated plasma compositions assuming a plasma temperature of 3 eV and 5 eV for titanium and 4 eV and 6 eV for tungsten. For these calculations, ionization energies and partition functions have been taken from Refs. [21-23]. For the lowering of the ionization energies we used the Debye-Hückel model which is valid for weakly non-ideal plasmas.

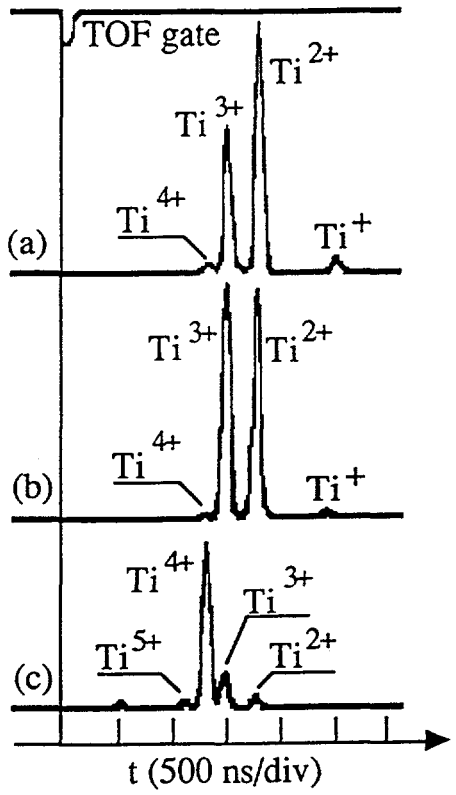

Fig. 2 TOF spectra of titanium ion beams: (a) "standard" ion source, 150 A, 100 µs after triggering; (b) 30 µs after triggering, using a 100 µF capacitor, 560 A, 60 µs pulse; (c) 3 µs after triggering, 12 µF capacitor, 1.8 kA; 6 µs pulse.

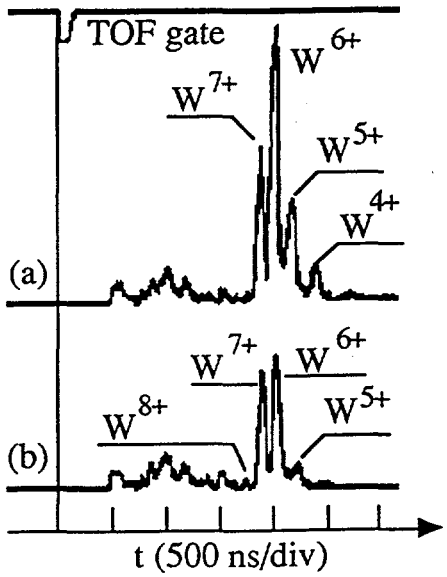

Fig. 3 TOF spectra of tungsten ion beams: (a) 6 µs after triggering, 100 µF capacitor, 3.4 kA; 12 µs pulse; (b) same as (a) showing the large shot-by-shot variation.

The calculation for tungsten are somewhat uncertain since we used self-consistent-field Hartree-Fock results for the ionization energies [21] and estimates for the partition functions (to our knowledge, no experimental data are available).

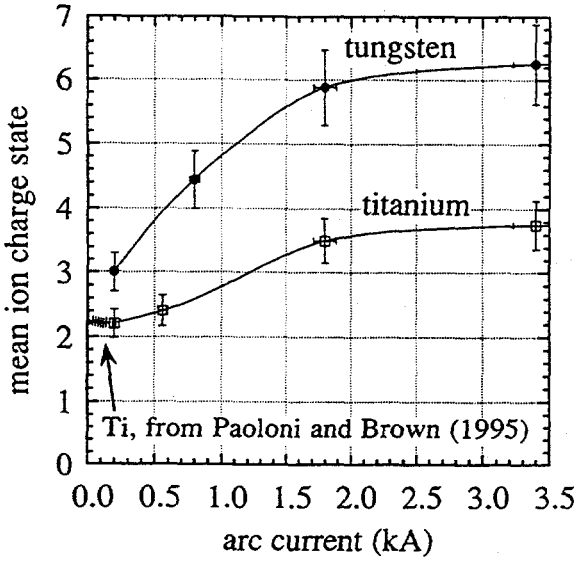

Fig. 4 Increase of the mean ion charge state with discharge current. Each point represents an average of 16 discharges.

When ionizing/recombining collisions become infrequent the composition of the plasma "freezes". Although "freezing" is actually a step-wise process [15], it is reasonable to look for a combination of plasma density and temperature which approximately gives the experimentally observed CSD. In this way, we determined a "freezing temperature" and "freezing density" as indicated in Figs. 5-8.

At low current, plasma is produced at a single cathode spot or very few spots. The plasma of each spot can expand independently from the plasma of other spots, and the plasma density decreases as r^{-2} where r is the distance from the spot center. Freezing typically occurs at a density of heavy particles $n_h \approx 10^{25}$ m^{-3} ([17] and Figs. 5, 6).

At high current, the freezing process and the resulting CSDs are changed by two effects. First, more energy is invested in each heavy particle. If we assume that (i) the amount of plasma produced is proportional to the current and (ii) the plasma conductivity does not change significantly with increasing current, then the energy per particle is approximately proportional to the current. Therefore, the plasma temperature increases with current. Second, many spots are simultaneously active at high current, and the plasma of each spot expands under the influence of neighboring plasmas. Thus the expansion is not as rapid as in the previous case, and the density drops as $r^{-\nu}$ with $\nu < 2$. The characteristic expansion time becomes longer, and freezing occurs at lower densities and larger distances from the cathode. These effects are illustrated in Figs. 7 and 8.

New effects must be expected at much higher currents (many kA). Erosion of material occurs not only from the cathode but also from the anode. Compression and plasma heating by the self-magnetic field leads to much higher charge states in "hot spots" within the plasma [10, 12]. More effort will be needed these effects for the formation of beams of even higher charged metal ions. A broad beam metal ion implanter based of multiply charged ions is under construction at LBNL.

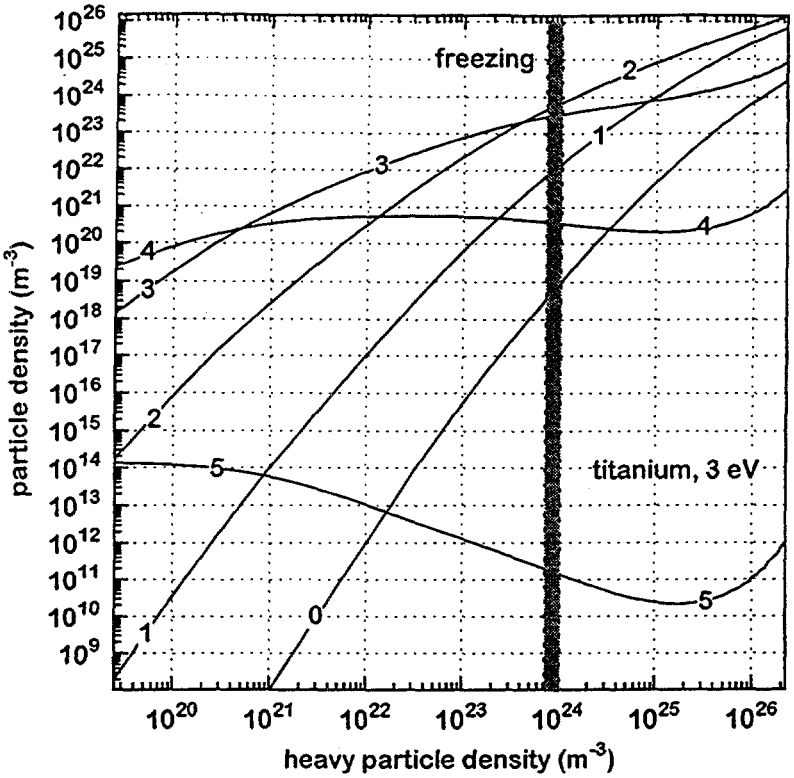

Fig. 5 Composition of a Ti plasma in equilibrium at 3 eV (Saha calculation); the freezing in the case of low current is indicated.

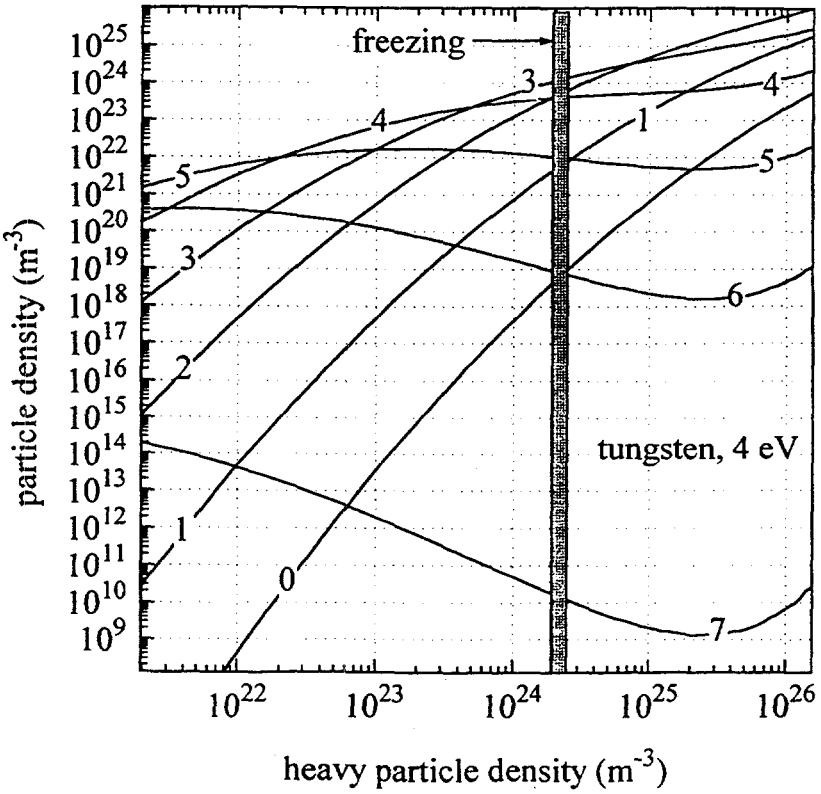

Fig. 6 As Fig. 5 but for tungsten at 4 eV.

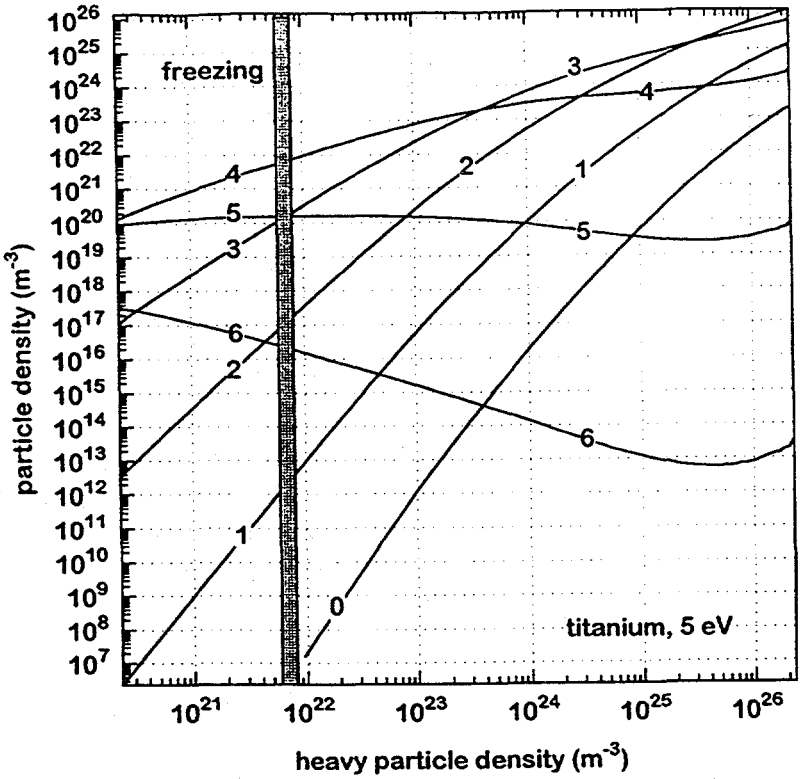

Fig. 7 Composition of a Ti plasma in equilibrium at 5 eV; the freezing in the case of high current is indicated.

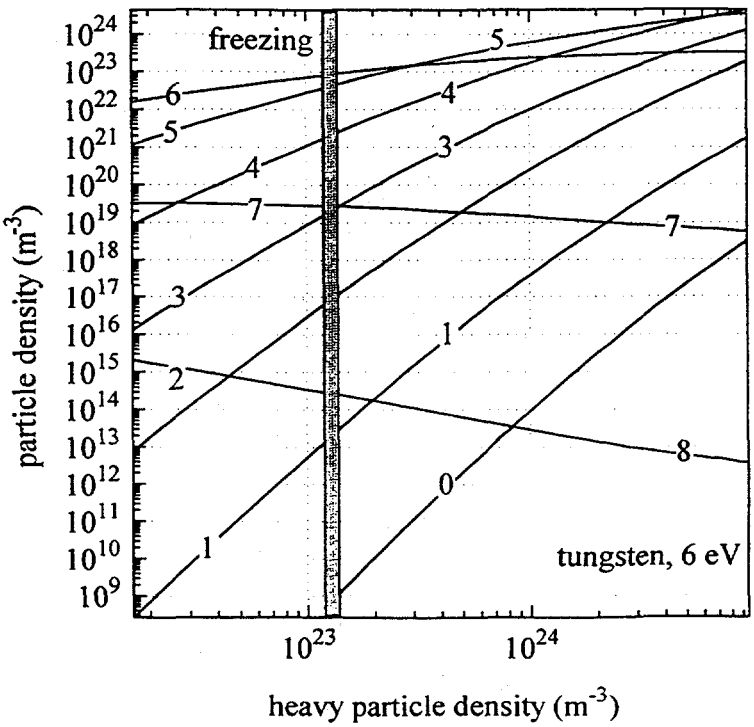

Fig. 8 As Fig. 7 but for tungsten at 6 eV

Acknowledgments

We would like to acknowledge the generous help of Thomas Schülke, Germany, in performing the numerical calculations. This work was supported by the U.S. Department of Energy, Division of Advanced Energy Projects, under contract No. DE-AC03-76SF00098.

References

[1] I. G. Brown, Rev. Sci. Instrum. **65**, 3081 (1994).

[2] I. G. Brown, in The Physics and Technology of Ion Sources, edited by I. G. Brown (Wiley, New York, 1989), p.331.

[3] I. G. Brown and X. Godechot, IEEE Trans. Plasma Sci. **PS-19**, 713 (1991).

[4] I. G. Brown, B. Feinberg, and J. E. Galvin, J. Appl. Phys. **63**, 4889 (1988).

[5] J. E. Galvin, I. G. Brown, and R. A. MacGill, Rev. Sci. Instrum. **61**, 583 (1990).

[6] A. Anders, S. Anders, B. Jüttner, and I. G. Brown, IEEE Trans. Plasma Sci. **PS-21**, 305 (1993).

[7] E. M. Oks, I. G. Brown, M. R. Dickinson, R. A. MacGill, H. Emig, P. Spätke, and B. H. Wolf, Appl. Phys. Lett. **67**, 200 (1995).

[8] E. M. Oks, I. G. Brown, M. R. Dickinson, R. A. MacGill, this Conf. (6th ICIS, Whistler, Canada, 1995), to be published in Rev. Sci. Instrum.

[9] F. J. Paoloni and I. G. Brown, Rev. Sci. Instrum. **66**, 3855 (1995).

[10] R. Beier and H.-J. Kunze, Z. Physik A **285**, 347 (1978).

[11] C. R. Negus and N. J. Peacock, J. Phys. D: Appl. Phys. **12**, 91 (1979).

[12] I. G. Brown, J. E. Galvin, R. A. MacGill, and R. T. Wright, Rev. Sci. Instrum. **58**, 1589 (1987).

[13] S. Anders, Contrib. Plasma Phys. **26**, 416 (1986).

[14] C. Wieckert, Contrib. Plasma Phys. **27**, 309, (1987).

[15] S. Anders, A. Anders, J. Phys. D: Appl. Phys. **21**, 213, (1988).

[16] N. Radic and B. Santic, Proc. XIII Int. Symp. Discharges and Electrical Insulation in Vacuum (Paris), edited by J. M. Buzzi and A. Septier, 217, 1988.

[17] S. Anders, A. Anders, Contrib. Plasma Phys. **29**, 537, (1989).

[18] N. B. Volkov and A. Z. Nemirovsky, J. Phys. D: Appl. Phys. **24**, 693, (1991).

[19] A. Anders, S. Anders, A. Förster, and I. G. Brown, Plasma Sources Sci. Technol. **1**, 263, (1992).

[20] E. M. Oks, A. Anders, I. G. Brown, M. R. Dickinson, R. A. MacGill, submitted to IEEE Trans. Plasma Sci.

[21] T. A. Carlson, C. W. Nestor, N. Wasserman, and J. D. McDowell, Atomic Data **2**, 63, (1970).

[22] S. Bashkin and J. O. Stoner, *Atomic Energy-Level and Grotrian Diagrams, vol. II, Sulfur I - Titanium XXII*, (North-Holland Publ. Comp., Amsterdam, 1978).

[23] H.-W. Drawin and P. Felenbok, *Data for Plasmas in Local Thermodynamic Equilibrium*, (Gauthier-Villars, Paris, 1965).

List of Participants

André Anders
LBNL, MS-53
University of California, Berkeley, CA 94720, USA
Ph: 510-486-6745
Fax: 510-486-4374
EMail: AAnders@LBL.Gov

Simone Anders
LBNL, MS-53
University of California, Berkeley, CA 94720, USA
Ph: 510-486-5928
Fax: 510-486-4374
EMail: SAnders@LBL.Gov

Ian Brown
LBNL, MS-53
University of California, Berkeley, CA 94720, USA
Ph: 510-486-4174
Fax: 510-486-4374
EMail: IBrown@LBL.Gov

Michael Dickinson
LBNL, MS-53
University of California, Berkeley, CA 94720, USA
Ph: 510-486-7792
Fax: 510-486-4374

Evgeni Donets
JINR, Laboratory of High Energies
141980 Dubna, Russia
Ph: 7-09621-65806
Fax: 7-095-975-2381
EMail: Donets@LHE26.jinr.dubna.su

Peter Evans
ANSTO
PMB 1, Menai, NSW 2234, Australia
Ph: 61-2-717-3696
Fax: 61-2-717-9265
Email: PEV@atom.ansto.gov.au

Xavier Godechot
Sodern
20 Ave. Descartes, 94451 Limeil-Brevannes, France
Ph: 33-1-4595-7000
Fax: 33-1-4569-1402

Steve Gower
University of Wollongong, Elec. & Computer Eng. Dept.
PO Box 1144, Wollongong, NSW 2500, Australia
Ph: 61-42-21-3401
Fax: 61-42-21-3555
EMail: steveg@uow.edu.au

Othon Monteiro
LBNL, MS-53
University of California, Berkeley, CA 94720, USA
Ph: 510-486-6159
Fax: 510-486-4374
EMail: ORMonteiro@LBL.Gov

Efim Ox
High Current Electronics Institute
4 Akademicheskaya Avenue, Tomsk 634055, Russia
Ph: 7-3822-258-776
Fax: 7-3822-259-410
EMail: Oks@hcei.tomsk.su

Dinesh Sood
RMIT
GPO Box 2476V, Melbourne, Vic 3001, Australia
Ph: 61-3-660-2459
Fax: 61-3-662-1921
Email: REEDS@Whitetail.cse.rmit.edu.au

Peter Spädtke
GSI
Postfach 110052, Darmstadt 64220, Germany
Ph: 49-6159-71-2323
Fax: 49-6159-71-2988
EMail: UL13@GSI.DE

Zhi Wang
LBNL, MS-53
University of California, Berkeley, CA 94720, USA
Ph: 510-486-5441
Fax: 510-486-4374
EMail: Z_Wang@LBL.Gov

Bernhard Wolf
GSI
Postfach 110052, Darmstadt 64220, Germany
Ph: 49-6159-71-2320
Fax: 49-6159-71-2988
EMail: BWolf@CLR16F.GSI.DE

George Yushkov
High Current Electronics Institute
4 Akademicheskaya Avenue, Tomsk 634055, Russia
Ph: 7-3822-258-776
Fax: 7-3822-259-410
EMail: GYushkov@hcei.tomsk.su